NBS

Technical Note No. 313

ON THE EFFECT OF HEAVY IONS ON LF PROPAGATION, WITH SPECIAL REFERENCE TO A NUCLEAR ENVIRONMENT

J. RALPH JOHLER AND LESLIE A. BERRY

U. S. DEPARTMENT OF COMMERCE
NATIONAL BUREAU OF STANDARDS

THE NATIONAL BUREAU OF STANDARDS

The National Bureau of Standards is a principal focal point in the Federal Government for assuring maximum application of the physical and engineering sciences to the advancement of technology in industry and commerce. Its responsibilities include development and maintenance of the national standards of measurement, and the provisions of means for making measurements consistent with those standards; determination of physical constants and properties of materials; development of methods for testing materials, mechanisms, and structures, and making such tests as may be necessary, particularly for government agencies; cooperation in the establishment of standard practices for incorporation in codes and specifications; advisory service to government agencies on scientific and technical problems; invention and development of devices to serve special needs of the Government; assistance to industry, business, and consumers in the development and acceptance of commercial standards and simplified trade practice recommendations; administration of programs in cooperation with United States business groups and standards organizations for the development of international standards of practice; and maintenance of a clearinghouse for the collection and dissemination of scientific, technical, and engineering information. The scope of the Bureau's activities is suggested in the following listing of its four Institutes and their organizational units.

Institute for Basic Standards. Applied Mathematics. Electricity. Metrology. Mechanics. Heat. Atomic Physics. Physical Chemistry. Laboratory Astrophysics.* Radiation Physics. Radio Standards Laboratory:* Radio Standards Physics; Radio Standards Engineering. Office of Standard Reference Data.

Institute for Materials Research. Analytical Chemistry. Polymers. Metallurgy. Inorganic Materials. Reactor Radiations. Cryogenics.* Materials Evaluation Laboratory. Office of Standard Reference Materials.

Institute for Applied Technology. Building Research. Information Technology. Performance Test Development. Electronic Instrumentation. Textile and Apparel Technology Center. Technical Analysis. Office of Weights and Measures. Office of Engineering Standards. Office of Invention and Innovation. Office of Technical Resources. Clearinghouse for Federal Scientific and Technical Information.**

Central Radio Propagation Laboratory.* Ionospheric Telecommunications. Tropospheric Telecommunications. Space Environment Forecasting. Aeronomy.

---

* Located at Boulder, Colorado 80301.

** Located at 5285 Port Royal Road, Springfield, Virginia 22171.

NATIONAL BUREAU OF STANDARDS

Technical Note 313

ISSUED June 7, 1965

ON THE EFFECT OF HEAVY IONS ON LF PROPAGATION, WITH SPECIAL REFERENCE TO A NUCLEAR ENVIRONMENT

J. Ralph Johler and Leslie A. Berry
Central Radio Propagation Laboratory
National Bureau of Standards
Boulder, Colorado

For sale by the Superintendent of Documents, U. S. Government Printing Office
Washington, D.C. 20402
Price: 45¢

Contents

Foreword

This paper is the annual comprehensive report on LF propagation part of Advanced Research Projects Agency (ARPA) Order No. 183, Amendment No. 13, Task IV, or NBS Project 51013-12-5100415. This is a theoretical study of low frequency signals in the presence of ambient and disturbed ionosphere models. In particular, this paper introduces the effects of heavy ions into the theoretical analysis. These ions are known to exist in the ambient atmosphere and ionosphere, but the effect on propagation has not been studied in a systematic manner. Indeed large quantities of ions, in addition to electrons, are produced by solar disturbances, proton events, and high altitude nuclear detonations. This paper introduces an equation of motion for a gas mixture of four constituents: positive ions, negative ions, electrons, and neutrals together with the interaction of these constituents via collisions resulting from velocity differentials and the superposed terrestrial magnetic field.

The resultant electrical properties of the magneto-plasma are formulated in a format which can be readily introduced in the previously published analytical methods of Johler and Harper [1962].

On the Effects of Heavy Ions on LF Propagation, with Special Reference to a Nuclear Environment†

J. Ralph Johler and Leslie A. Berry

Natural disturbances and high altitude nuclear detonations produce large quantities of ions in the ionosphere and in the atmosphere. The effect of such ionization on the propagation of LF radio waves is not in general negligible. In fact, physically realizable production rates can be postulated in which the ions rather than the electrons control the propagation of radio waves around the terrestrial sphere. Therefore, considering only an electron gas type plasma as an ionosphere model is subject to possible grave errors in the theoretical prediction of LF propagation. The theoretical solution of the heavy ion problem requires the introduction of an equation of motion or hydrodynamic equation for each gas constituent.

1. Introduction to Ionosphere Models

1.1. Ambient Model

The propagation of LF (low frequency) radio waves is, in large measure, dependent upon the electrification in the upper atmosphere and lower ionosphere. This electrification can be quantitatively described as a microprocess in the plasma by a set of rate equations [Chapman, 1931; Nicolet and Aikin, 1960; Ginzburg, 1960; Crain, 1961; Pierce and Arnold, 1962; Arnold and Pierce, 1963; Pierce, 1963; Arnold, 1964; and Moler, 1960]:

$$\frac{dN_e}{dt} = Q - AN_e - BN_eN_+ + (C + D)N_-$$

$$\frac{dN_-}{dt} = AN_e - (C + D)N_- - EN_-N_+$$

$$\frac{dN_+}{dt} = Q - BN_eN_+ - EN_-N_+, \qquad (1.1)$$

where $N_+ = N_e + N_-$ and $\frac{dN_+}{dt} = \frac{d}{dt}(N_e + N_-)$.

† This work was sponsored by ARPA under Order No. 183, Amendment No. 13, Task IV or NBS Project 51013-12-5100415.

The number density, N, is identified with three gas constituents by the subscripts: e, elctrons; +, positive ions; -, negative ions. The quantities on the right side of the differential equations comprise ion-electron pair production rate, Q, causing dissociation into positive ions and electrons, and the various rate coefficients, A, B, C, D, and E. The electron attachment coefficient is designated by A, the electron-ion recombination coefficient by B, the photo detachment coefficient by C, The detachment coefficient by D, and the ion-ion recombination coefficient by E. An extensive survey of the state of knowledge concerning these rate coefficients has been given by Archer [1963].

The attachment coefficient, A, is calculated [Arnold and Pierce, 1963; Pierce, 1963; and Arnold, 1964] from atomic oxygen number density, cm^{-3}, [O], molecular oxygen number density $[O_2]$ and nitrogen number density $[N_2]$ temperature, T, °K (degrees Kelvin) obtained from model atmospheres such a Minzner and Ripley [1956], Minzner, Ripley, and Condron [1958], and Minzner, Champion, and Pond [1959] by,

$$A \sim 1.3[O](10^{-15}) + [O_2](10^{-17}) + \left(\frac{T+100}{400}\right)[O_2]\left\{[O_2] + \frac{[N_2]}{50}\right\} 3(10^{-30}),\ sec^{-1} \tag{1.2}$$

This equation has recently been verified by Hirsch, Eisner, and Selvin [1964]. Hirsch et al., however, get $2.1(10^{-30})$ instead of $3(10^{-30})$ for the numerical constant assuming T = 300°K. The electron-ion recombination coefficient, B, is [Arnold and Pierce, 1963]

$$B \sim 2(10^{-7}),\ cm^3\ sec^{-1}. \tag{1.3}$$

This is valid for altitudes 40 to 100 km above the surface of the earth.

The photo detachment term C is [Arnold and Pierce, 1963; Pierce, 1963; and Arnold, 1964]

$$C = \frac{0.1[O_2^-] + 1.4[O^-] + 5(10^{-3})[O_3^-] + 10^{-3}[OH^-] + 10^{-6}[NO_2^-]}{[O_2^-] + [O^-] + [O_3^-] + [OH^-] + [NO_2^-]} \cos\chi,\ sec^{-1}, \tag{1.4}$$

where χ, the zenith angle of the sun, has been introduced. Several negative ions: ozone O_3^-, OH^-, NO_2^-, O^-, and O_2^-, have also been included.

The detachment coefficient, D, comprises two parts, $D = D_c + D_A$ where D_c is the collisional detachment and D_A is the associative detachment. The collisional detachment, D_c, is,

$$D_c = \frac{[O_2^-]}{N_-} [O_2] P_r \, 1.3(10^{-9}) \left(\frac{E_a}{\varkappa T}\right) \exp\left(-\frac{E_a}{\varkappa T}\right) \text{sec}^{-1}. \qquad (1.5)$$

Boltzmann's constant, $\varkappa (\varkappa \sim 1.38(10^{-16})$ ergs/deg Kelvin), and the electron affinity, E_a, electron volts (1 electron volt $\sim 1.602\,(10^{-12})$ ergs), together with the probability, P_r, that detachment occurs for a particular ion, have been introduced. Here N_- is the sum of the concentrations of all negative ions. The contribution to D_c from an ion except O_2^- is negligible. Hence, O_2^- is ordinarily the only negative ion used to calculate D_c. It has also been found that O_2 is the only efficient molecule for detaching the electron from O_2^-. Pierce and Arnold [1962] pointed out the wide variation in E_a estimates in the literature which strongly influences D_c. Indeed, published values of E_a range from 0.76 to 0.15 electron volts. The value $E_a = 0.46$ electron volts was recommended by Pierce and Arnold [1962].

The associative detachment, D_A, is,

$$D_A = \frac{10^{-12}}{N_-/N_e} \left\{ \frac{[O_2^-]}{N_e}[O] + 10^{-1} \frac{[O_3]}{N_e}[O] + \frac{[O^-]}{N_e}[O] + \frac{[OH^-]}{N_e}[H] + \frac{[NO_2^-]}{N_e}[N] \right\}, \quad \text{sec}^{-1}. \qquad (1.6)$$

Atomic hydrogen concentration [H] has here been introduced. The detachment coefficient, $D \sim D_A$ has, in this paper, been increased by a factor of 50 in the daytime over the value given by Arnold and Pierce [1963, 1964]. This was found to be necessary as a consequence of a study of the Loran-C ionospheric wave propagated between Cape Fear, North Carolina, and Boulder, Colorado. Thus it was found necessary, when calculating reflection coefficients and propagated fields at LF for the Loran-C, to modify the model somewhat at this point in the procedure to obtain the correct values of attenuation, Doherty [1964].

Measurements of the ionic recombination coefficient, E, have been given by Arnold and Pierce [1963] as $\sim 2(10^{-7})$ cm^3 sec^{-1}. More recently, LeLevier [1964] has given estimates,

$$E \sim 3(10^{-7}) \text{ to } 7(10^{-7}) \text{ cm}^3 \text{ sec}^{-1}. \qquad (1.7)$$

The ionizing radiations during quiet conditions comprise cosmic Lyman α and X-ray radiation. The cosmic radiation, q_c, for

$$q_o \sim 38 \cos^{-4} \theta, \tag{1.8}$$

where q_o is the rate of ionization production in ion pairs per cm^3 per second per atmosphere pressure and θ is the geomagnetic latitude, is

$$q_c(h, \theta) \sim q_o \frac{N_h}{N_g} \sim 38 \cos^{-4} \theta \frac{N_h}{N_g} \sim 38 \cos^{-4} \theta \frac{N_h}{2.55(10^{19})}, \ cm^{-3} \ sec^{-1} \tag{1.9}$$

where q_c is the rate of ionization production due to cosmic rays at a height, h; N_h is the total number density at height, h; N_g is the number density at height, h = 0. An annual variation for cosmic radiation exists [Arnold and Pierce, 1963]:

$$q_c = 1.5(10^{-18}) N_h \cos^{-4} \theta \left[1 - \frac{3}{22}(Y - 1964)\right] \tag{1.10}$$

$$(1964 \leq Y \leq 1967)$$

$$q_c = 1.5(10^{-18}) N_h \cos^{-4} \theta \left[\frac{5}{11} + \frac{6}{77}(Y - 1968)\right] \tag{1.11}$$

$$(1968 \leq Y \leq 1976),$$

where Y denotes the Gregorian calendar year.

The Lyman α radiation, q_h^α, for

$$I_h = I_\infty^\alpha \exp\left(-\sec \chi \frac{P_h}{21.2}\right) \tag{1.12}$$

where I_∞^α is the incident flux of Lyman α equal to $3(10^{11})$ photos cm^{-2} sec^{-1} and I_h is the flux at any height, h; and P is the atmospheric pressure at a height, h, in microbars, is

$$q_h^\alpha = \sum_j \sigma_j' N_j(I_h), \tag{1.13}$$

where q_h^α is the production ionization at a height, h; σ_j' is the ionization cross section of the constituent, j; and N_j is the number density of the constituent, j. The dominant ionization from Lyman α in the ionosphere is due primarily to Nitric Oxide, NO, according to Arnold and Pierce [1963]. There is also an annual variation for Lyman α radiation given by the factors:

$$q_h = \tfrac{1}{8}\,[4 + (Y - 1964)] \quad (1964 \le Y \le 1968) \tag{1.14}$$

$$q_h = \tfrac{1}{14}\,[14 - (Y - 1968)] \quad (1968 \le Y \le 1975) \tag{1.15}$$

The ionization production due to X-rays is

$$q_h^x = 1.8\,(10^{10})\, I_\infty^x\, \mu_m\, \rho_h \exp\left(-\frac{\mu_m \sec \chi\, P_h}{960}\right), \tag{1.16}$$

where q_h^x is the rate of ion production at height, h, μ_m is the mass absorption coefficient; ρ_h is the mass density at a height, h; P_h is the atmospheric pressure at a height, h; and I_∞^x is the incident flux. For,

$$0.6\ \text{Å} < \lambda < 20\ \text{Å},\ \mu_m = (3.1)\,\lambda^{2.8}, \tag{1.17}$$

$$\lambda < 0.25\ \text{Å},\ \mu_m = (0.36)\,\lambda^{0.38}. \tag{1.18}$$

The rate of ion production represented by the incident flux is determined by a complicated calculation involving a summation over all wavelengths. However, a reasonable approximation can be made by splitting the flux into different wavelength ranges. X-ray radiation also has an annual variation given by:

$$I_\infty^x(\lambda) = \frac{I'_\infty(\lambda)}{1000}\left[1 + \frac{999}{4}\,(Y - 1964)\right] \quad (1964 \le Y \le 1968)$$

$$I_\infty^x(\lambda) = \frac{I'_\infty(\lambda)}{7000}\left[7000 - 999(Y - 1968)\right] \quad (1968 \le Y \le 1975) \qquad (\lambda < 8\text{A}), \tag{1.19}$$

$$I_\infty^x(\lambda) = \frac{I'_\infty(\lambda)}{135}\left[3 + 33\,(Y - 1964)\right] \quad (1964 \le Y \le 1968)$$

$$I_\infty^x(\lambda) = \frac{I'_\infty(\lambda)}{315}\left[315 - 4(Y - 1964)\right] \quad (1968 \le Y \le 1975), \qquad (\lambda > 8\text{A}), \tag{1.20}$$

where $I'_\infty(\lambda)$ is the intensity at solar maximum.

Additional radiations exist which affect the ionosphere at greater altitudes. Among these are meteoric ionizations, solar ultraviolet radiation ionization, soft X-ray radiation ionization, and radiation ionization resulting from chemical reactions which have been calculated by Poppoff and Whitten [1963] and Arnold and Pierce [1963].

The equilibrium conditions for the ambient ionosphere permit approximations to (1.1) using

$$\frac{dN_e}{dt} \sim \frac{dN_-}{dt} \sim \frac{dN_+}{dt} \sim 0, \text{ or,} \tag{1.21}$$

$$Q - AN_e - BN_e N_+ + (C + D) N_- \sim 0 \tag{1.22}$$

$$AN - (C + D) N_- - BN_- N_+ \sim 0 \tag{1.23}$$

$$Q - BN_e N_+ - BN_- N_+ = Q - B(N_+)^2 \sim 0. \tag{1.24}$$

Since,[2] $B \sim E \sim 2(10^{-7})$ and $N_+ = N_e + N_-$, and introducing $F = C + D$,

$$N_{q,+} = \left(\frac{Q}{B}\right)^{\frac{1}{2}}, \tag{1.25}$$

$$N_{q,-} = \left(\frac{Q}{B}\right)^{\frac{1}{2}} \left(\frac{A}{A + F + \sqrt{QB}}\right), \tag{1.26}$$

$$N_{q,e} = \left(\frac{Q}{B}\right)^{\frac{1}{2}} \left(\frac{F + \sqrt{QB}}{A + F + \sqrt{QB}}\right). \tag{1.27}$$

Figure 1 illustrates theoretical estimates of the electron density profile of the lower ionosphere during the day, J, and at night, A′, according to the Arnold and Pierce [1963] method. The collisional detachment coefficient, D_c, has however been reduced by a factor of 20 over the value used by these authors, since higher values at the lower altitudes do not give correct reflection coefficient for experimental observations to be discussed below.

[2] Crain [1964] uses $B \sim 2(10^{-7})$, $E \sim (10^{-8})$.

Figure 2 illustrates the ambient daytime noon ionosphere model. Positive ions, negative ions, and electrons are given. This profile was deduced from Loran-C measurements of Doherty [1964] between Cape Fear, North Carolina, and Boulder, Colorado. To produce the observed attenuation of the first ionospheric wave hop relative to the groundwave it was found necessary to increase D in (1.6) by a factor of approximately 200 and in addition increase the chemionization, q_{ch}, by a factor of 100 over those given by Popoff and Whitten [1963] and Arnold and Pierce [1963]. Apparently, the best estimates of chemionization production q_{ch} and the detachment coefficient do not predict the correct Loran-C pulse attenuation. It should be noted that the ionospheric wave is variable with time and geographic location. This would indicate temporal geographic variations in the profile. The effect of reflection height in the above mentioned measurement was obtained from measurements of the first ionospheric wave delay and theoretically from a study of the transmission coefficient U_m [see (3.2)] into the ionosphere. Thus, the transmission coefficient, figure 20 for example, exhibits a sharp break at approximately 23-24 km above the bottom of the ionosphere. This resolves the effective reflection height within a very few kilometers so that the remaining variable, the precise shape of the profile can be resolved at this point. Figure 3 illustrates a profile predicted by the theory at another geographic location. Figure 4 illustrates a possible nighttime profile. Figure 5 illustrates a daytime profile similar to figure 3 except the detachment coefficient has been increased by a factor of 50, and the chemionization q_{ch} is as given by Popoff and Whitten [1963] and Arnold and Pierce [1963].

1.2. Ionization Introduced by Nuclear Detonations

Abnormal ionization of the atmosphere follows nuclear detonations as a consequence of beta and gamma radiation arising from the decay of fission fragments in the atmosphere as a function of time after detonation. A model for such an abnormal ionosphere has been investigated by Crain [1964] and Crain and Booker [1963, 1964]. There are ionization peaks at 30 km as a result of gamma rays and at 65 km as a result of beta rays if the debris from the detonation is above 80-90 km. Crain [1964] estimates maximum production rates for fission debris Q_m of 10^0, 10^{-1}, 10^{-2} depending upon fission yield, time, and distance from detonation. Thus,

$$Q_m = \frac{5(10^{13})\, F_y}{R_{km}^2\, t_{sec}^{1.2}} \text{ el/cm}^3/\text{sec}, \qquad (1.28)$$

where F_y is the fission yield in megatons, R_{km} is the distance from detonation and t is the time elapsed. Production rates for the ambient ionosphere can be estimates by an approximate formula, using cosmic rays only:

$$Q = Q_0 \, f(z),$$

where f(z) is the ARDC normalized model atmospheric mass density, $\frac{\rho}{\rho_0}$ [Minzner, Champion, and Pond, 1959], and Q_0 is 50 for a typical ambient low geomagnetic latitude. In the nuclear model ionosphere, $Q_0 \sim 10^4$ to 10^8. Figures 6 and 7 illustrate models developed by Crain [1964]. Here, the conductivity parameter $\frac{N}{\nu m}$ has been introduced where ν is the collision frequency. It should be noted that the conductivity, σ, of an isotropic electron or ion plasma, using number density, N; mass, m; angular frequency, ω, can be written

$$\sigma = \frac{Ne^2}{m(\nu + i\omega)}.$$

In the lower atmosphere, $\nu \gg \omega$, at LF, or

$$\sigma \sim \frac{Ne^2}{m\nu} \propto \frac{N}{\nu m}.$$

In these models, the ions are assumed to be O_2^+. Based on these models, Crain and Booker [1964] made estimates of the effect of the ions on oblique ionospheric wave transmissions. It is of interest to note in these models, figures 6 and 7, the conductivity, σ_i for the ions can be greater than the conductivity for the electrons and in most cases of interest certainly not completely negligible. Thus, for example, at 30 km, for a production rate per atmosphere of 10^8 $\frac{\sigma_i}{e^2} \sim 2.6(10^{30})$ whereas for the electrons $\frac{\sigma_e}{e^2} \sim 10^{29}$ for the daytime model, figure 6.

An extensive computer program has been developed by McKee and Kostigen [1964] which can give electron, positive ion, and negative ion profiles, provided the time after detonation, yield of weapon, height of detonation, time of day, and distance from detonation are specified; figures 8, 9, and 10 illustrate computations performed with the aid of this computer program.

2. Propagation Effects of Heavy Ions

Ordinarily, a theory of propagation of radio waves involves electron plasmas and ion plasmas in the ionosphere in the form of profiles $N_e(h)$, $N_1(h)$, $\nu(h)$ which exist as a consequence of natural phenomena. Under natural conditions the effect of ions, $N_1(h)$ is small and indeed is usually neglected. In a previous paper [Johler, 1963] the effects of heavy ions were not included. Johler and Berry [1962] have presented an analytical procedure for taking these ions into account. Thus, the ion gyro resonance is < 50 cycles per second, except for the hydrogen nucleus which is ~ 800 cycles per second. In the case of a nuclear environment in which fission and other radioactive debris is found in large quantities in the upper atmosphere, the natural ionosphere model is no longer appropriate for propagation of ionospheric waves. The effect of heavy ions, in fact, is no longer a small effect. In fact, under certain conditions these ions can exhibit a dominant role in the propagation.

The effect of the heavy ions, i.e., the effect other than the collisions with electrons, cannot in general be neglected at extra low and ultra low radiofrequencies. The mathematical formulation of such a problem has been presented in a general manner by Ginzburg [1960], for example, but considerable elaboration as to detail is required to reduce the equations to practical computation. The mathematical technique which has been employed on the IBM 7090 computer is therefore discussed here in some detail following Johler and Berry [1962].

The number of positive ions, N_+, the number of negative ions, N_-, in addition to the number of electrons, $N = N_e$, are to be considered. The convection current components are

$$J_x = -Ne\,V_x = -e\,[N_e V_e^x - N_+ V_+^x + N_- V_-^x] = J_x^e + J_x^+ + J_x^-$$

$$J_y = -Ne\,V_y = -e\,[N_e V_e^y - N_+ V_+^y + N_- V_-^y] = J_y^e + J_y^+ + J_y^-$$

$$J_z = -NeV_z = -e\,[N_e V_e^z - N_+ V_+^z + N_- V_-^z] = J_z^e + J_z^+ + J_z^-. \qquad (2.1)$$

In the classical magneto-ionic theory collision frequency types, ν can be described in connection with certain constant, C_1, C_2, C_3, . . . , (see for example, Pfister [1955]),

$$C_1=\nu_{e,0}\frac{m_0}{m_e+m_0},\ C_4=\nu_{+,0}\frac{m_0}{m_++m_0},\ C_7=\nu_{-,0}\frac{m_0}{m_-+m_0},\ C_{10}=\nu_{0,-}\frac{m_-}{m_0+m_-},$$

$$C_2=\nu_{e,-}\frac{m_-}{m_e+m_-},\ C_5=\nu_{+,-}\frac{m_-}{m_++m_-},\ C_8=\nu_{-,+}\frac{m_+}{m_-+m_+},\ C_{11}=\nu_{0,+}\frac{m_+}{m_0+m_+},$$

$$C_3=\nu_{e,+}\frac{m_+}{m_e+m_+},\ C_6=\nu_{+,e}\frac{m_e}{m_++m_e},\ C_9=\nu_{-,e}\frac{m_e}{m_-+m_e},\ C_{12}=\nu_{0,e}\frac{m_e}{m_0+m_e}, \qquad (2.2)$$

where $\nu_{e,0}$ is the electron-neutral molecule average collision frequency $\nu_{e,-}$ is an electron-negative average collision frequency, etc., where the average differential velocity of like particles is assumed to be zero, and m_0, m_e, m_+, and m_- are the masses of the neutral molecules, electrons, positive and negative ions, respectively. The components of the Langevin equation can then be written, [Johler and Berry, 1962] for purposes of developing a practical computation form,

$$i\omega V_{e,x}+\frac{e}{m_e}E_x+\frac{\mu_0 e}{m_e}[V_{e,y}\,\mathcal{H}_z-V_{e,z}\,\mathcal{H}_y]+(C_1+C_2+C_3)V_{e,x}-C_1V_{0,x}-C_2V_{-,x}-C_3V_{+,x}=0$$

$$i\omega V_{e,y}+\frac{e}{m_e}E_y+\frac{\mu_0 e}{m_e}[V_{e,z}\,\mathcal{H}_x-V_{e,x}\,\mathcal{H}_z]+(C_1+C_2+C_3)V_{e,y}-C_1V_{0,y}-C_2V_{-,y}-C_3V_{+,y}=0$$

$$i\omega V_{e,z}+\frac{e}{m_e}E_z+\frac{\mu_0 e}{m_e}[V_{e,x}\,\mathcal{H}_y-V_{e,y}\,\mathcal{H}_x]+(C_1+C_2+C_3)V_{e,z}-C_1V_{0,z}-C_2V_{-,z}-C_3V_{+,z}=0$$

$$i\omega V_{+,x}+\frac{-e}{m_+}E_x+\frac{-\mu_0 e}{m_+}[V_{+,y}\,\mathcal{H}_z-V_{+,z}\,\mathcal{H}_y]+(C_4+C_5+C_6)V_{+,x}-C_4V_{0,x}-C_5V_{-,x}-C_6V_{e,x}=0$$

$$i\omega V_{+,y}+\frac{-e}{m_+}E_y+\frac{-\mu_0 e}{m_+}[V_{+,z}\,\mathcal{H}_y-V_{+,z}\,\mathcal{H}_z]+(C_4+C_5+C_6)V_{+,y}-C_4V_{0,y}-C_5V_{-,y}-C_6V_{e,y}=0$$

$$i\omega V_{+,z}+\frac{-e}{m_+}E_z+\frac{-\mu_0 e}{m_+}[V_{+,x}\,\mathcal{H}_y-V_{+,y}\,\mathcal{H}_x]+(C_4+C_5+C_6)V_{+,z}-C_4V_{0,z}-C_5V_{-,z}-C_6V_{e,z}=0$$

$$i\omega V_{-,x}+\frac{e}{m_-}E_x+\frac{\mu_0 e}{m_-}[V_{-,y}\,\mathcal{H}_z-V_{-,z}\,\mathcal{H}_y]+(C_7+C_8+C_9)V_{-,x}-C_7V_{0,x}-C_8V_{+,x}-C_9V_{e,x}=0$$

$$i\omega V_{-,y}+\frac{e}{m_-}E_y+\frac{\mu_0 e}{m_-}[V_{-,z}\,\mathcal{H}_x-V_{-,x}\,\mathcal{H}_z]+(C_7+C_8+C_9)V_{-,y}-C_7V_{0,y}-C_8V_{+,y}-C_9V_{e,y}=0$$

$$i\omega V_{-,z}+\frac{e}{m_-}E_z+\frac{\mu_0 e}{m_-}[V_{-,x}\,\mathcal{H}_y-V_{-,y}\,\mathcal{H}_x]+(C_7+C_8+C_9)V_{-,z}-C_7V_{0,z}-C_8V_{+,z}-C_9V_{e,z}=0$$

$$\begin{aligned}
&(C_{10}+C_{11}+C_{12})V_{0,x}-C_{10}V_{-,x}-C_{11}V_{+,x}-C_{12}V_{e,x}=0\\
&(C_{10}+C_{11}+C_{12})V_{0,y}-C_{10}V_{-,y}-C_{11}V_{+,y}-C_{12}V_{e,y}=0\\
&(C_{10}+C_{11}+C_{12})V_{0,z}-C_{10}V_{-,z}-C_{11}V_{+,z}-C_{12}V_{e,z}=0,
\end{aligned}\qquad (2.3)$$

where the components of $\bar{E}$, and the velocity components of $\bar{V}$ are designated by the subscripts x, y, and z for plane local coordinate system at the ionosphere boundary. $\mathcal{H}_x$, $\mathcal{H}_y$, and $\mathcal{H}_z$ are the components of the static magnetization.

The simultaneous solution of these (2. 3) with Maxwell's equations utilizing (2. 1) results in two coupled matrix equations:

$$\begin{bmatrix} a_{11} & a_{12} & a_{13} & a_{14} & 0 & 0 & a_{17} & 0 & 0 \\ a_{21} & a_{22} & a_{23} & 0 & a_{25} & 0 & 0 & a_{28} & 0 \\ a_{31} & a_{32} & a_{33} & 0 & 0 & a_{36} & 0 & 0 & a_{39} \\ a_{41} & 0 & 0 & a_{44} & a_{45} & a_{46} & a_{47} & 0 & 0 \\ 0 & a_{52} & 0 & a_{54} & a_{55} & a_{56} & 0 & a_{58} & 0 \\ 0 & 0 & a_{63} & a_{64} & a_{65} & a_{66} & 0 & 0 & a_{69} \\ a_{71} & 0 & 0 & a_{74} & 0 & 0 & a_{77} & a_{78} & a_{79} \\ 0 & a_{82} & 0 & 0 & a_{85} & 0 & a_{87} & a_{88} & a_{89} \\ 0 & 0 & a_{93} & 0 & 0 & a_{96} & a_{97} & a_{98} & a_{99} \end{bmatrix} \cdot \begin{bmatrix} J_x^e \\ J_y^e \\ J_z^e \\ J_x^+ \\ J_y^+ \\ J_z^+ \\ J_x^- \\ J_y^- \\ J_z^- \end{bmatrix} + \begin{bmatrix} E_x \\ E_y \\ E_z \\ E_x \\ E_y \\ E_z \\ E_x \\ E_y \\ E_z \end{bmatrix} = 0 \qquad (2.4)$$

and

$$\begin{bmatrix} b_{11} & b_{12} & b_{13} \\ b_{21} & b_{22} & b_{23} \\ b_{31} & b_{32} & b_{33} \end{bmatrix} \cdot \begin{bmatrix} E_x \\ E_y \\ E_z \end{bmatrix} + \begin{bmatrix} C(J_x^e + J_x^+ + J_x^-) \\ C(J_y^e + J_y^+ + J_y^-) \\ C(J_z^e + J_z^+ + J_z^-) \end{bmatrix} = 0, \qquad (2.5)$$

where $C = -1/i\omega\epsilon_0$, and

$$a_{11} = a_{22} = a_{33} = \frac{m_e}{e^2 N_e}\left(-i\omega - \sum\nolimits_1 + \frac{C_1 C_{12}}{\Sigma_{10}}\right)$$

$$a_{12} = -a_{21} = \frac{\mu_0 \mathcal{H}_z}{-e N_e}$$

$$a_{13} = -a_{31} = \frac{\mu_0 \mathcal{H}_y}{e N_e}$$

$$a_{23} = -a_{32} = \frac{\mu_0 \mathcal{H}_x}{-e N_e} = 0, \text{ if } \mathcal{H} \text{ is in the yz-plane}$$

$$a_{14} = a_{25} = a_{36} = \frac{-m_e}{e^2 N_+}\left(C_3 + \frac{C_1 C_{11}}{\Sigma_{10}}\right)$$

$$a_{17} = a_{28} = a_{39} = \frac{m_e}{e^2 N_-}\left(C_2 + \frac{C_1 C_{10}}{\Sigma_{10}}\right)$$

$$a_{41} = a_{52} = a_{63} = \frac{-m_+}{e^2 N_e}\left(C_6 + \frac{C_4 C_{12}}{\Sigma_{10}}\right)$$

$$a_{44} = a_{55} = a_{66} = \frac{m_+}{e^2 N_+}\left(-i\omega - \Sigma_4 + \frac{C_4 C_{11}}{\Sigma_{10}}\right)$$

$$a_{45} = -a_{54} = \frac{\mu_0 \mathcal{H}_z}{eN_+}$$

$$a_{46} = -a_{64} = \frac{\mu_0 \mathcal{H}_y}{-eN_+}$$

$$a_{56} = a_{65} = \frac{\mu_0 \mathcal{H}_x}{eN_+} = 0, \text{ if } \vec{\mathcal{H}} \text{ is in the yz-plane}$$

$$a_{47} = a_{58} = a_{59} = \frac{-m_+}{e^2 N_-}\left(C_5 + \frac{C_4 C_{10}}{\Sigma_{10}}\right)$$

$$a_{71} = a_{82} = a_{93} = \frac{m_-}{e^2 N_e}\left(C_9 + \frac{C_7 C_{12}}{\Sigma_{10}}\right)$$

$$a_{74} = a_{85} = a_{96} = \frac{-m_-}{e^2 N_+}\left(C_8 + \frac{C_7 C_{11}}{\Sigma_{10}}\right)$$

$$a_{77} = a_{88} = a_{99} = \frac{m_-}{e^2 N_-}\left(-i\omega - \Sigma_7 + \frac{C_7 C_{10}}{\Sigma_{10}}\right)$$

$$a_{78} = a_{87} = \frac{\mu_0 \mathcal{H}_z}{-eN_-}$$

$$a_{79} = -a_{97} = \frac{\mu_0 \mathcal{H}_y}{eN_-}$$

$$a_{89} = -a_{98} = \frac{\mu_0 \mathcal{H}_x}{-eN_-} = 0, \text{ if } \vec{\mathcal{H}} \text{ is in the yz plane}$$

where the C_i are defined in (2.2) and $\Sigma_i = C_i + C_{i+1} + C_{i+2}$.

$$b_{11} = a_L^2 + \zeta^2 - 1$$

$$b_{12} = -a_L a_T$$

$$b_{13} = -a_T \zeta$$

$$b_{21} = -a_T a_L$$

$$b_{22} = \zeta^2 + a_T^2 - 1$$

$$b_{23} = -a_L \zeta$$

$$b_{31}=a_L\zeta$$

$$b_{32}=a_La_T$$

$$b_{33}=a_T{}^2+a_Ta_L-1.$$

The two equations (2. 4) and (2. 5) are equivalent to the single equation,

$$\left[\begin{array}{ccccccccc:ccc}
a_{11} & a_{12} & a_{13} & a_{14} & 0 & 0 & a_{17} & 0 & 0 & 1 & 0 & 0 \\
a_{21} & a_{22} & a_{23} & 0 & a_{25} & 0 & 0 & a_{28} & 0 & 0 & 1 & 0 \\
a_{31} & a_{32} & a_{33} & 0 & 0 & a_{36} & 0 & 0 & a_{39} & 0 & 0 & 1 \\
a_{41} & 0 & 0 & a_{44} & a_{45} & a_{46} & a_{47} & 0 & 0 & 1 & 0 & 0 \\
0 & a_{52} & 0 & a_{54} & a_{55} & a_{56} & 0 & a_{58} & 0 & 0 & 1 & 0 \\
0 & 0 & a_{63} & a_{64} & a_{65} & a_{66} & 0 & 0 & a_{69} & 0 & 0 & 1 \\
a_{71} & 0 & 0 & a_{74} & 0 & 0 & a_{77} & a_{78} & a_{79} & 1 & 0 & 0 \\
0 & a_{82} & 0 & 0 & a_{85} & 0 & a_{87} & a_{88} & a_{89} & 0 & 1 & 0 \\
0 & 0 & a_{93} & 0 & 0 & a_{96} & a_{97} & a_{98} & a_{99} & 0 & 0 & 1 \\
\hdashline
C & 0 & 0 & C & 0 & 0 & C & 0 & 0 & b_{11} & b_{12} & b_{13} \\
0 & C & 0 & 0 & C & 0 & 0 & C & 0 & b_{21} & b_{22} & b_{23} \\
0 & 0 & C & 0 & 0 & C & 0 & 0 & C & b_{31} & b_{32} & b_{33}
\end{array}\right]
\cdot
\left[\begin{array}{c}
J_x^e \\ J_y^e \\ J_z^e \\ J_x^+ \\ J_y^+ \\ J_z^+ \\ J_x^- \\ J_y^- \\ J_z^- \\ \hdashline E_x \\ E_y \\ E_z
\end{array}\right]=0. \qquad (2.6)$$

The 12 × 12 matrix (2. 6), and the vector submatrices can be divided into block matrices as indicated by the dashed line:

$$\begin{bmatrix} M_{9\times9} & N_{9\times3} \\ P_{3\times9} & Q_{3\times3} \end{bmatrix} \quad \begin{bmatrix} J_{9\times1} \\ K_{3\times1} \end{bmatrix}=0. \qquad (2.7)$$

Then
$$\mathrm{M\cdot J+N\cdot K=0.} \qquad (2.8)$$

and
$$\mathrm{P\cdot J+Q\cdot K=0.} \qquad (2.9)$$

If M^{-1} exists, multiply (2. 8) by $\mathrm{P\cdot M}^{-1}$ and subtract from (2. 9). Then,

$$Q\cdot K-P\cdot M^{-1}\cdot N\cdot K=(Q-P\cdot M^{-1}\cdot N)\cdot K=0. \qquad (2.10)$$

But,

$$Q=\begin{bmatrix} b_{11} & b_{12} & b_{13} \\ b_{21} & b_{22} & b_{23} \\ b_{31} & b_{32} & b_{33} \end{bmatrix}, \text{and } K=\begin{bmatrix} E_x \\ E_y \\ E_z \end{bmatrix}$$

and $P\cdot M^{-1}\cdot N$ can be computed numerically [Johler and Harper, 1962; Johler and Walters, 1960]. Thus $(Q - P\cdot M^{-1}\cdot N)$ can be written as a matrix involving the complex number, ζ. $(Q - P\cdot M^{-1}\cdot N)\cdot K = 0$ has a nontrivial solution if, and only if, $|Q - P\cdot M^{-1}\cdot N| = 0$. This yields a polynominal in ζ which can be solved to find ζ [Johler and Walters, 1960]. These results depend on the existence of M^{-1} where M is the original 9×9 matrix, (2.4). If E exists, the nonexistence of M^{-1} would imply that (2.4) has no unique solution.

Writing,

$$\begin{vmatrix} b_{11}-\alpha_{11} & b_{12}-\alpha_{12} & b_{13}-\alpha_{13} \\ b_{21}-\alpha_{21} & b_{22}-\alpha_{22} & b_{23}-\alpha_{23} \\ b_{31}-\alpha_{31} & b_{32}-\alpha_{32} & b_{33}-\alpha_{33} \end{vmatrix} = \left| Q-P\cdot M^{-1}\cdot N \right| = 0, \tag{2.11}$$

and letting

$$\begin{array}{ll} a=a_L{}^2-1-\alpha_{11} & g=-a_L \\ b=-a_La_T-\alpha_{12} & h=-\alpha_{23} \\ c=-a_T & i=-a_T \\ d=-\alpha_{13} & j=-\alpha_{31} \\ e=-a_Ta_L-\alpha_{21} & k=a_La_T-\alpha_{32} \\ f=a_T{}^2-1-\alpha_{22} & l=a_T{}^2+a_Ta_L-1-\alpha_{33}, \end{array} \tag{2.12}$$

then (2.11) becomes

$$\begin{vmatrix} \zeta^2+a & b & c\zeta+d \\ e & \zeta^2+f & g\zeta+h \\ i\zeta+j & k & l \end{vmatrix} =$$

$$\zeta^4(l-ic)+\zeta^3(-cj-id-kg)+\zeta^2(la+lf+bgi-fic-jd-kh)+\zeta(bhi$$
$$+bjg+ekc-fcj-idf-kag)+(afl+bhj+ekd-fjd-kha-lbe),$$

or,

$$\begin{vmatrix} \zeta^2+a & b & c\zeta+d \\ e & \zeta^2+f & g\zeta+h \\ i\zeta+j & k & l \end{vmatrix} \tag{2.13}$$

$$= a_4\zeta^4+a_3\zeta^3+a_2\zeta^2+a_1\zeta+a_0 \tag{2.14}$$

where,

$$\begin{aligned} a_4&=l-a_T{}^2 \\ a_3&=a_T\alpha_{31}-a_T\alpha_{13}+ka_L \\ a_2&=la+lf+ba_La_T-a_T{}^2-\alpha_{13}\alpha_{31}+k\alpha_{23} \\ a_1&=ba_T\alpha_{23}+ba_L\alpha_{31}-eka_T-fa_T\alpha_{31}-fa_T\alpha_{13}+kaa_L \\ a_0&=afl+b\alpha_{23}\alpha_{31}-ek\alpha_{13}-f\alpha_{31}\alpha_{13}+ka\alpha_{23}-lbe. \end{aligned} \tag{2.15}$$

The solution is now in the form presented previously by Johler and Harper [1962], i.e., the reflection and transmission coefficients, T and U, at the lower ionosphere can now be calculated.

The index of refraction is found from,

$$\eta^2 = \zeta^2 + \sin^2 \varphi_1 ,$$

where φ_1 is the angle of incidence of the wave on the plasma, and

$$h = \frac{\omega_H \omega}{\omega_N^2} .$$

Also,

$h_L = - h \sin I$

$h_T = h \cos I$

$a = \sin \varphi_1$

$\omega_N^2 = N e^2 / \varepsilon_0 m$, the plasma frequency squared

$a_L = \sin \varphi_1 \cos \varphi_a$

$a_T = \sin \varphi_1 \sin \varphi_a$

$\omega_H = \mu_0 e \mathcal{H}/m$, the gyro frequency

$\varepsilon_0 = \frac{1}{c^2 \mu_0}$

and φ_a is the magnetic azimuth reckoned clockwise from magnetic north, I is the magnetic dip reckoned from the horizontal, μ_0 and ε_0 the permeability and permittivity of space, $\mu_0 = 4\pi(10^{-7})$, e is the electronic charge, and m_e, m_+, m_-, and m_0 are the electron, positive ion, negative ion, and neutral mass, respectively.

The various collision frequencies ν_{+0}, ν_{0+}, ν_{-0}, ν_{0-}, ... or in general ν_{ij} represent the average number of times an i-th type particle collides with j type particles in one second. Assuming the positive ions are NO^+ and the negative ions are O_2^- and the collision cross section for collisions between i-th and j-th type particles is $\pi\sigma_{ij}^2$ where [McKee, 1964; see also Ginzburg, 1960, p. 78 et seq.]

$$\sigma_{+0} = \sigma_{0+} = \sigma_{-0} = \sigma_{0-} = \sigma_{O_2N_2} = 3.45(10^{-8}) \text{ cm},$$

then,

$$\nu_{+o} = 3.9(10^{11})\ \rho\sqrt{T}, \tag{2.16}$$

$$\nu_{o+} = 1.9(10^{-11})\ (1+\lambda')\ N_e\sqrt{T}, \tag{2.17}$$

$$\nu_{-o} = 3.7(10^{11})\ \rho\sqrt{T}, \tag{2.18}$$

$$\nu_{o-} = 1.86(10^{-11})\ \lambda' N_e\sqrt{T} \tag{2.19}$$

$$\nu_{+-} = 2.16(10^{-2})\ \lambda' N_e\ T^{-\frac{3}{2}}\ \mathrm{Ln}\ \frac{2.4(10^3)\ T}{[(1+2\lambda')\ N_e]^{\frac{1}{3}}}\ , \tag{2.20}$$

$$\nu_{-+} = 2.16(10^{-2})\ (1+\lambda')\ N_e\ T^{-\frac{3}{2}}\ \mathrm{Ln}\ \frac{2.4(10^3)\ T}{[(1+2\lambda')\ N_e]^{\frac{1}{3}}}\ , \tag{2.21}$$

$$\nu_{e+} = 3.62\ (1+\lambda')\ N_e\ T^{-\frac{3}{2}}\ \mathrm{Ln}\ \frac{2.4\ (10^3)\ T}{[(2+\lambda')\ N_e]^{\frac{1}{3}}}\ , \tag{2.22}$$

$$\nu_{+e} = \left(\frac{N_e}{N_+}\right)\nu_{e+} = \left(\frac{1}{1+\lambda'}\right)\nu_{e+}, \tag{2.23}$$

$$\nu_{e-} = 3.62\ \lambda' N_e T^{-\frac{3}{2}}\ \mathrm{Ln}\ \frac{2.4\ (10^3)T}{[(1+\lambda')\ N_e]^{\frac{1}{3}}}\ , \tag{2.24}$$

$$\nu_{-e} = \left(\frac{N_e}{N_-}\right)\nu_{e-} = \left(\frac{1}{\lambda'}\right)\nu_{e-}, \tag{2.25}$$

$$\nu_{eo} = 1.6(10^{11})\left(\frac{P}{P_o}\right), \tag{2.26}$$

$$\nu_{oe} = 1.6(10^{11})\left(\frac{N_e}{N_o}\right)\left(\frac{P}{P_o}\right) = \left(\frac{N_e}{N_o}\right)\nu_{eo}, \tag{2.27}$$

where T is the temperature, °K, ρ is the mass density of neutral particles (grams/cm^3), $\lambda' = N_-/N_e$, $N_+ = N_e + N_- = (1+\lambda')\ N_e$ is the positive ion concentration (cm^{-3}), P is the pressure at the atmospheric height and temperature concerned, and P_o is the pressure at ground level and ambient temperature.

Equations (2.16) to (2.27) represent twelve possible collision frequencies $\nu_{i\,j}$, $i \neq j$. The following inequalities or approximations can be noted:

$$\nu_{o-} \ll \nu_{+-}$$

$$\nu_{o+} \ll \nu_{-+}$$

$$\nu_{-e} \sim \nu_{+e}$$

$$\nu_{oe} \ll \nu_{+e}$$

$$\nu_{-o} \sim \nu_{+o}$$

$$\nu_{e+} \ll \nu_{eo}$$

for the height range 40 to 100 km, and assuming ambient conditions illustrated in figures 1 and 2. Of course, these values change in the case of disturbed or nuclear ionosphere, with the number densities such that these approximations are no longer valid. In the ambient environment the neutral particle, N_0, are very much greater than any of the other constituents near the surface of the earth to considerable height (see Minzner, Champion, and Pond [1959]).

It is of interest to note that the velocities in the equations of motion (2.3) for each of the gas constituent are coupled by collisions. The ion velocities in each equation of motion are also coupled by the charge, e, to Maxwell's equations. If the collision coupling is negligible, the velocity equations of the ions are no longer coupled to the equations representing neutral particles of the gas. Then, only neutral collisions have an effect on the ion velocities. Thus, for example, only the 3×3 diagonal submatricies exist to the left and above dotted line in (2.6). This can be interpreted to mean that the velocity differentials between gas constituents are negligible. Although this results in considerable simplification of the analysis, the rigorous solution (2.6) was retained since the numerical significance for the collision coupling was indeed established for this analysis. This was accomplished by comparing numerical solutions of the reflection coefficient with and without collision coupling. Changes were noted in the first significant figure of the LF-VLF reflection coefficient as a result of this comparison.

Some simplification can also be obtained by dropping the Lorentz term $\mu_0 e (\vec{V} \times \vec{\mathcal{H}})$ in the case of the ions for $f \gg f_H$ where for the ions $f_H < 100$ c/s. To keep the analysis procedure general, however, the Lorentz terms were retained. In fact, some interesting phenomena occur as the reflection process switches between the almost isotropic ions and the anisotropic electrons during the progress of a wave in the

gas mixture (figures 42, 43, and 44). Thus, the ions reflect at LF and VLF as an isotropic plasma whereas the reflections from the electrons produce an abnormal component resulting from anisotropy. Hence, production rates, $Q_0 = 10^8$, cause reflection from ions and zero abnormal component T_{em}, T_{me}. On the other hand, reflections from models with $Q_0 = 10^6$ cause reflections from anisotropic electrons with absorption from the ions resulting from attenuation of the waves in the plasma.

3. Propagation in a Nuclear Environment

To illustrate the propagation of LF, VLF, ELF waves in a nuclear environment, reflection coefficients were computed for the mixed ion-electron ionosphere models, shown in figure 6, as a function of frequency. These reflection coefficients were then used as input to the wave hop (time mode) propagation program described in the previous paper [Berry, 1964]. As a first approximation, the bottom of the ionosphere model was chosen as the reflection height. Figures 11, 12, and 13 show the propagation characteristics of the ground wave and various hops as a function of frequency at a distance of 1609 km (1000 miles). These curves can be compared directly with those for an ambient day shown in figure 45 at 100 kc/s as a function of distance by Johler [1963]. The most significant differences are the decreased magnitude at all frequencies, and the change in crest of the curves as a function of frequency.

The models shown in figure 6 and 7 start at much lower heights than ambient day, and much of the effect mentioned above might be due to this difference. It was also conjectured that the wave might travel a considerable distance into the model, losing energy by absorption, before reflection. Such a change in reflection height would change the characteristics of propagation versus distance, and would, probably be frequency dependent. To clarify these points, propagation of waves into a stratified plasma was investigated.

The computer program used to calculate the reflection coefficient for a wave incident on a stratified, anisotropic ionosphere [Johler and Harper, 1962] can also provide information on the progress of the wave into the ionosphere, in the form of a transmission coefficient. Let φ_a be the angle between the vertical plane containing the earth's magnetic field vector and the direction of the incident ray and let φ_i be the angle of incidence on the ionosphere. Let $E_{y,i}$ be the normal component of the incident electric field in the plane of incidence ("vertical polarization") and let $E_{x,i}$ be the component perpendicular to the plane of

incidence ("horizontal polarization"). Let $E_{y,u}$ and $E_{x,u}$ be the corresponding upgoing waves inside the ionosphere and $E_{y,d}$ and $E_{x,d}$ be the downgoing waves. Then the ratios[3] $\frac{\hat{E}_{x,u}}{\hat{E}_{x,i}}$ and $\frac{\hat{E}_{y,u}}{\hat{E}_{x,i}}$ show the propagation of the waves into the ionosphere. In the Johler and Harper [1962] formulation the quantity

$$U_e \sim \frac{\hat{E}_{y,u}}{\hat{E}_{y,u}} \cos \varphi_i \cos \varphi_a \tag{3.1}$$

This is an equality for an isotropic plasma, in an anisotropic plasma there are additional small terms caused by the anisotropy. Similarly,

$$U_m \sim \frac{\hat{E}_{x,u}}{\hat{E}_{x,i}} \sin \varphi_a \tag{3.2}$$

Thus, the transmission of a vertically polarized wave into the ionosphere can be conveniently studied when $\varphi_a = 0$, while $\varphi_a = 270°$, 90° is best for the horizontally polarized wave. Figures 14 through 20 show $|U_e|$ and $|U_m|$ for both upgoing and downgoing waves as a function of distance into the ionosphere. The J profile, figure 1, is the model, $\varphi_a = 270°$ and $\varphi_i = 80°$. Figure 14 is for a frequency of 1 kc/s, and the succeeding figures for 2, 5, 10, 20, 50, and 100 kc/s. In figure 21 $|U_{m,u}| \sim 1$ just inside the ionosphere ($z \sim 0$) shows that virtually no energy has yet been reflected. The gradual decline of $|U_{m,u}|$ with height shows that the wave is being partially reflected at each boundary, so there does not seem to be a "reflection height". In the 10 kc/s case, figure 17, $|U_{m,u}| \sim 1$ for 20 km into the ionosphere, then drops sharply in the next few kilometers, defining a reasonably sharp reflection height. The drop is even more pronounced at 100 kc/s, figure 20.

The same frequencies are shown for a more grazing angle of incidence, $\varphi_i = 83°$, in figures 21 through 27. As expected, the wave does not penetrate as far into the ionosphere, and at the lower frequencies, the reflection height is not so well defined (see figures 16 and 23).

The penetration of the vertically polarized wave is illustrated in figures 28 through 34 for $\varphi_i = 80°$. In these $|U_{e,u}| \sim \cos \varphi_i$ at the bottom of the ionosphere. In figure 29, $|U_{e,u}|$ grows slightly as the wave progresses into the ionosphere due to addition of abnormal components coupled in by the magnetic field. There is a region of strong coupling near z - 23 km, where $|U_{e,u}|$ peaks, and then drops rapidly.

[3] $\hat{x}$, $\hat{y}$ ... refer to transformed coordinate systems [Johler and Harper, 1962].

The effect of the abnormal components decreases with increasing frequency, and occurs at greater heights, figure 30 through 35. No abnormal components are seen in $|U_{e,u}|$ at 100 kc/s, figure 34, probably because the wave is reflected before it reaches the region of strong coupling. In figures 35 through 41 the angle of incidence is increased to 83°.

Crain and Booker [1964] employed an approximate formula to determine the effective height of the ionosphere and the height at which the principal contributions to reflection occur. This can be written,

$$\frac{e^2}{\epsilon_0 \omega}\left[\frac{N_e(h)}{m_e \nu_e} + \frac{N_i(h)}{m_i \nu_i}\right] = 2\cos^2 \varphi_i .$$

This formula in figure 27 gives a reflection height at 64.5 km or 24.5 km within the ionosphere model (J-profile) 100 kc/s. This is just beyond the point at which the attenuation of the upgoing wave U_e increases rapidly. This subject, however, requires further study, since the selection of the principal point of reflection does affect the propagation in the guide below the ionosphere. Wait and Walters [1963] and Wait [1965] have investigated this subject and conclude that the precise principal point of reflection is not always clear. Indeed, it should be noted that in general some reflection occrus all the way up the profile until the field vanishes. Two regions of principal reflection can apparently occur as indicated in figures 42 and 43 in the case of a gas mixture. In these examples, however, the effect of one such region cominates the other.

For the J profile, then, frequencies rom 5 kc/s to 100 kc/s penetrate twenty or more kilometers into the ionosphere before being reflected. In this range, the reflection height varies only a few kilometers with frequency. For field strength calculations, a reflection height of about 65 km would be more realistic than 40 km, the height to the bottom of the ionosphere model.

The conclusion above prompted investigation of the penetration of waves into the mixed ion-electron plasmas shown in figure 6. The Loran-C frequency, 100 kc/s, and an 82° angles of incidence were used. The reflection height, h', was defined as the height at which the upgoing wave was 10 db below the incident wave. For the normalized production rate $Q_o = 10^4$ (figure 42). This occurred at $z \sim 22$ km, or a reflection height of 58 km. For $Q_o = 10^6$ (figure 43) the wave decreases gradually with height so that no "natural" reflection height is apparent, but by the definition above, $h' \sim 42$ km. For $Q_o = 10^8$, $h' \sim 24$ km (figure 44).

Using these reflection heights, the propagation of a 100 kc/s wave was computed as a function of distance. The propagation for an ambient day is shown first, in figure 45 [Berry, 1964], for comparison. The reflection coefficients were modeled for a single plasma slab which gives approximately the same attenuation at 100 kc/s as the exact solution (multiple slabs) for the J-profile given in figure 1. The amplitude of the total field, the ground wave, and the first three hops are shown. The vertical mark on each hop shows the location of its caustic, or geometric-optic cut-off point. It is apparent that each hop diffracts into its shadow zone, and remains dominant far beyond its geometric-optic cut-off point. The relative minimum in the second hop near 3200 km is caused by the pseudo-Brewster angle in the ground reflection coefficient [Berry, 1964]. This does not occur in the first hop, since it is not reflected from the ground; and the minimum is sharper in the third hop, which is reflected twice. The pseudo-Brewster angle effect is very small for propagation over sea water.

Figure 46 shows the propagation in a nuclear environment for $Q_o = 10^4$, with effective reflection height, $h' = 58$ km. Comparison with figure 11 shows the effect of the greater reflection height. Similarly, figure 47, for $Q_o = 10^6$, and figure 48, for $Q_o = 10^8$, can be compared with figures 12 and 13, respectively.

The total field, for $Q_o = 10^4$ and $Q_o = 10^6$, is 15-20 db below that calculated for ambient day (figure 45). This shows that the gas mixture of ions and electrons is absorbing energy from the wave. Since the ion conductivities are close to or greater than the electron conductivities, figures 6 and 7, and since the effect of collision coupling discussed above also has a numerical effect on the results it is clear that ions play a significant role in the propagation of LF and VLF radio waves. However, for $Q_o = 10^8$, the propagation is almost as good as on an ambient day. There are now enough ions for a fairly good reflector. In fact, at 1000 km, the ambient day first hop is smaller than the first hop for nuclear conditions. The explanation is that at this point, the angle of incidence for the nuclear case is nearly five degrees greater because of the much lower reflection height.

4. Conclusions

The ions produced by nuclear detonation debris will, in general, produce increased attenuation of LF waves. The amount of this attenuation is dependent upon the ion production rate per atmosphere, Q_o, of the debris. The detail, such as the shift in the peak of the amplitude curve as a function of frequency is critically dependent on reflection

height assumed for the model. From theoretical studies of the LF field, as a function of reflection height and available experimental data, a model can be ascertained. However, the bottom of the model and the point of almost total reflection of the wave are readily ascertained, and, hence, the amplitude of the ambient and nuclear environment LF field can be bracketed. It can be concluded that an increased attenuation of LF wave can be anticipated when such a wave is propagated through the nuclear environment. A comparison of the LF region (100 kc/s) with the VLF region (10 kc/s) indicates better propagation at LF in a nuclear environment. In fact, attenuations in excess of ground wave are possible for the total field expressed as the sum of the wave hops.

5. Acknowledgments

The authors are indebted to Duane C. Hyovalti and Mary E. Chrisman for their valuable contribution to the numerical work reported. Valuable conversations and discussions with other workers in the subject area gave the authors considerable advantage in this study. In particular, the following should be noted: E. T. Pierce, H. R. Arnold, C. M. Crain, J. R. Wait, A. G. Jean, R. H. Doherty, J. McKee, T. Kostigen, and G. R. Underhill. However, these individuals should in no way be held responsible for any shortcomings in this technical note. Also, the work performed in a companion project (NBS Project 5100441 initiated under DASA RA-2 938/04, 067 dated February 27, 1964) supported by the Defense Atomic Support Agency had a technical effect on the course of this work.

This research was supported by the Advanced Research Projects Agency, Nuclear Test Detection Office, and was monitored by Major Hillman Dickinson, Contract No. 183, Amendment No. 13, Task IV.

6. References

Archer, D. H. (1963), Reaction rate coefficients for ambient and heated air, DASA 1437 RM 63 TEMP-45 (G. E. Tempo, Santa Barbara, California).

Arnold, H. R. (1964), Comments on a paper "Collisional detachment and the formation of an ionosphere" by E. T. Pierce, Radio Sci. J. Res. NBS/USNC-URSI 68D, No. 2, 215-217.

Arnold, H. R., and E. T. Pierce (1963), The ionosphere below 100 km (D-region), A simple model, Research Memorandum 11 (Stanford Research Institute, Menlo Park, California).

Berry, L. A. (Dec. 1964), Wave hop theory of long distance propagation of low frequency radio waves, Radio Sci. J. Res. NBS/USNC-URSI 68D, No. 12.

Chapman, S. (1931), The absorbing and dissociative or ionizing effect of monochromatic radiation in an atmosphere on a rotating earth, Proc. Phys. Soc. 42, p. 26 (London).

Crain, C. M. (1961), Ionization loss rates below 90 km, J. Geophys. Res. 66, No. 4, 117-1126.

Crain, C. M. (Nov. 1964), A note on persisting radio propagation effects after high-altitude nuclear bursts, J. Geophys. Res. 66, No. 21, 4-117.

Crain, C. M., and H. G. Booker (Apr. 1963), The effect of nuclear bursts in space on the propagation of HF radio waves between separated earth terminals, J. Geophys. Res.

Crain, C. M., and H. G. Booker (Nov. 1964), The effect of ions on LF and VLF propagation in an abnormally ionized atmosphere, J. Geophys. Res. 69, No. 21, 4713-4716.

Doherty, R. H. (1964), Private communication on Loran-C measurements.

Ginzburg, V. L. (1960), Propagation of electromagnetic waves in plasmas (Gordon and Breach, Inc., New York, N. Y.).

Hirsh, M. N., P. N. Eisner, and J. A. Selvin (1964), An experimental investigation of the effects of radiation on the propagation of EM signals, Annual Technical Report R-P73-4 (The G. C. Demg Corp., New York, N. Y.).

Johler, J. R. (Sept.-Oct. 1963), Radio pulse propagation by a reflection process at the lower ionosphere, J. Res. NBS 67D, No. 5, 481-499.

Johler, J. R., and L. A. Berry (1962), Propagation of terrestrial radio wave of long wavelength--theory of zonal harmonics, J. Res. NBS 66D, No. 6, 737-773.

Johler, J. R., and J. D. Harper, Jr. (Jan.-Feb. 1962), Reflection and transmission of radio waves at a continuously stratified plasma with arbitrary magnetic induction, J. Res. NBS 66D (Radio Prop.), No. 1, 81-99.

Johler, J. R., and L. C. Walters (1960), On the theory of reflection of low- and very low-radiofrequency waves from the ionosphere, J. Res. NBS 64D (Radio Prop.), No. 3, 269-285.

LeLevier, R. E. (Feb. 1964), Determination of the D-layer dissociative recombination coefficient from a high-altitude nuclear explosion, J. Geophys. Res. 69, No. 3, 481-485.

McKee, J. (1964), (G. E. Tempo), Private communication.

McKee, J., and T. Kostigen (1964), Computer program (G. E. Tempo), Private communication.

Minzner, R. A., K. A. W. Champion, and H. L. Pond (Aug. 1959), The ARDC model atmosphere 1959, Air Force Surveys in Geophysics No. 115, ARCRC, Bedford, Massachusetts.

Minzner, R. A., and W. S. Ripley (1956), The ARDC model atmosphere 1956, ASTIA Document 110233.

Minzner, R. A., W. S. Ripley, and T. P. Condron (1958), U. S. extension to the ICAO standard atmosphere tables and data to 300 standard geopotential kilometers (Geophys. Res. Directorate and U. S. Weather Bureau, Washington, D. C.).

Moler, W. F. (1960), VLF propagation effects of a D-region layer produced by cosmic rays, J. Geophys. Res. 65, No. 4, 1459-1468.

Nicolet, M., and A. C. Aikin (May 1960), The formation of the D-region of the ionosphere, J. Geophys. Res. 65, No. 5, 1469-1483.

Pfister, W. (1955), Conf. on Physics of the Ionosphere, Cambridge, 1954 (London, Physical Society) p. 394.

Pierce, E. T. (1963), Collisional detachment and the formation of an ionospheric C-region, J. Res. NBS 67D (Radio Prop.), No. 5, 525-532.

Pierce, E. T., and H. R. Arnold (Oct. 1962), Sudden ionospheric disturbances and the propagation of VLF radio waves, SRI Report No. 3684.

Poppoff, B., and R. C. Whitten (1963), Ionization and deionization in the lower ionosphere, SRI Project 3624, Final Report.

Thrane, E. (1962), Private communication via R. H. Doherty.

Wait, J. R., and L. C. Walters (1963), Reflection of VLF radio waves from an inhomogeneous ionosphere, J. Res. NBS 67D (Radio Prop.), Pt. I, No. 3, 261-367; Pt. II, No. 5, 519-523; Pt. III, No. 6, 747-752.

Wait, J. R. (1965), Concerning the mechanism of reflection of EM waves from an inhomogeneous lossy plasma, To be published in Radio Sci. J. Res.

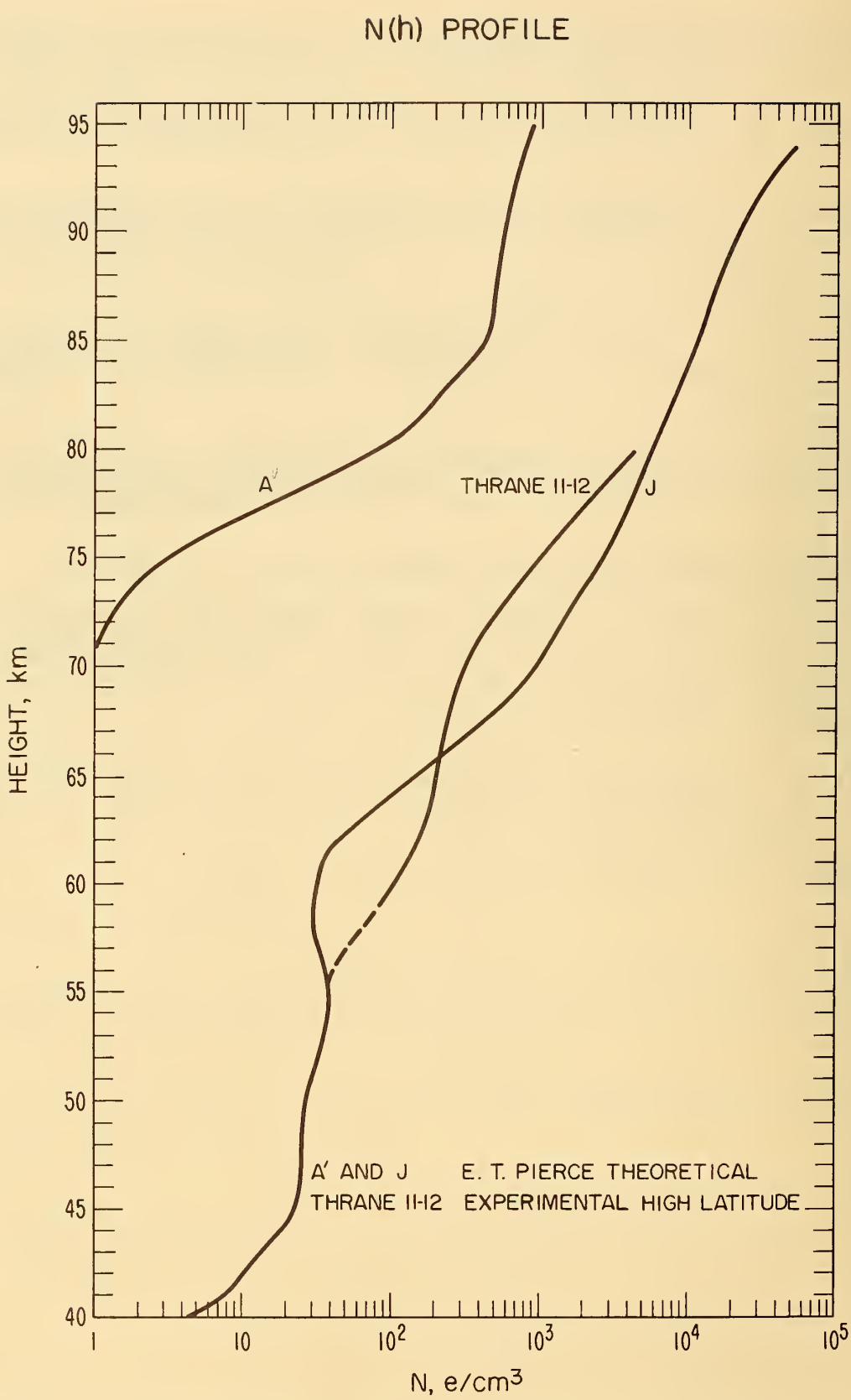

Figure 1. Typical profiles. Thrane 11-12 and J are for daytime, A′ is a night profile.

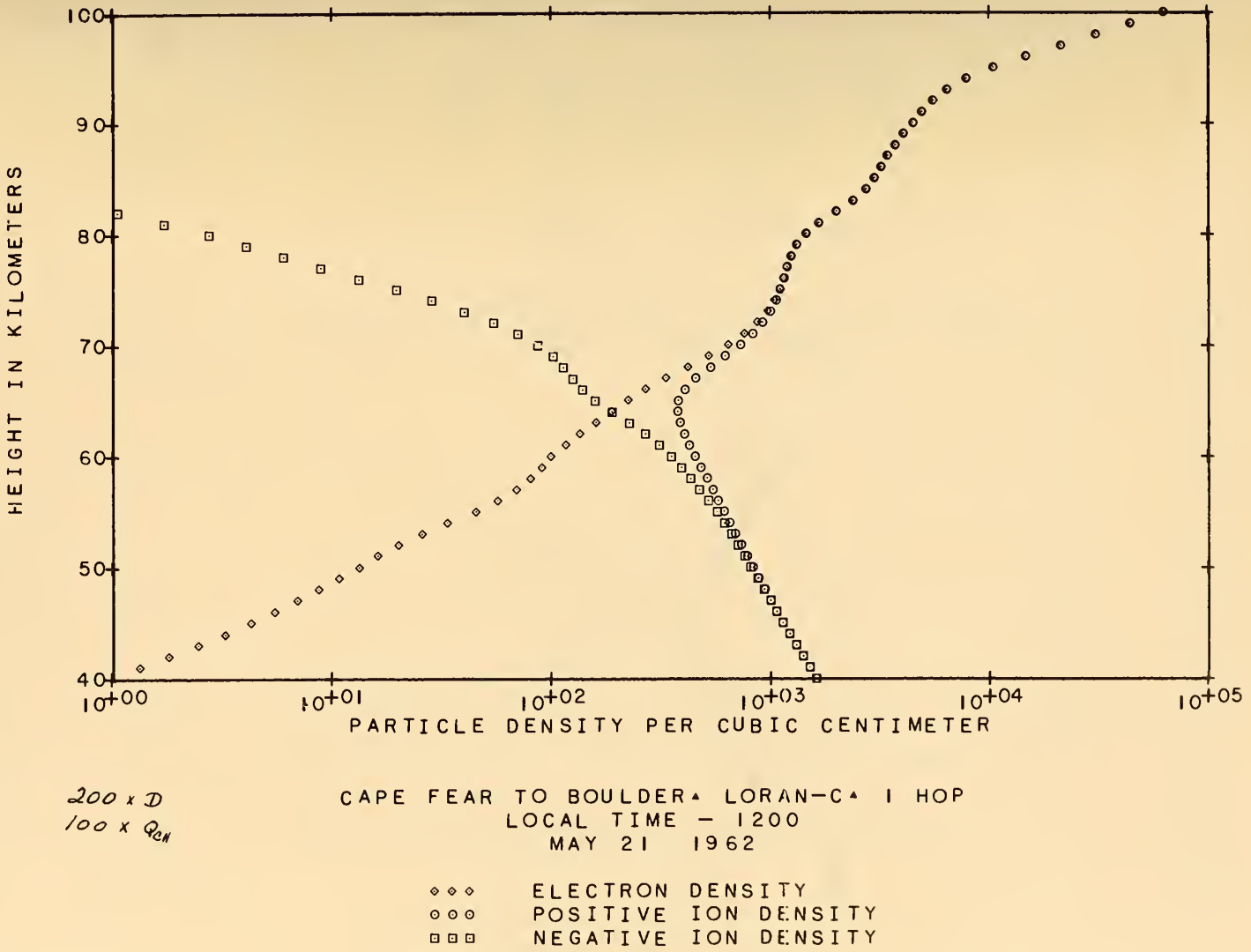

Figure 2. Model daytime ionosphere for Cape Fear to Boulder Loran-C propagation circuit. Chemionization was increased by a factor of 100 and D was increased by a factor of 200 in the balance equations to obtain observed attenuation .

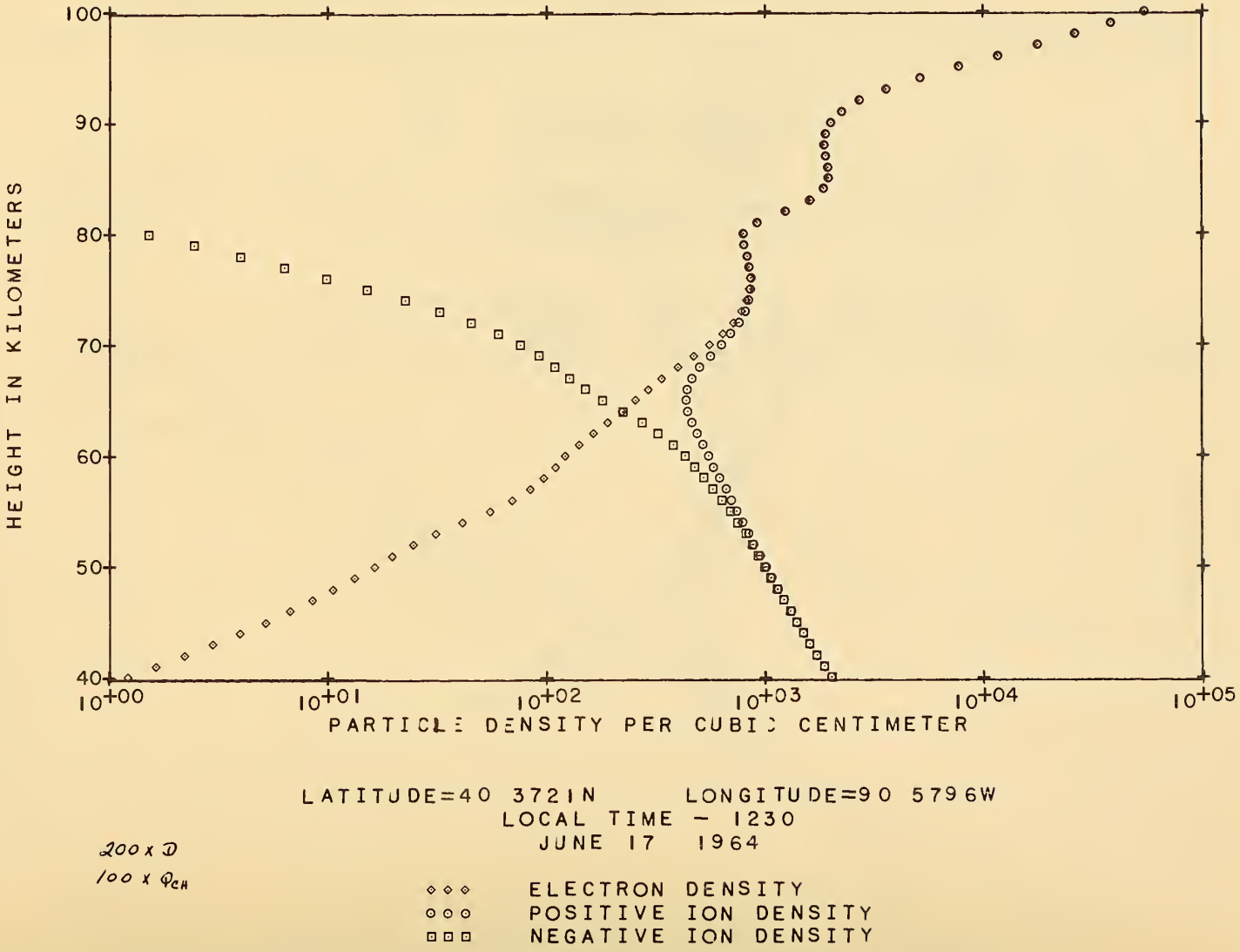

Figure 3. Model daytime ionosphere for typical propagation over northern continental United States with enhanced chemionization and D.

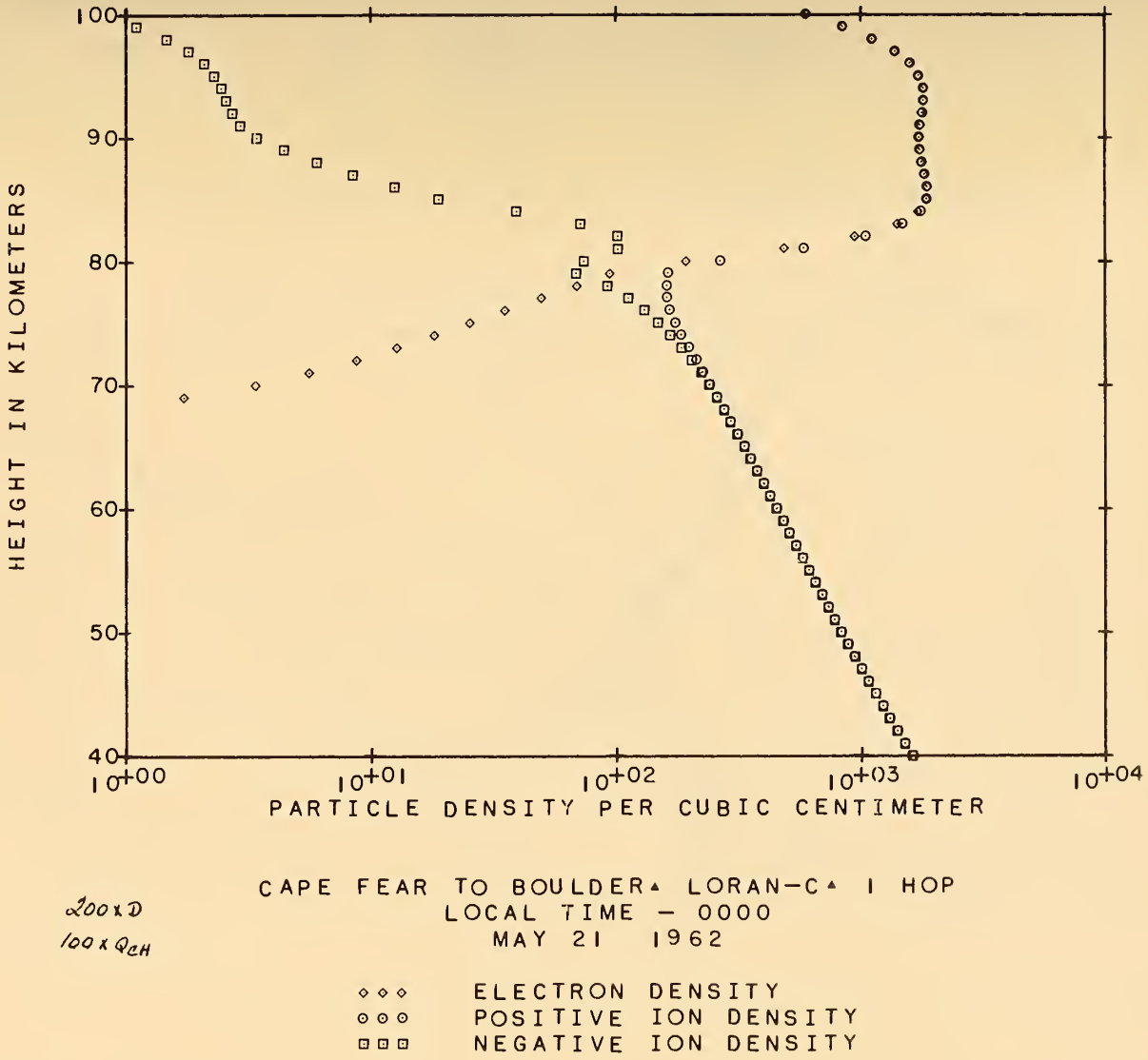

Figure 4. Nighttime model for ionosphere with enhamced chemionization and D.

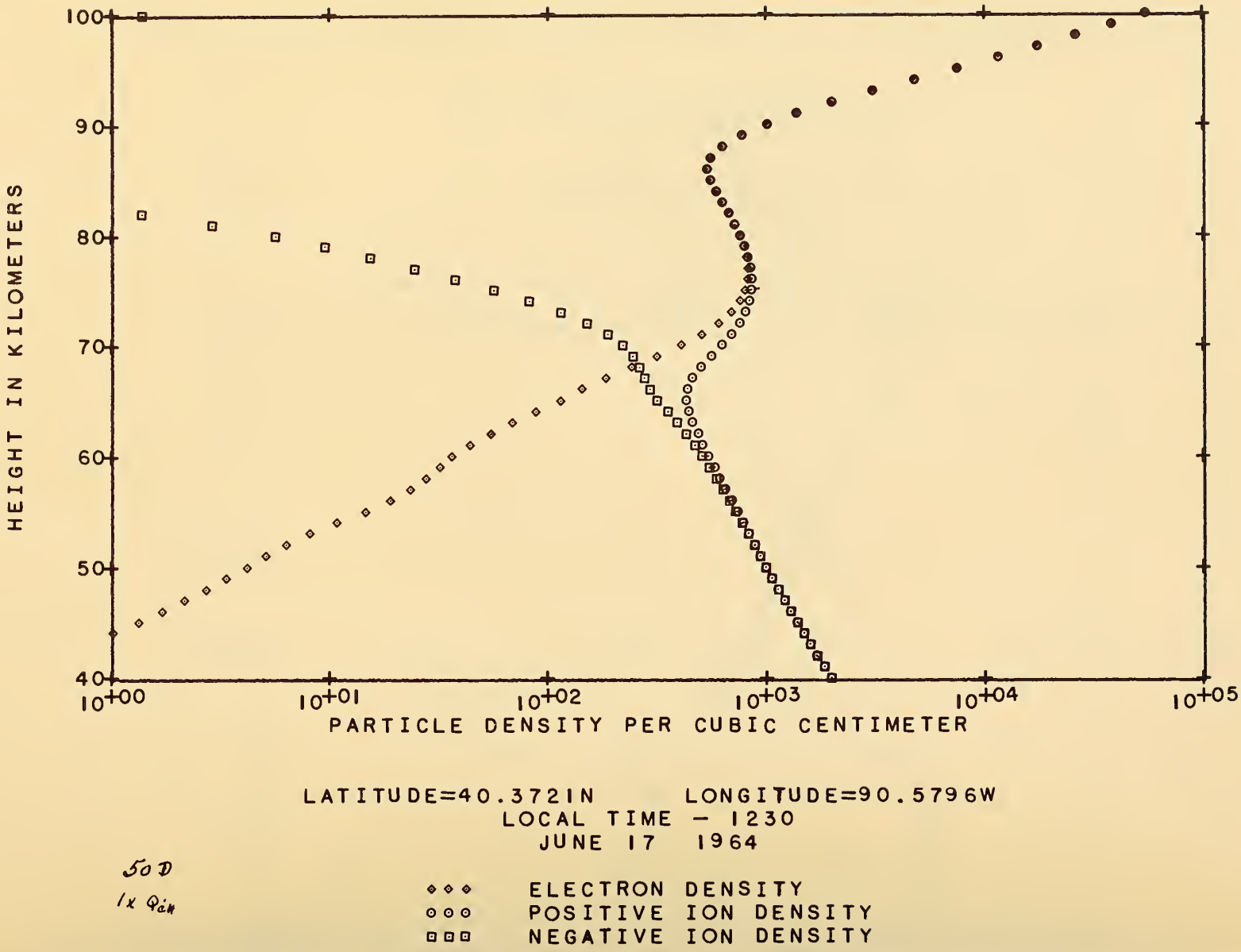

Figure 5. Model daytime ionosphere without enhanced chemionization and 50 D.

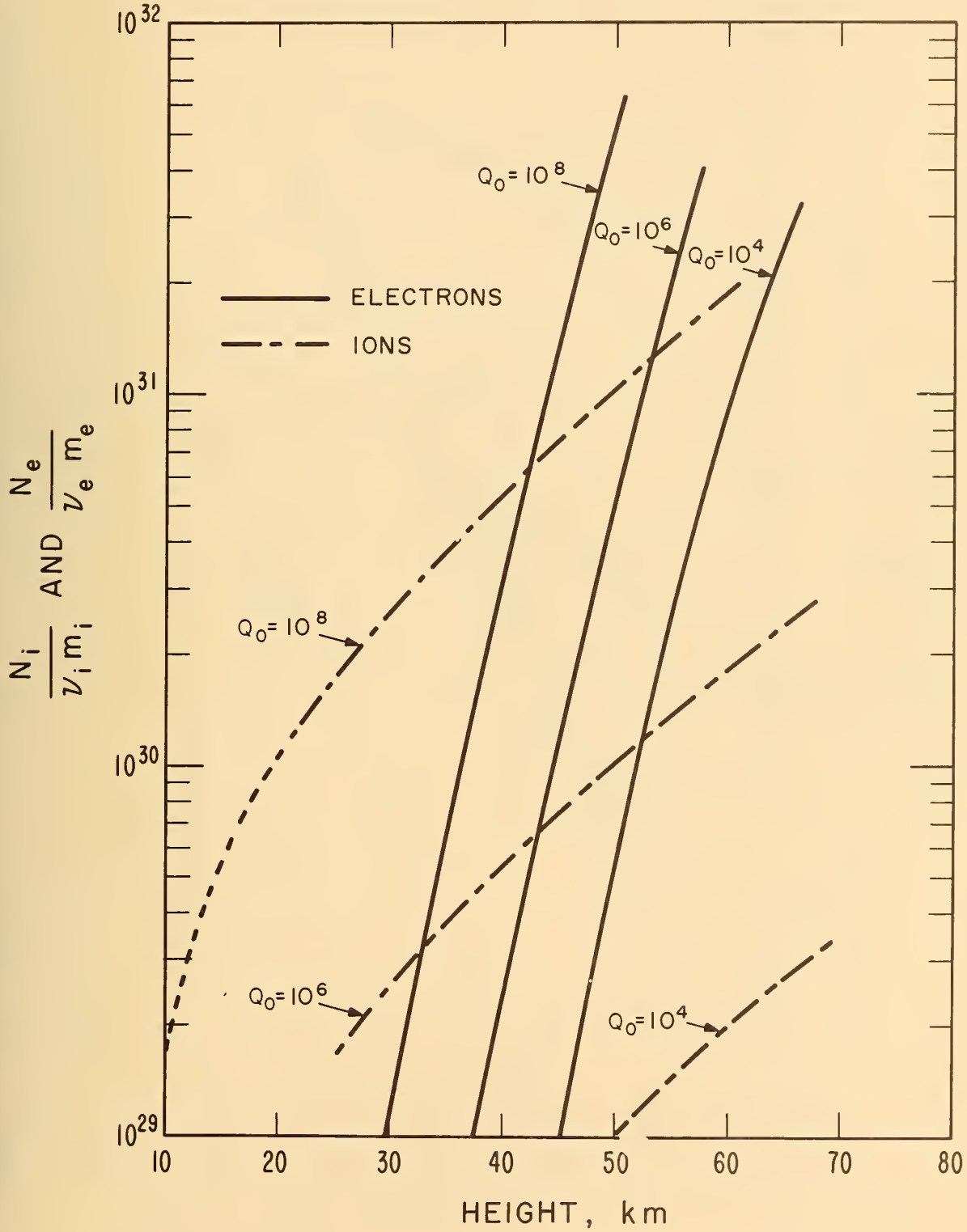

Figure 6. Daytime nuclear profiles (after Crain).

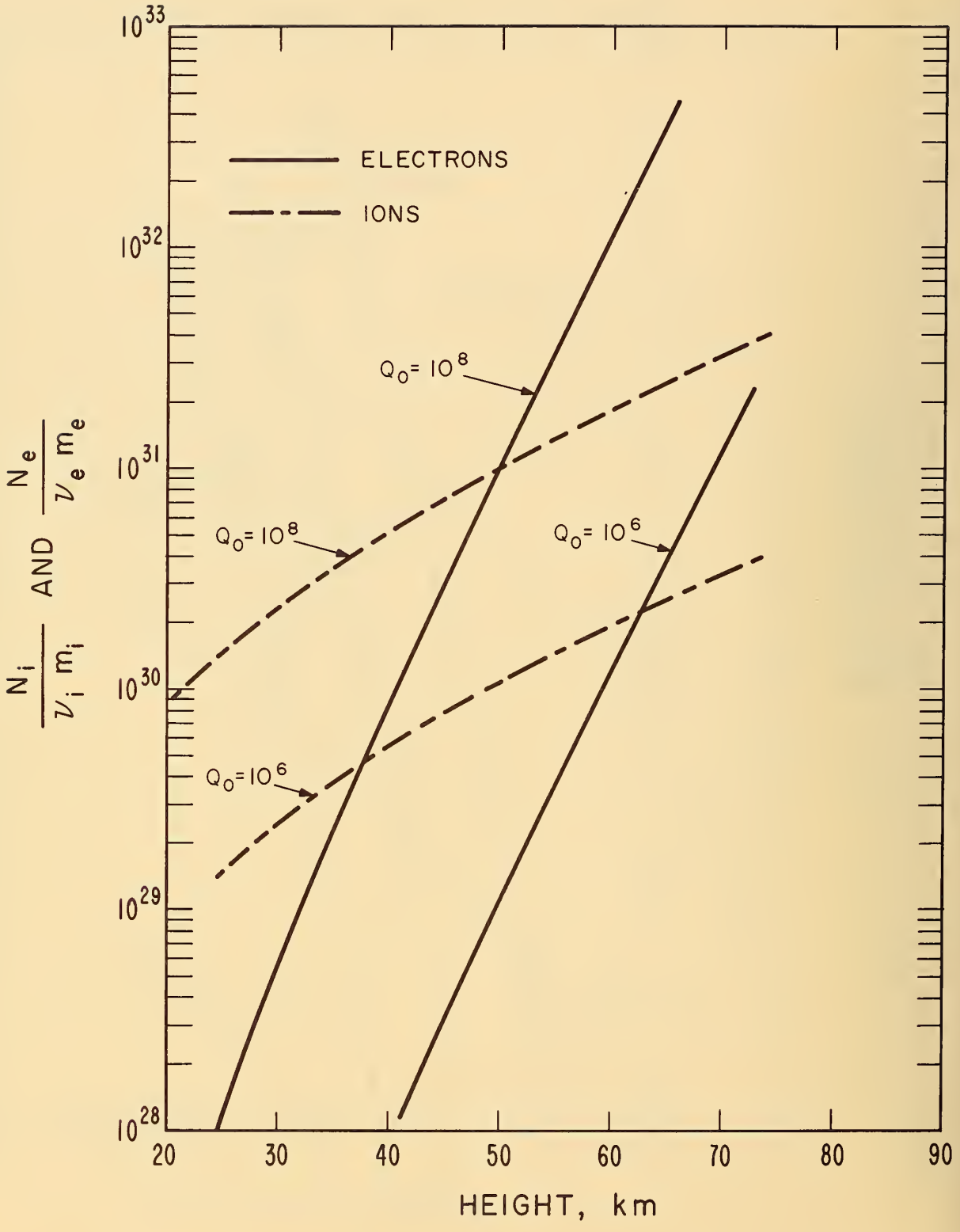

Figure 7. Nighttime nuclear profiles (after Crain).

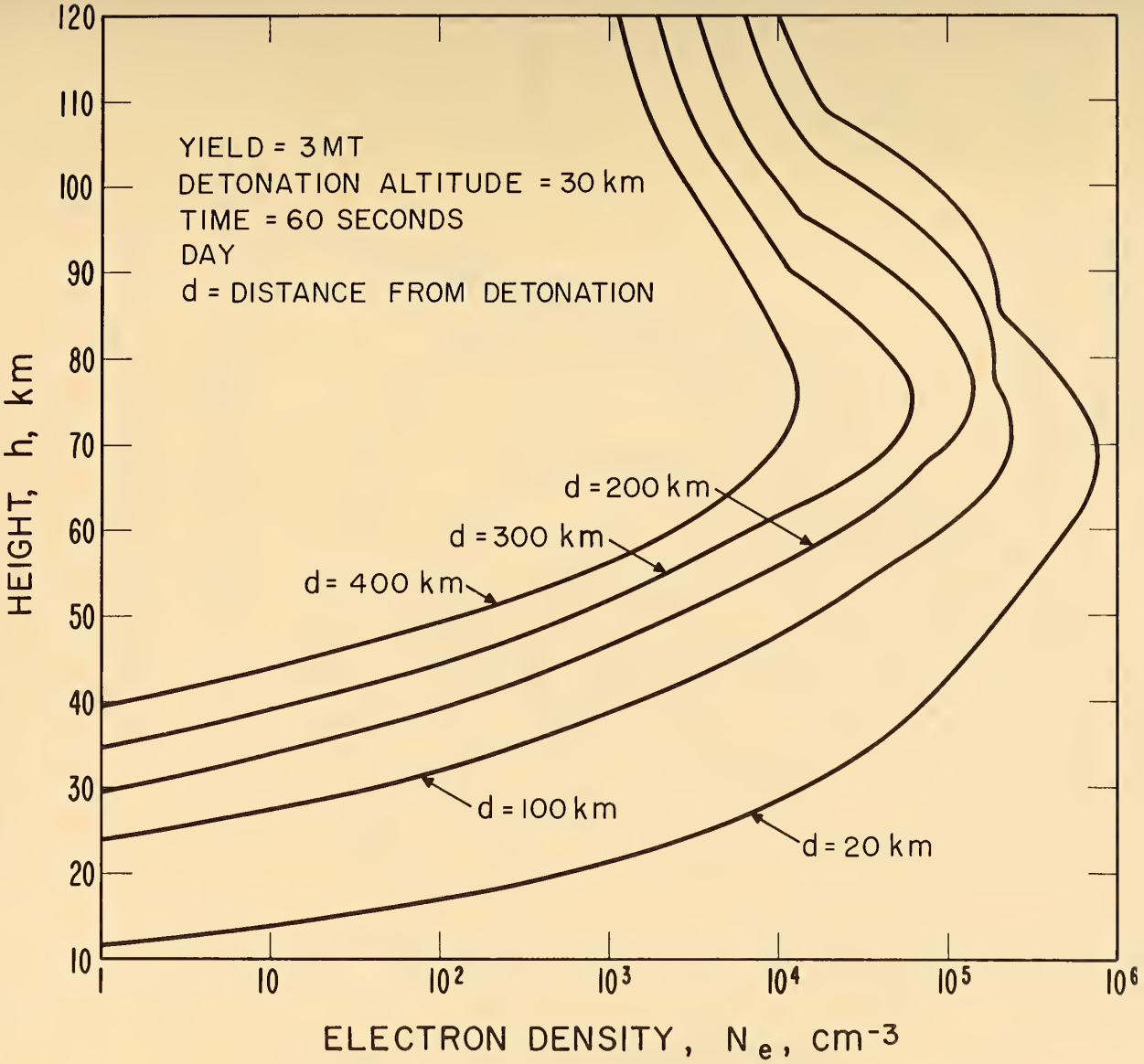

Figure 8. Daytime nuclear profiles of electron density for various distances.

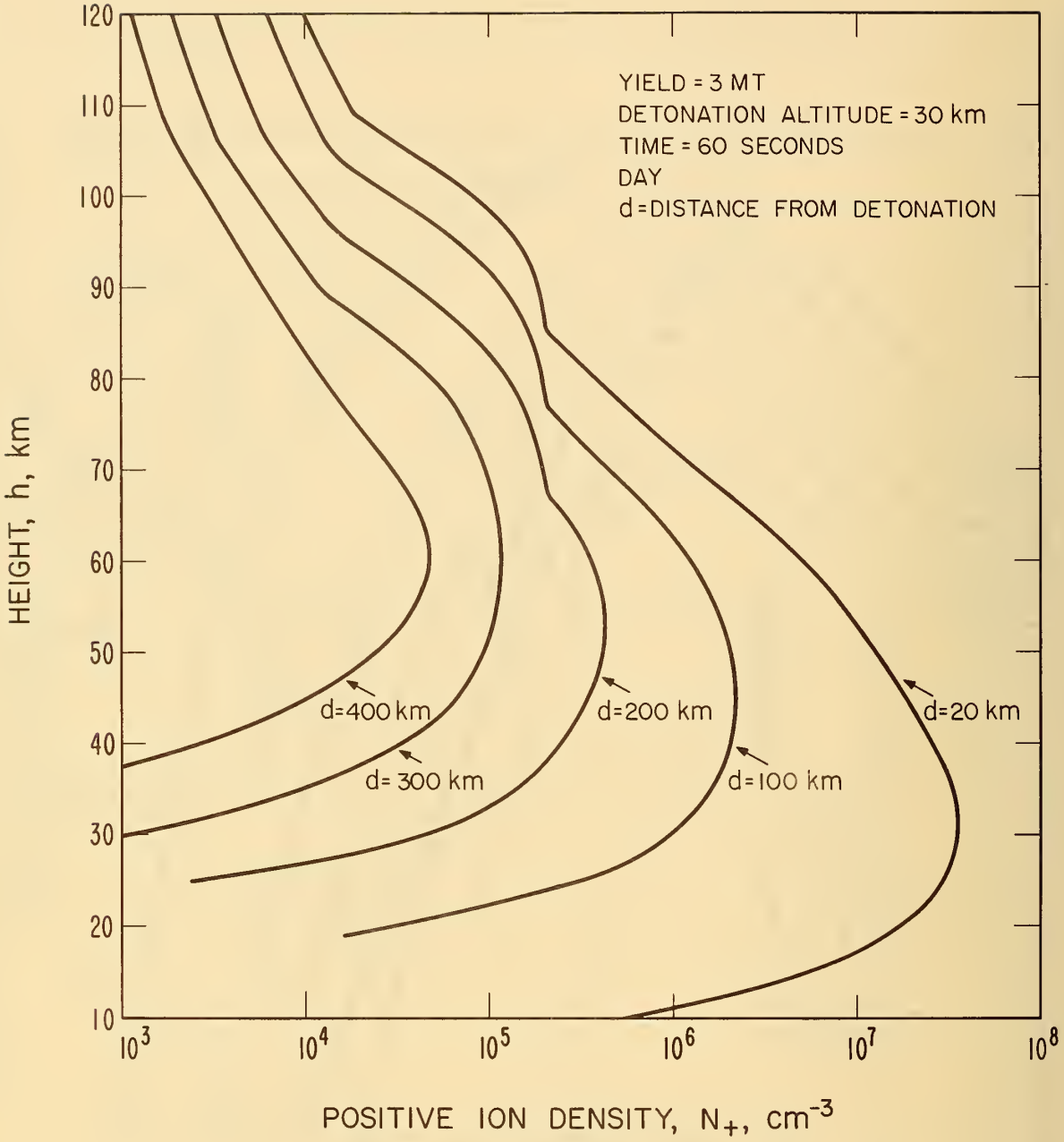

Figure 9. Daytime nuclear profiles of positive ion density for various distances.

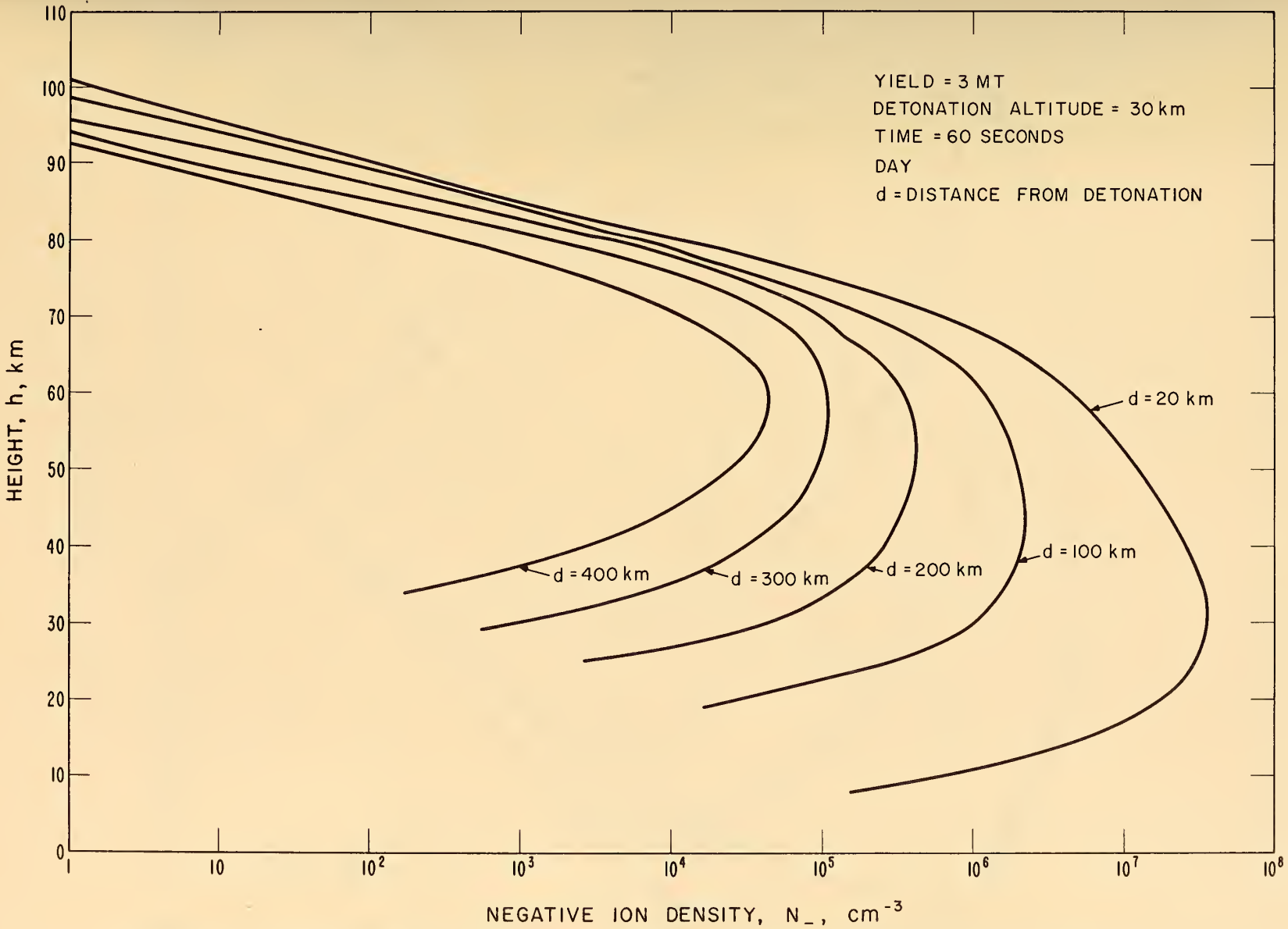

Figure 10. Daytime nuclear profiles of negative ion density for various distances.

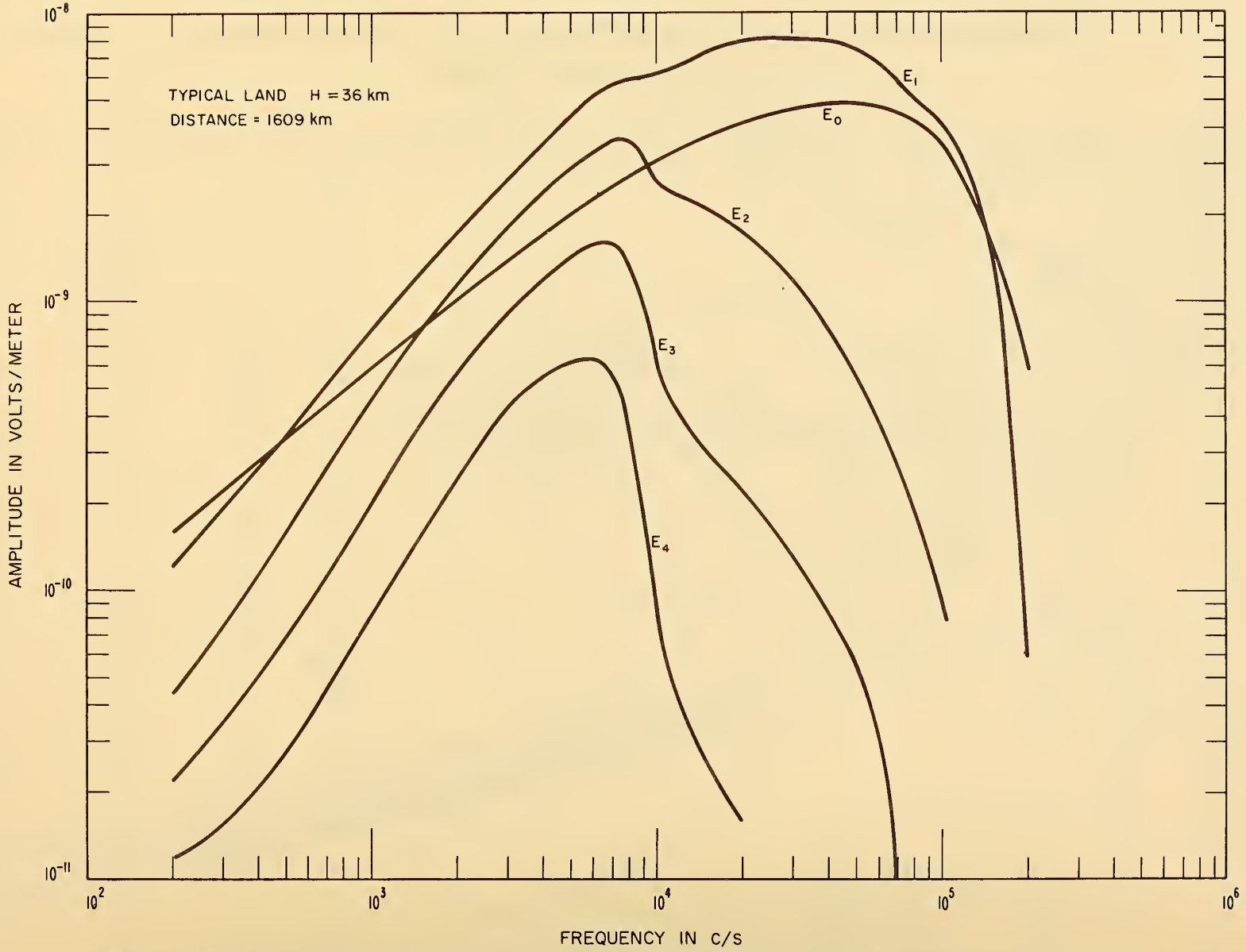

Figure 11. Magnitude of first four hops and ground wave vs. frequency, day, $Q_o = 10^4$.

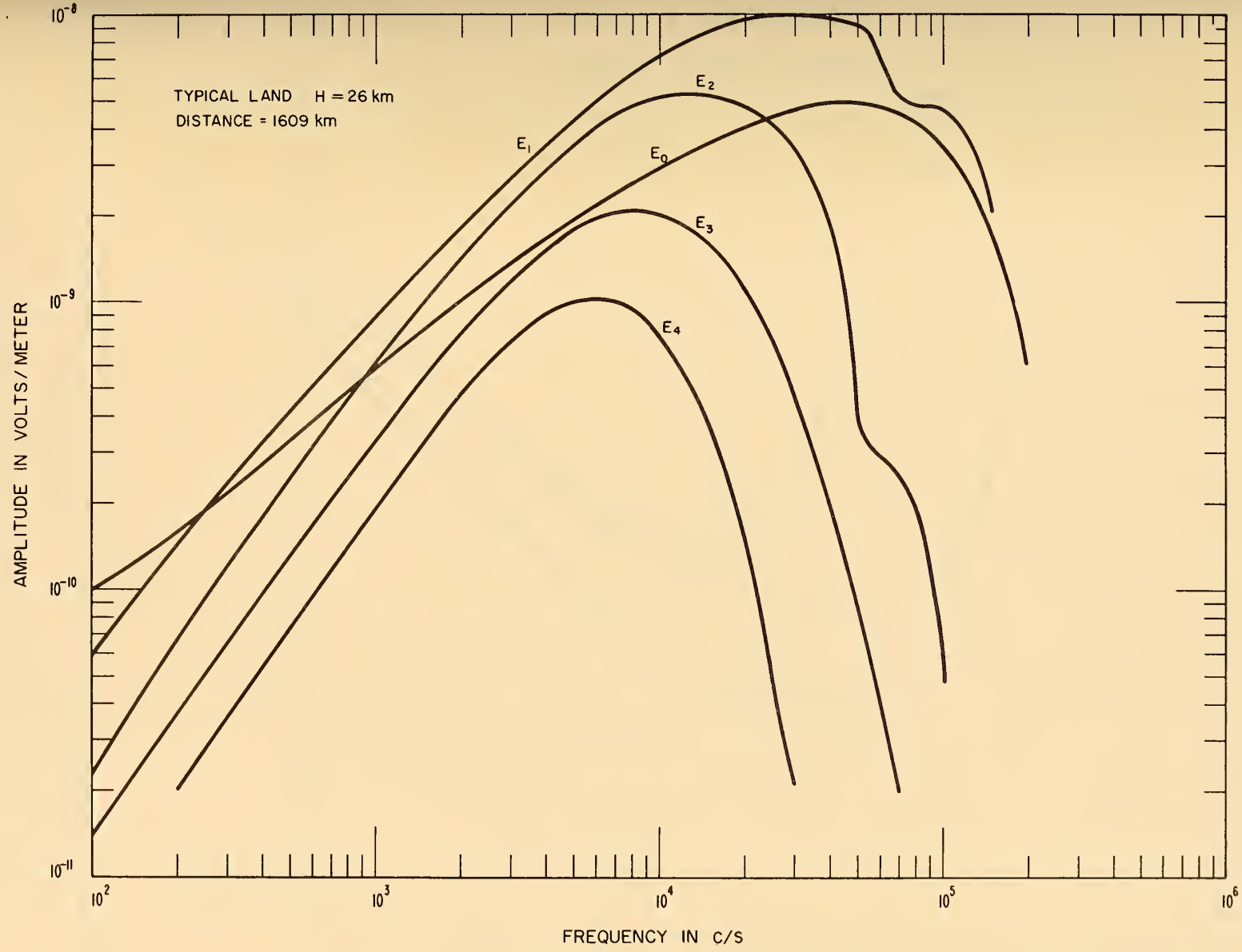

Figure 12. Magnitude of first four hops and ground wave vs. frequency, day, $Q_o = 10^6$.

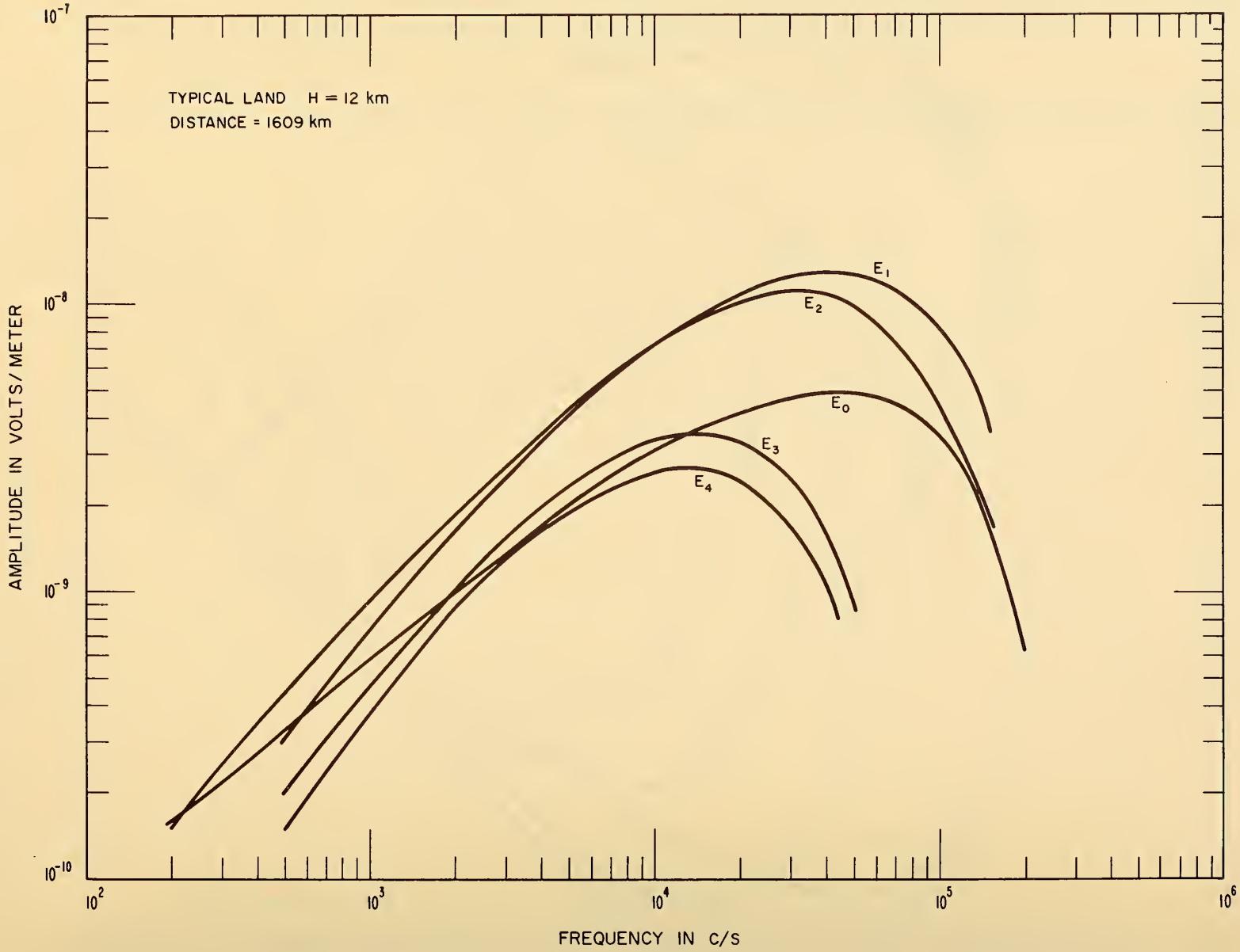

Figure 13. Magnitude of first four hops and ground wave vs. frequency, day, $Q_o = 10^8$

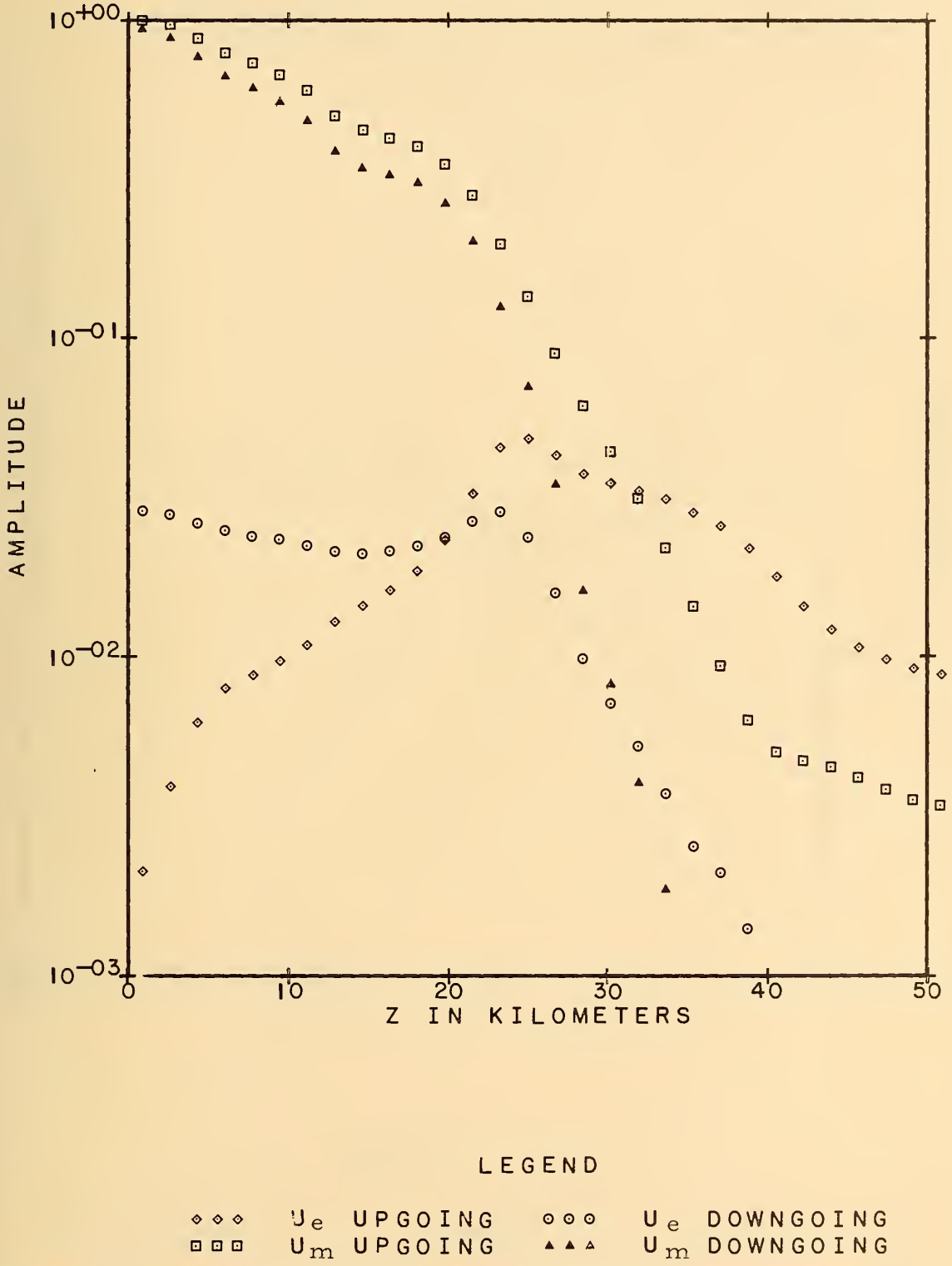

Figure 14. Penetration of horizontally polarized wave into model ionosphere, $\phi_a = 270°$, $\phi_1 = 80°$, f = 1 kc/s, h = 40 km, J profile.

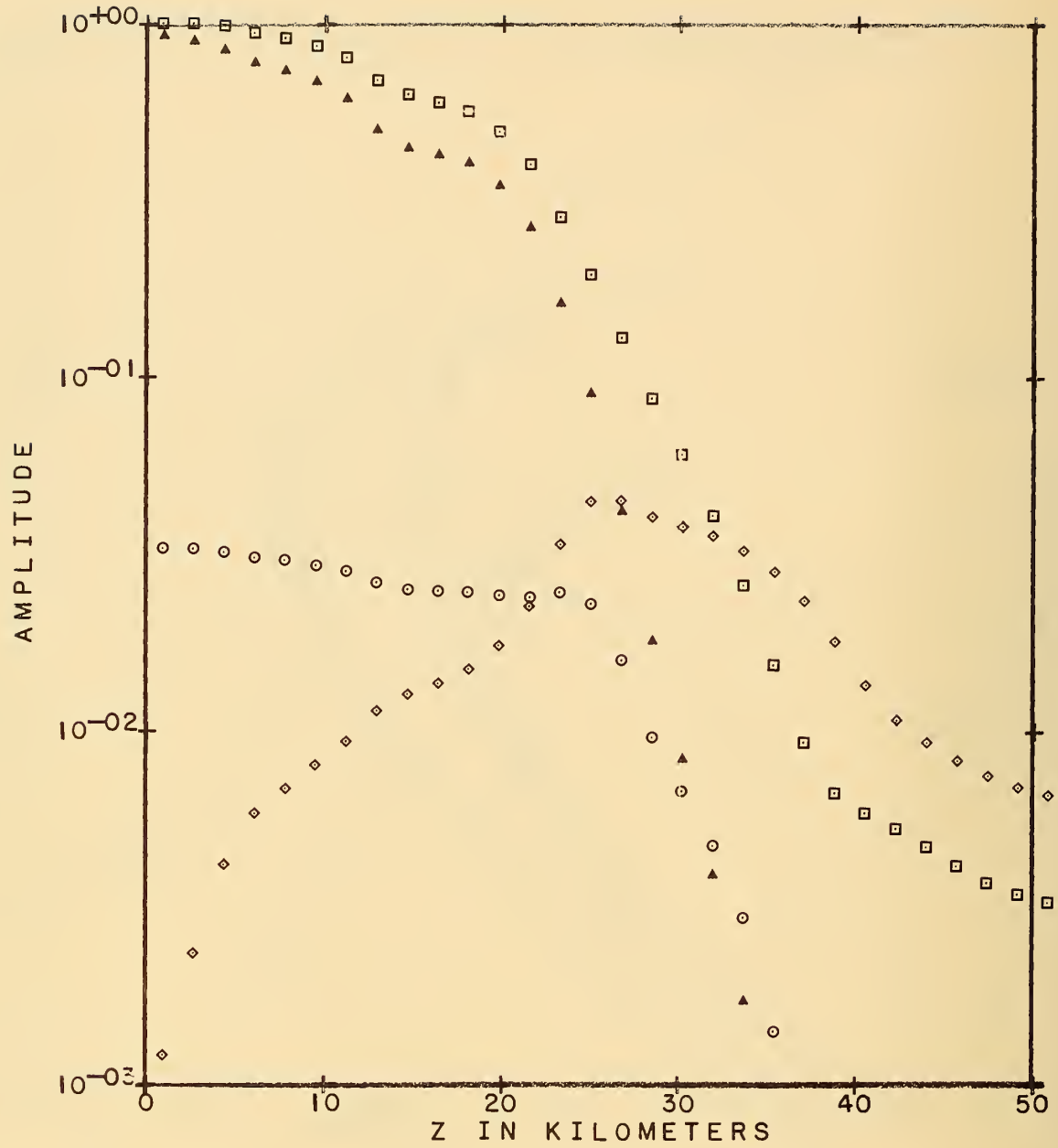

Figure 15. Penetration of horizontally polarized wave into model ionosphere, $\phi_a = 270°$, $\phi_i = 80°$, f = 2 kc/s, h = 40 km, J profile.

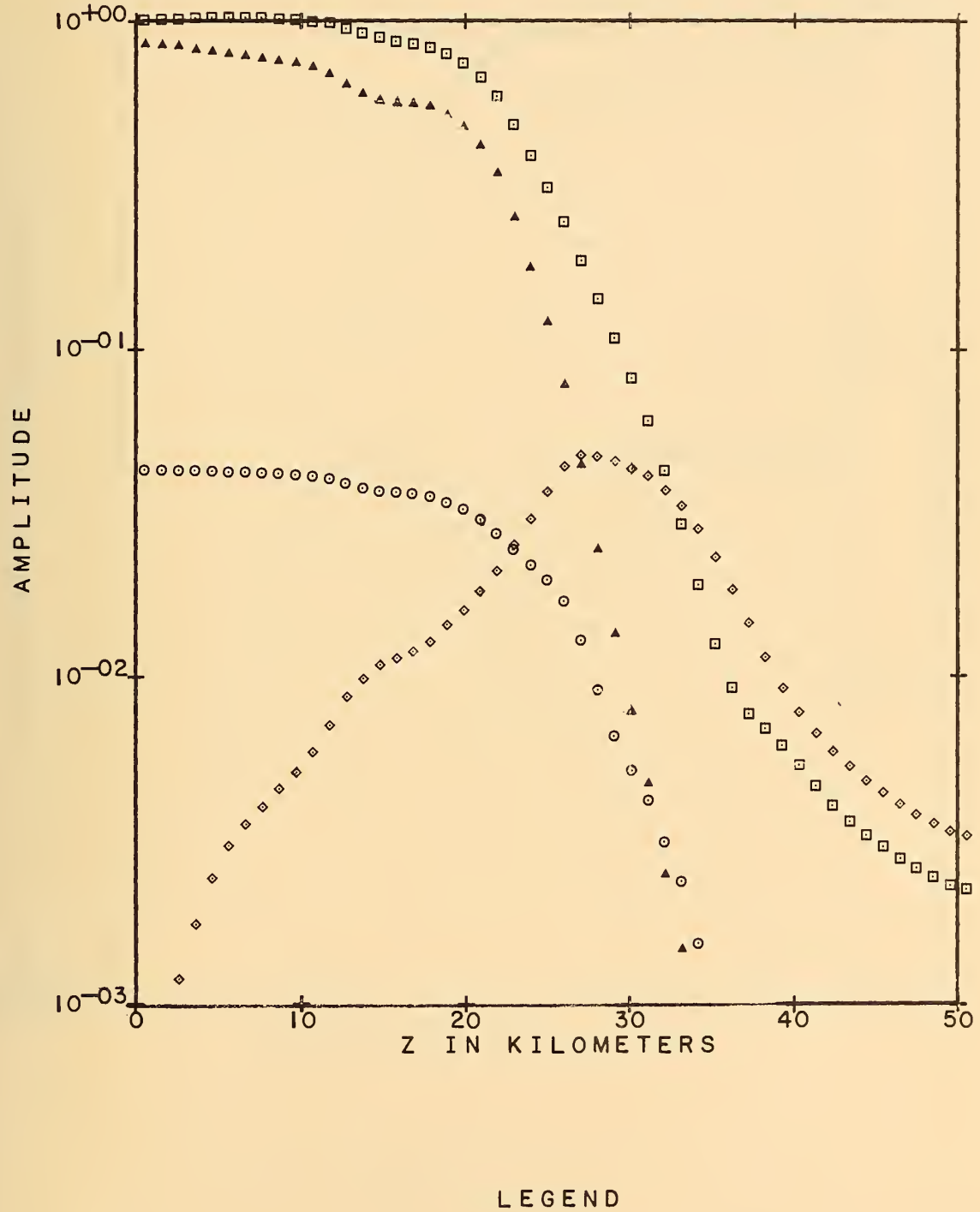

Figure 16. Penetration of horizontally polarized wave into model ionosphere, $\phi_a = 270°$, $\phi_i = 80°$, f = 5 kc/s, h = 40 km, J profile.

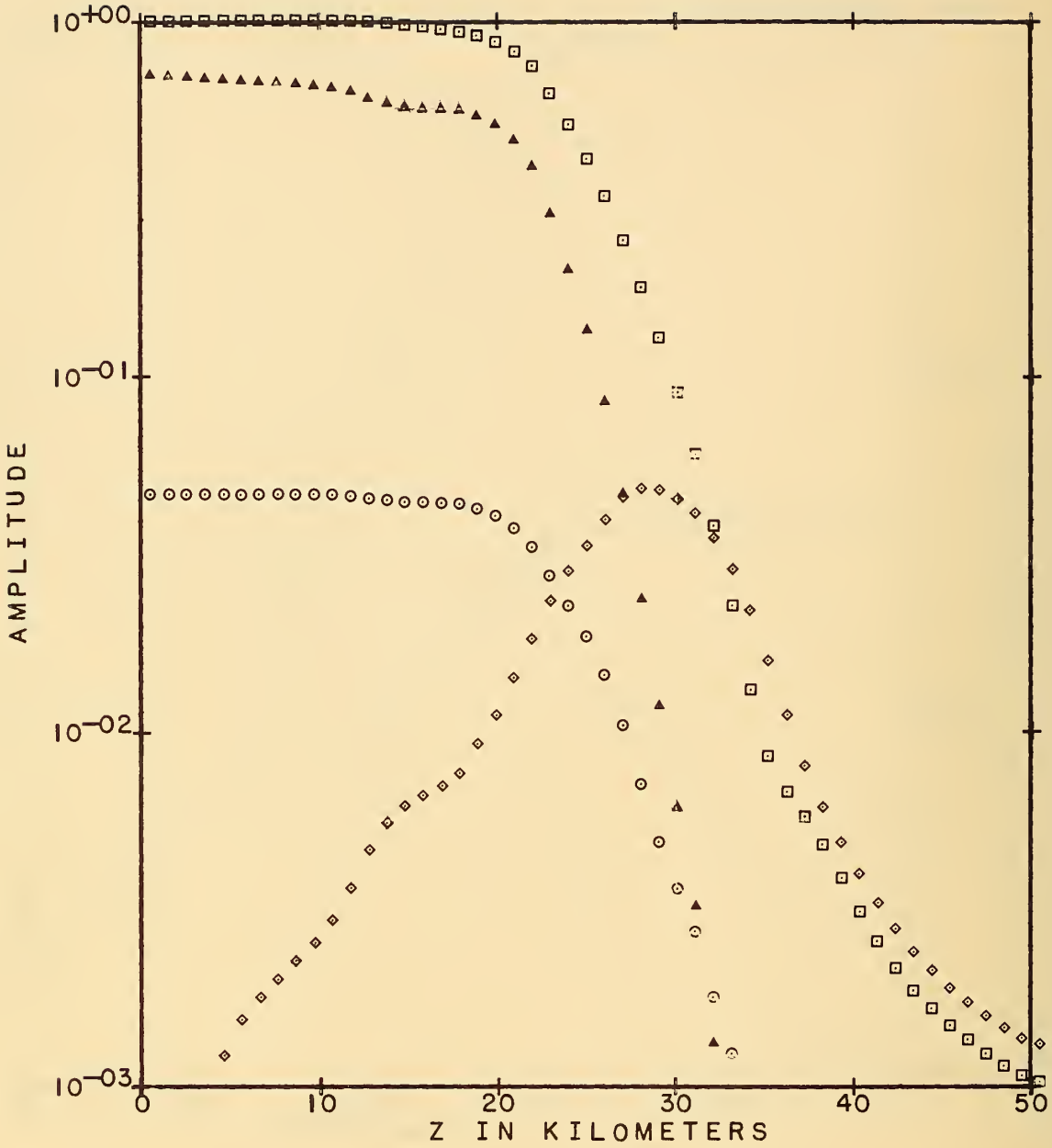

Figure 17. Penetration of horizontally polarized wave into model ionosphere, $\phi_a = 270°$, $\phi_i = 80°$, f = 10 kc/s, h = 40 km, J profile.

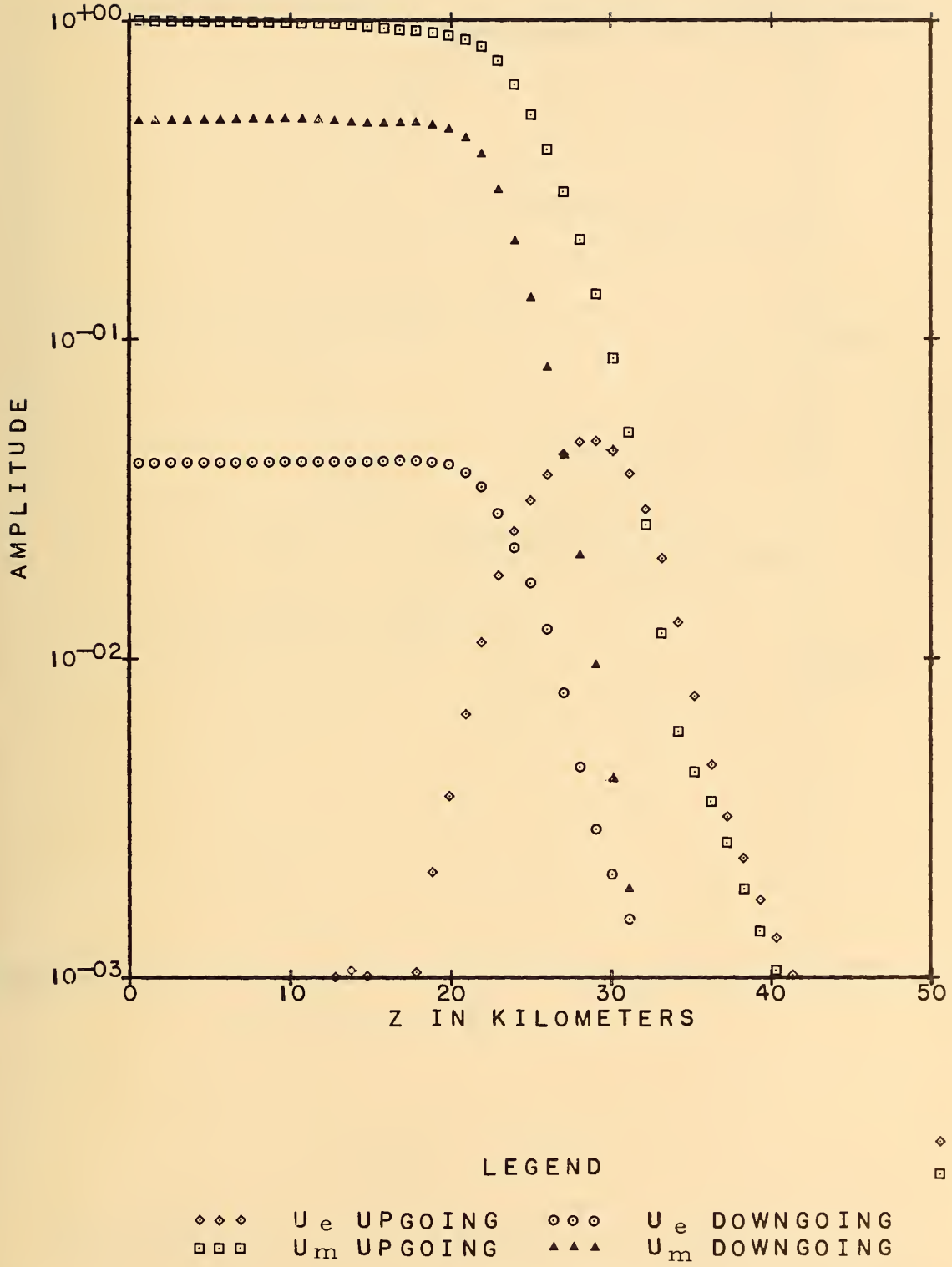

Figure 18. Penetration of horizontally polarized wave into model ionosphere, $\phi_a = 270°$, $\phi_i = 80°$, f = 20 kc/s, h = 40 km, J profile.

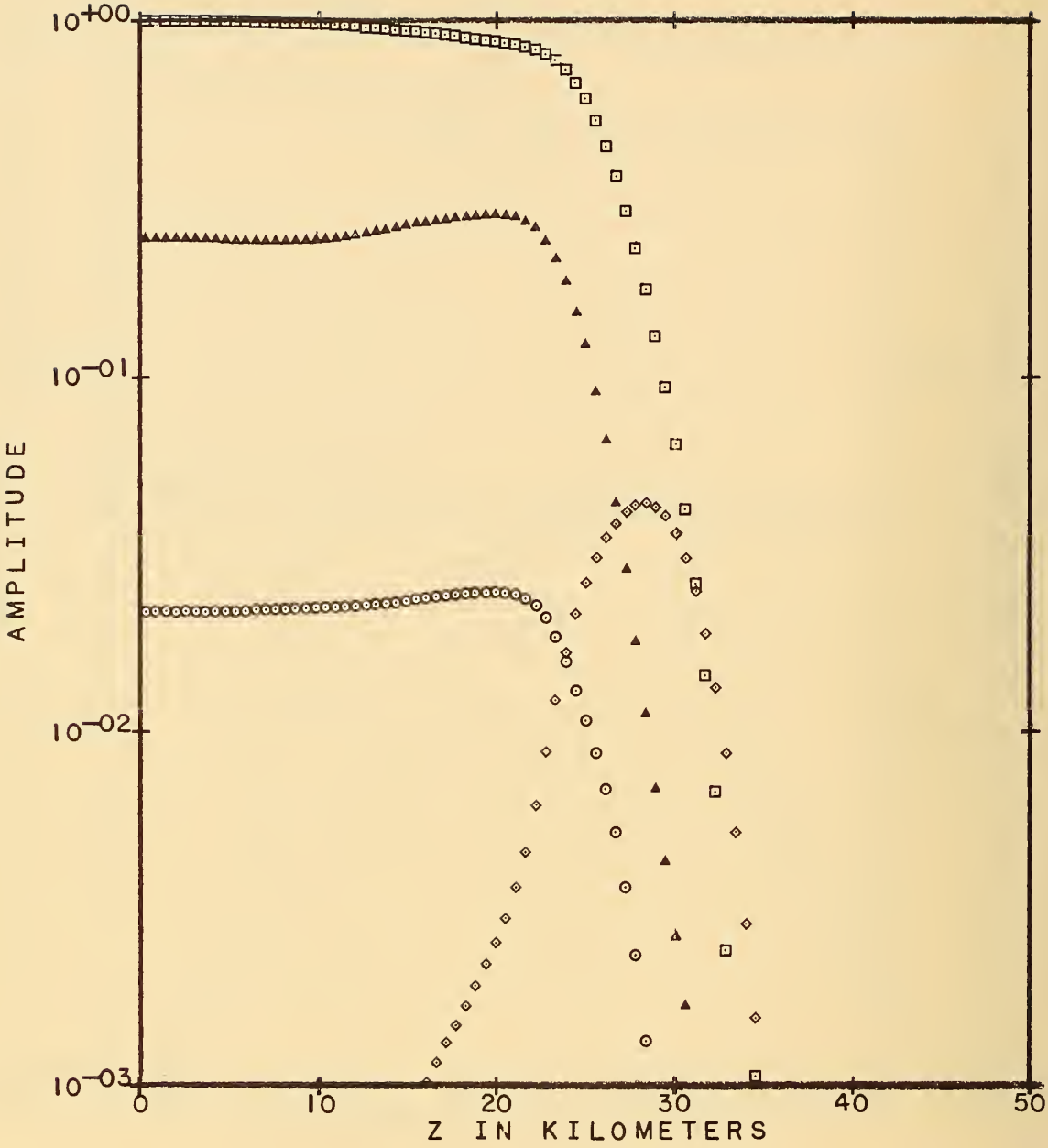

Figure 19. Penetration of horizontally polarized wave into model ionosphere, $\phi_a = 270°$, $\phi_1 = 80°$, f = 50 kc/s, h = 40 km, J profile.

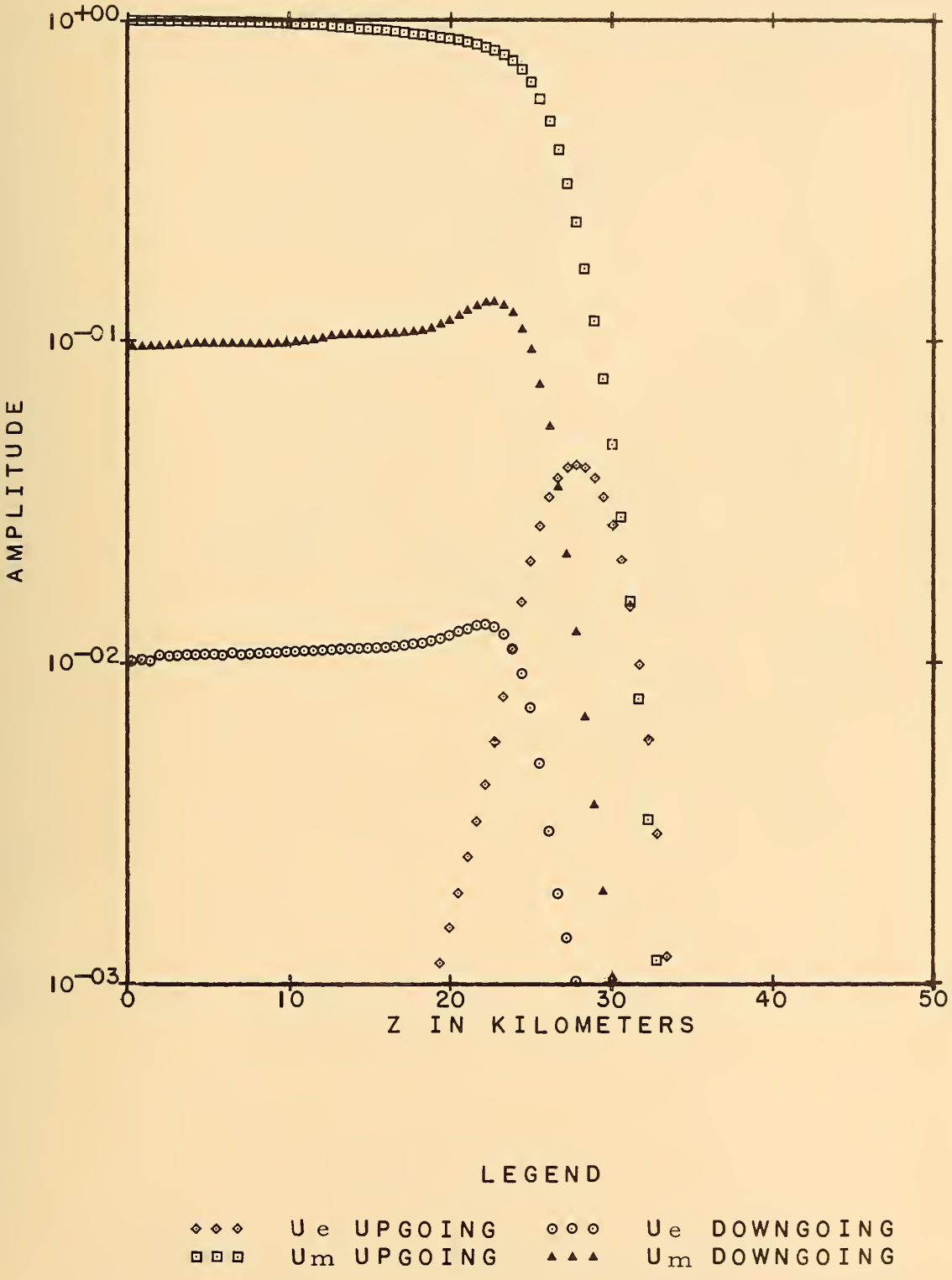

Figure 20. Penetration of horizontally polarized wave into model ionosphere, $\phi_a = 270°$, $\phi_i = 80°$, f = 100 kc/s, h = 40 km, J profile.

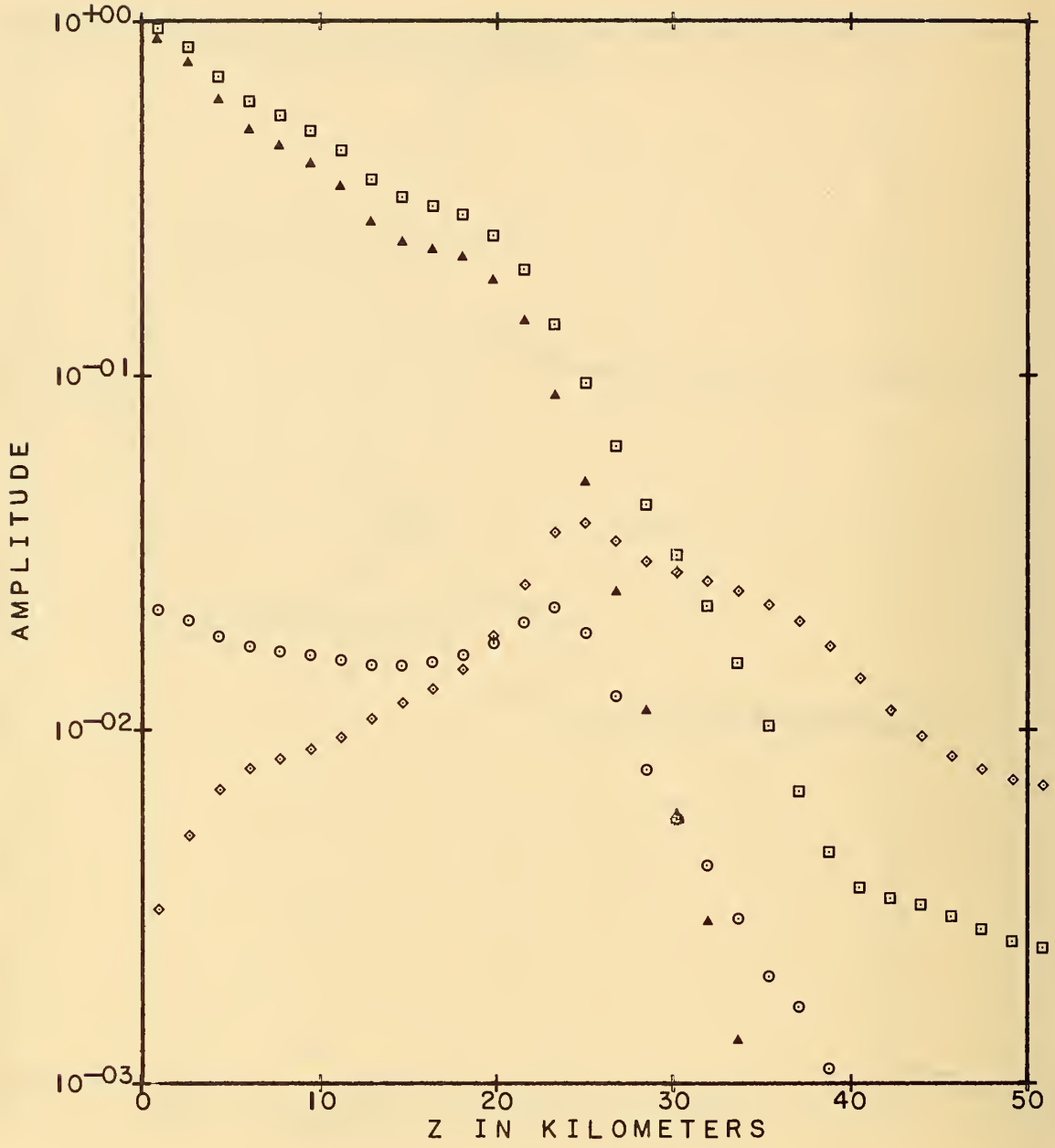

Figure 21. Penetration of horizontally polarized wave into model ionosphere, $\phi_a = 270°$, $\phi_i = 83°$, f = 1 kc/s, h = 40 km, J profile.

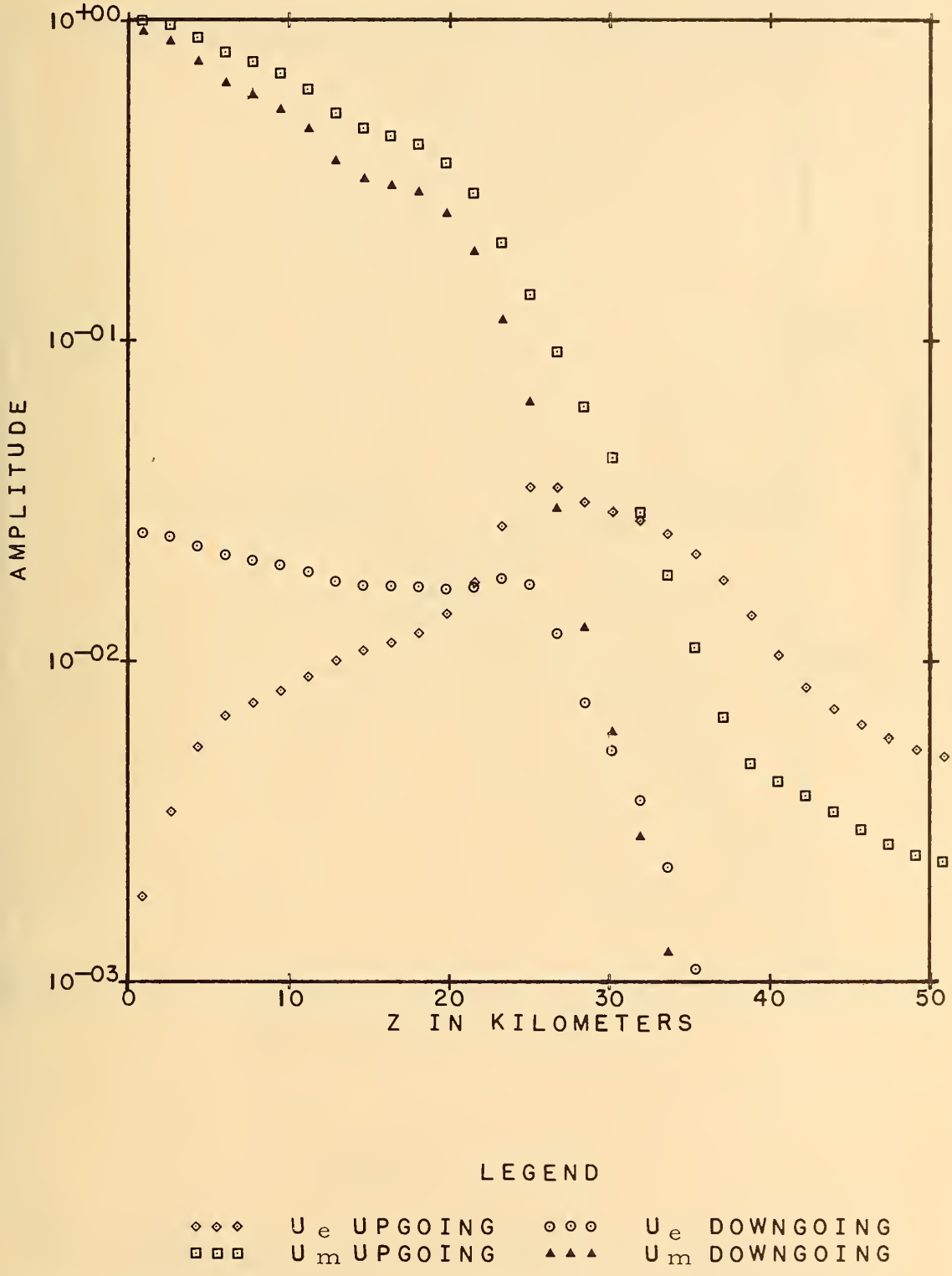

Figure 22. Penetration of horizontally polarized wave into model ionosphere, $\phi_a = 270°$, $\phi_i = 83°$, f = 2 kc/s, h = 40, J profile.

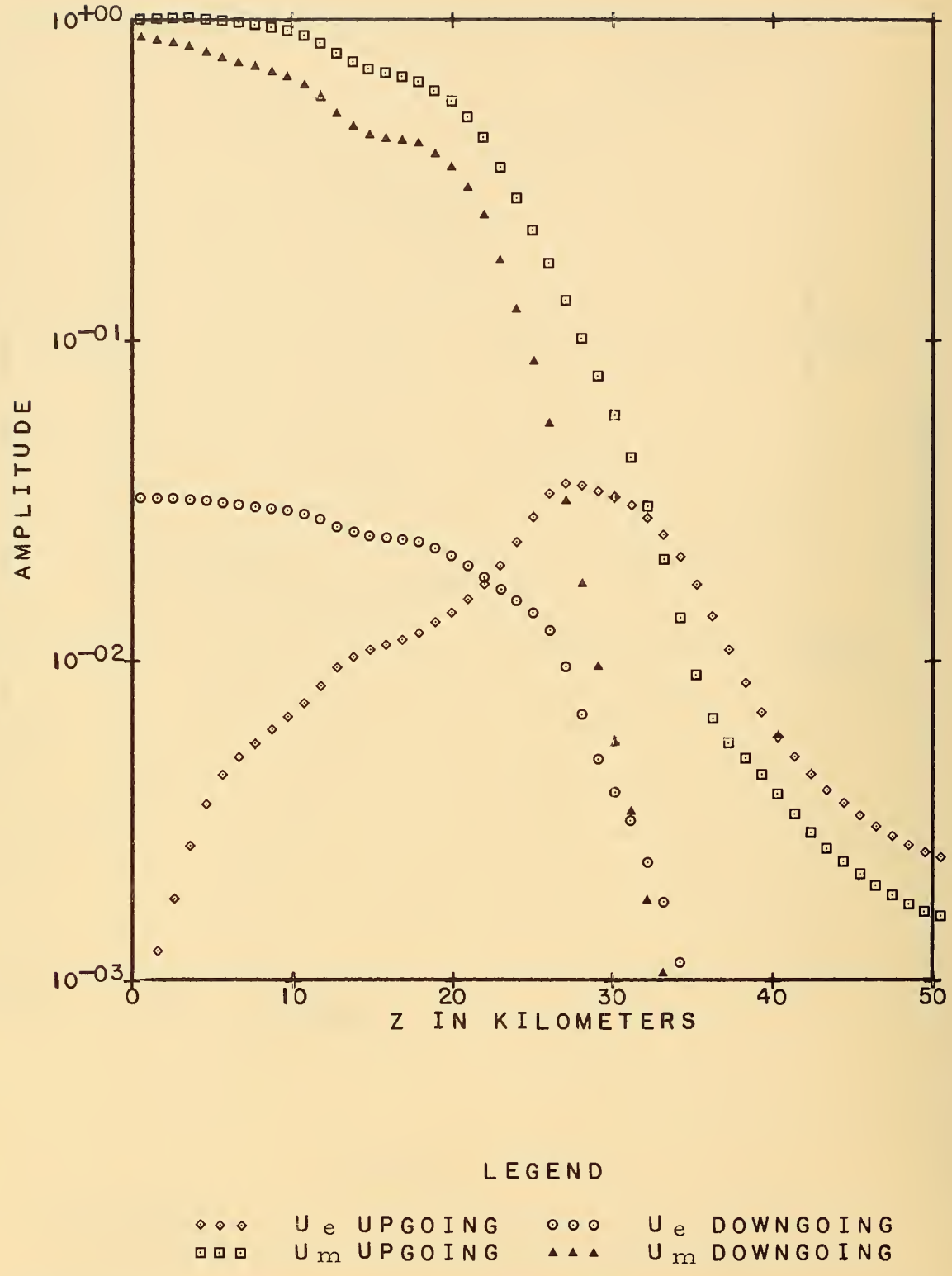

Figure 23. Penetration of horizontally polarized wave into model ionosphere, ϕ_a = 270°, ϕ_i = 83°, f = 5 kc/s, h = 40 km, J profile.

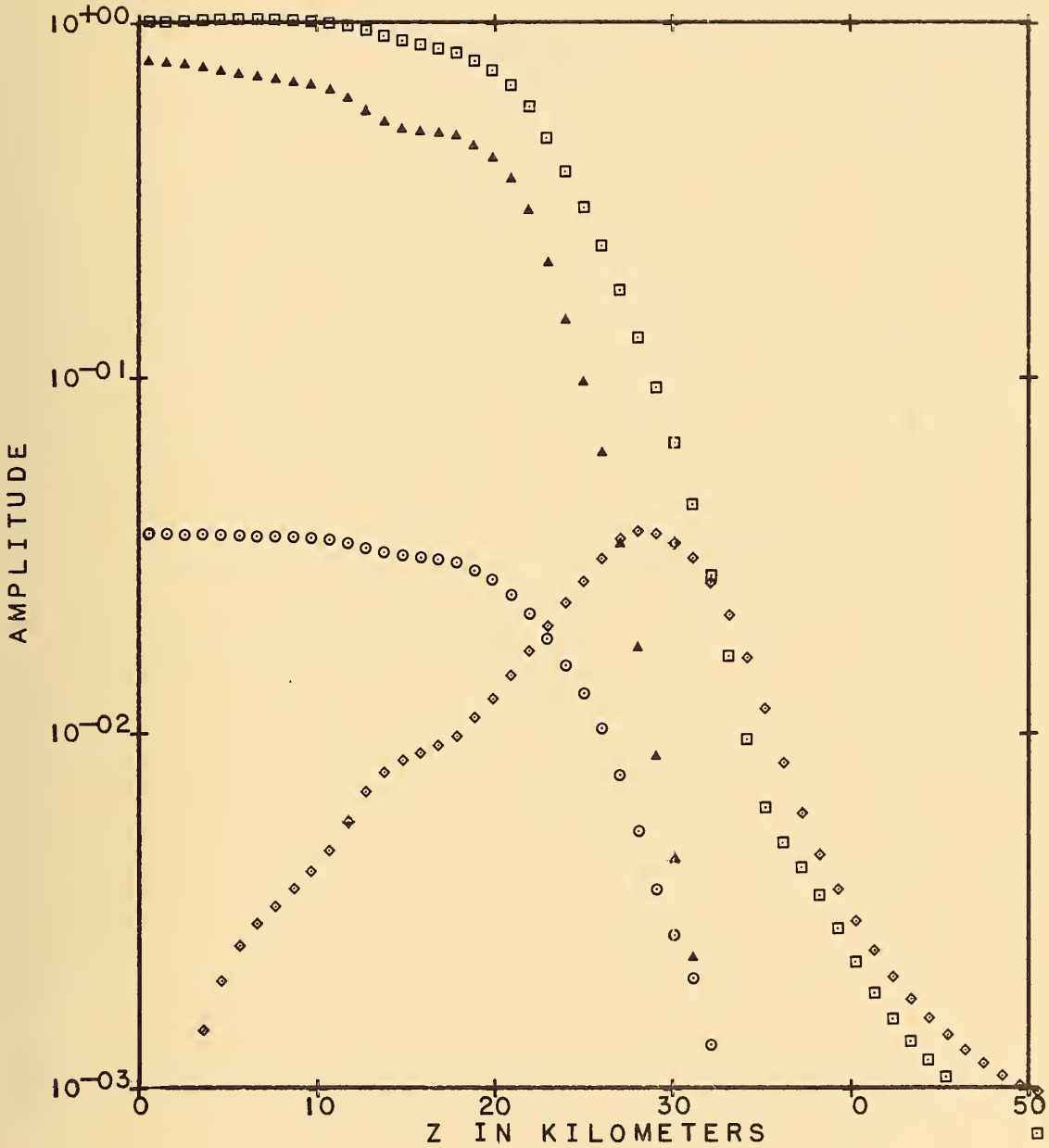

Figure 24. Penetration of horizontally polarized wave into model ionosphere, $\phi_a = 270°$, $\phi_i = 83°$, f = 10 kc/s, h = 40 km, J profile.

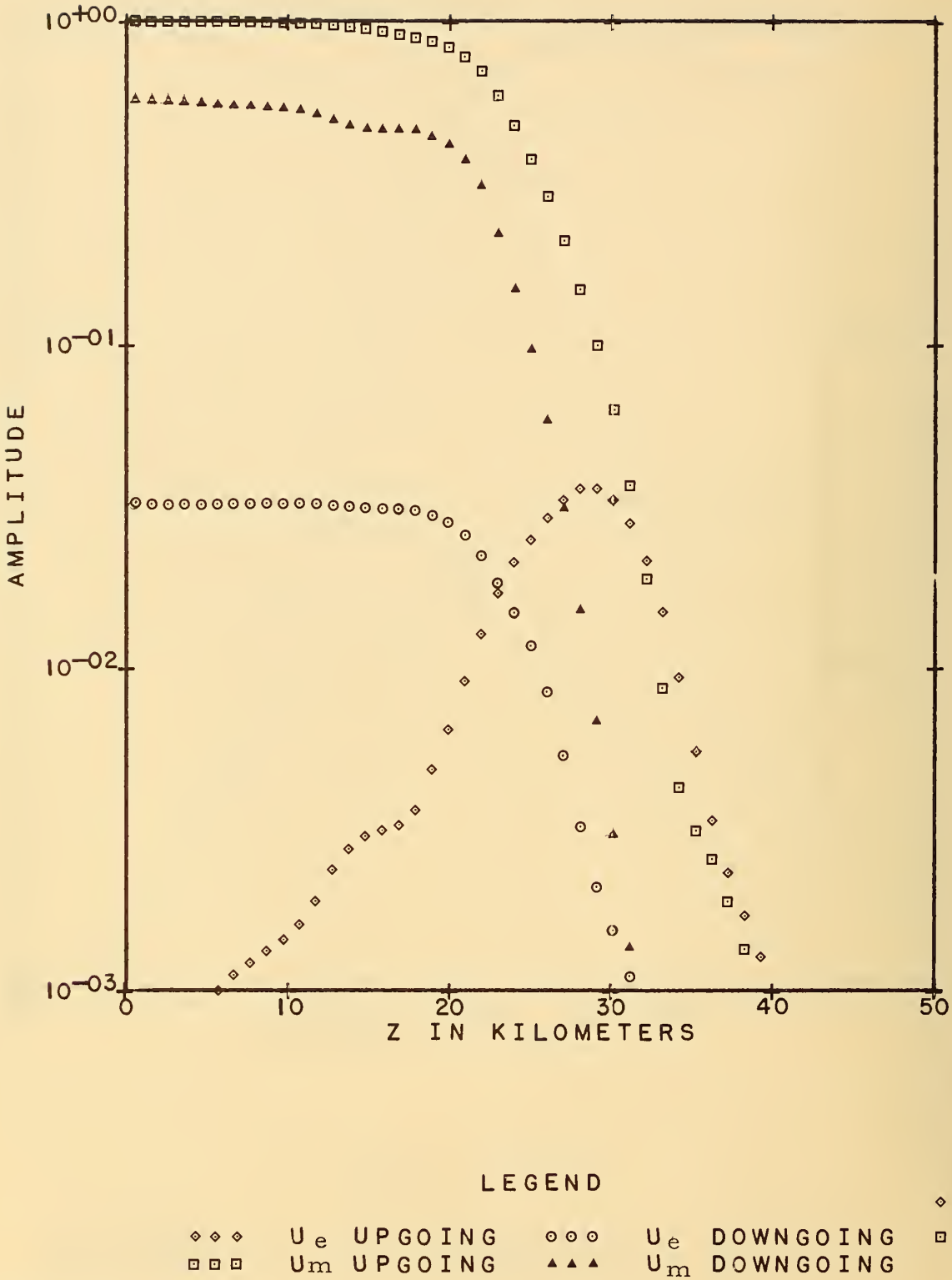

Figure 25. Penetration of horizontally polarized wave into model ionosphere, $\phi_a = 270°$, $\phi_i = 83°$, f = 20 kc/s, h = 40 km, J profile.

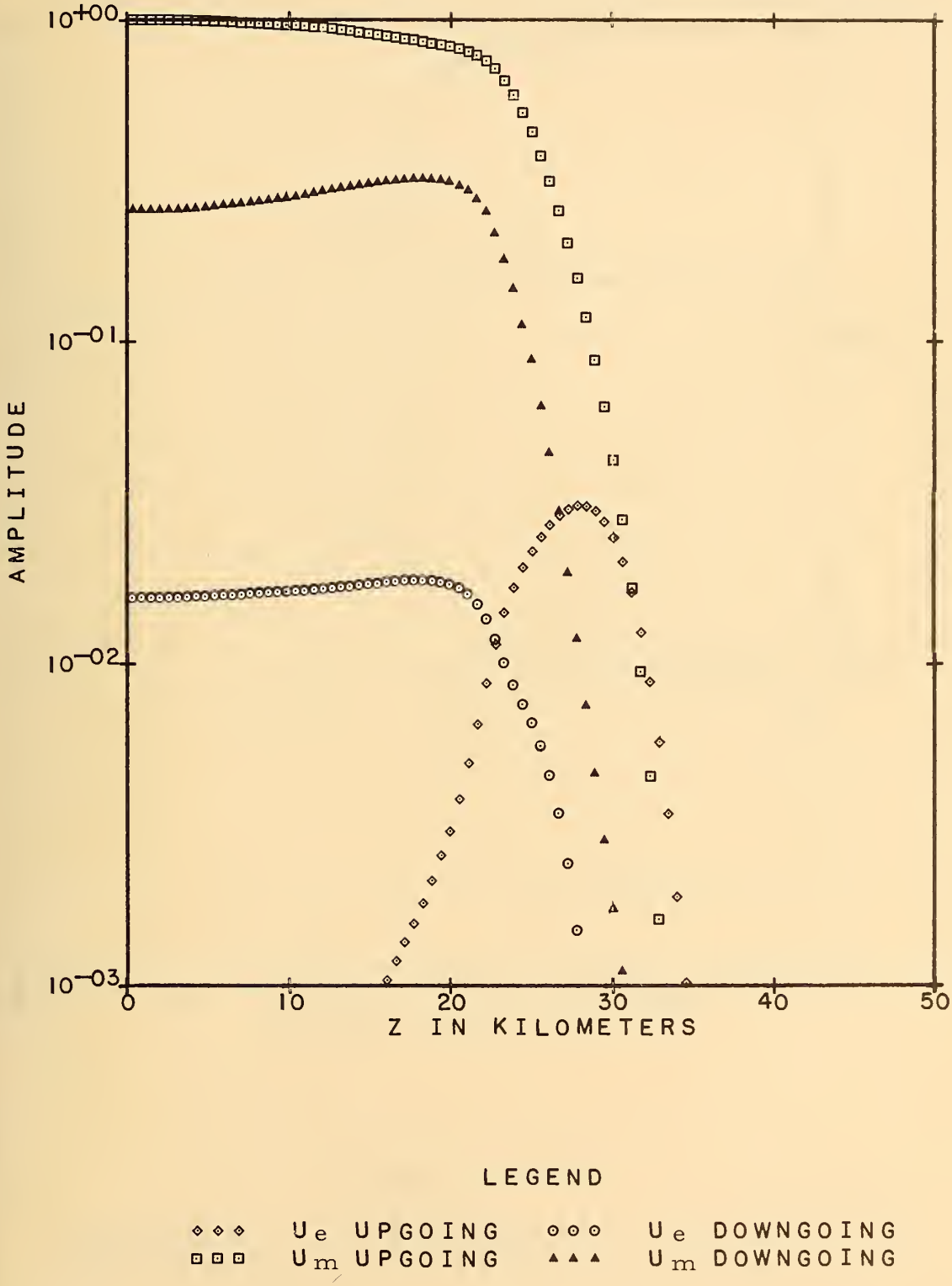

Figure 26. Penetration of horizontally polarized wave into model ionosphere, ϕ_a = 270°, ϕ_i = 83°, f = 50 kc/s, h = 40 km, J profile.

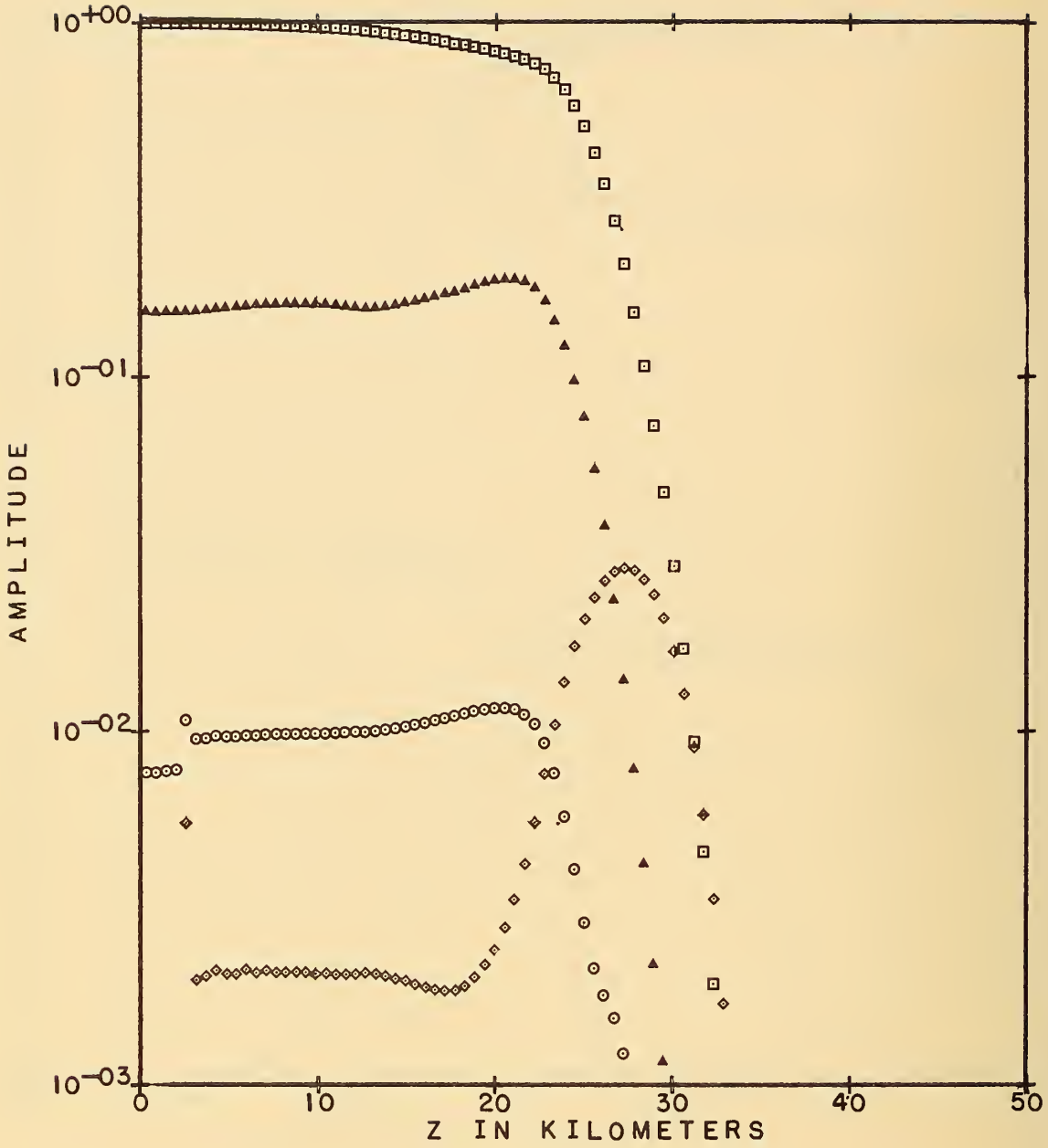

Figure 27. Penetration of horizontally polarized wave into model ionosphere, $\phi_a = 270°$, $\phi_i = 83°$, f = 100 kc/s, h = 40 km, J profile.

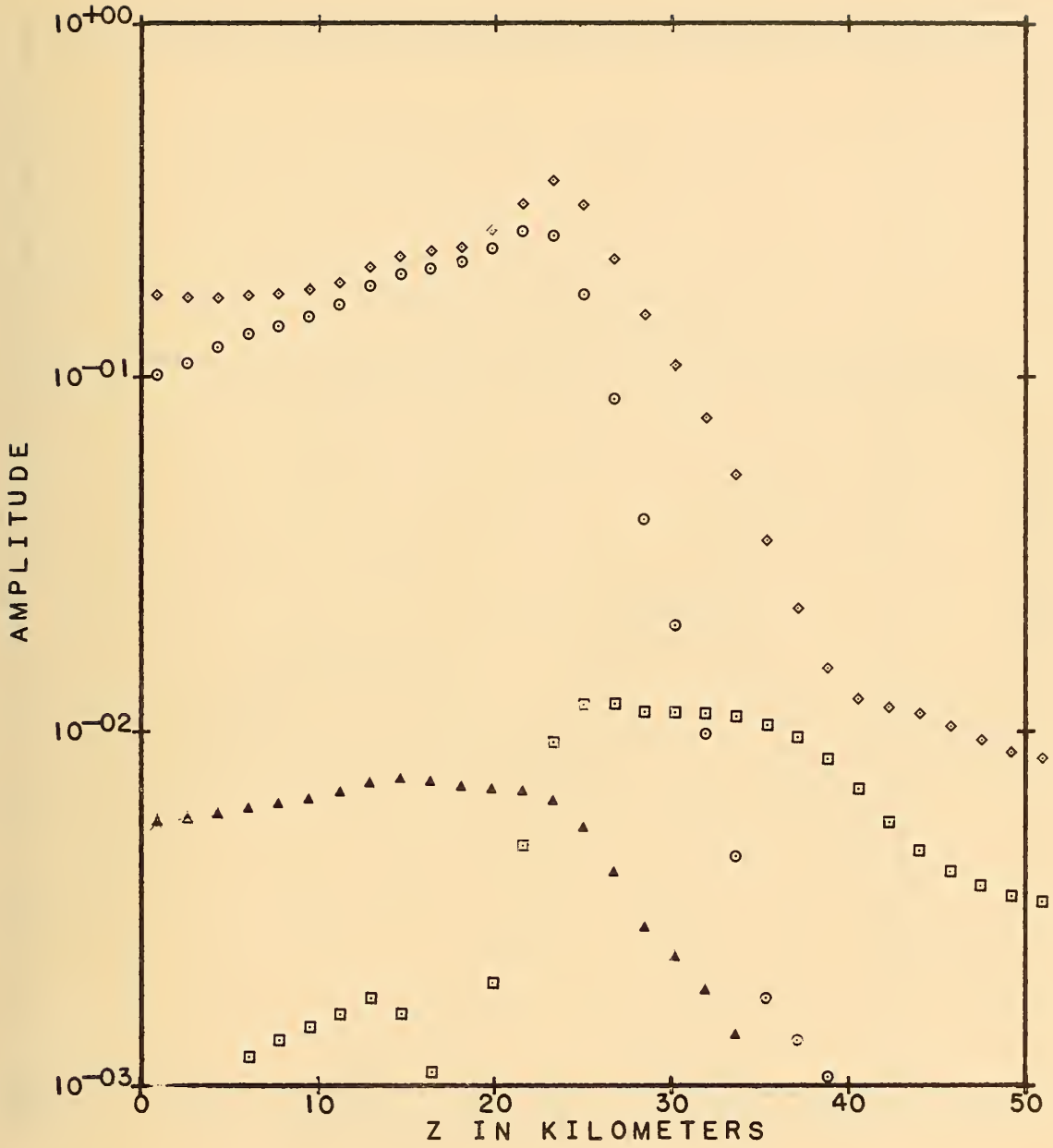

Figure 28. Penetration of vertically polarized wave into model ionosphere, $\phi_a = 0°$, $\phi_i = 80°$, f = 1 kc/s, h = 40 km, J profile.

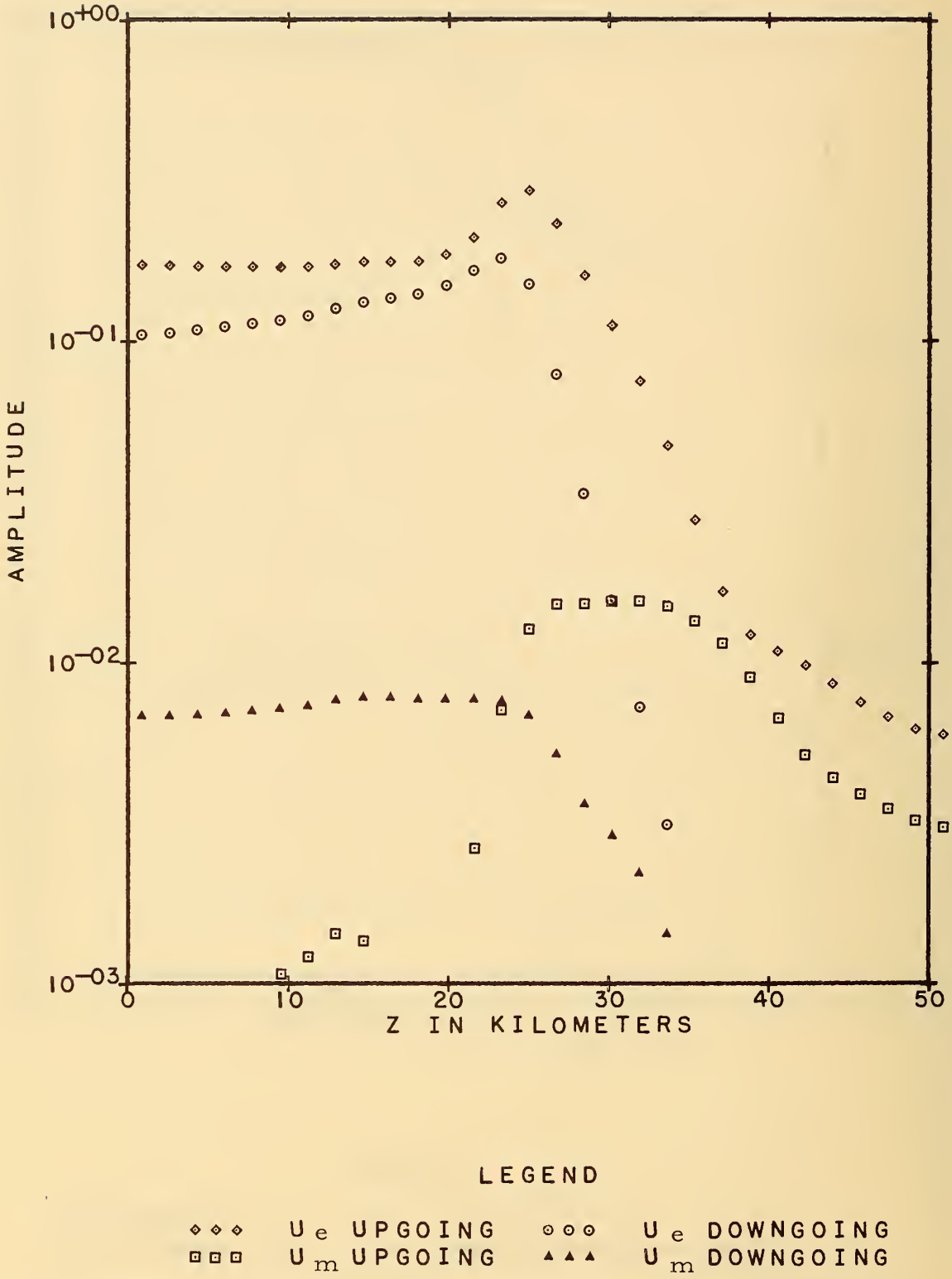

Figure 29. Penetration of vertically polarized wave into model ionosphere, $\phi_a = 0°$, $\phi_i = 80°$, f = 2 kc/s, h = 40 km, J profile.

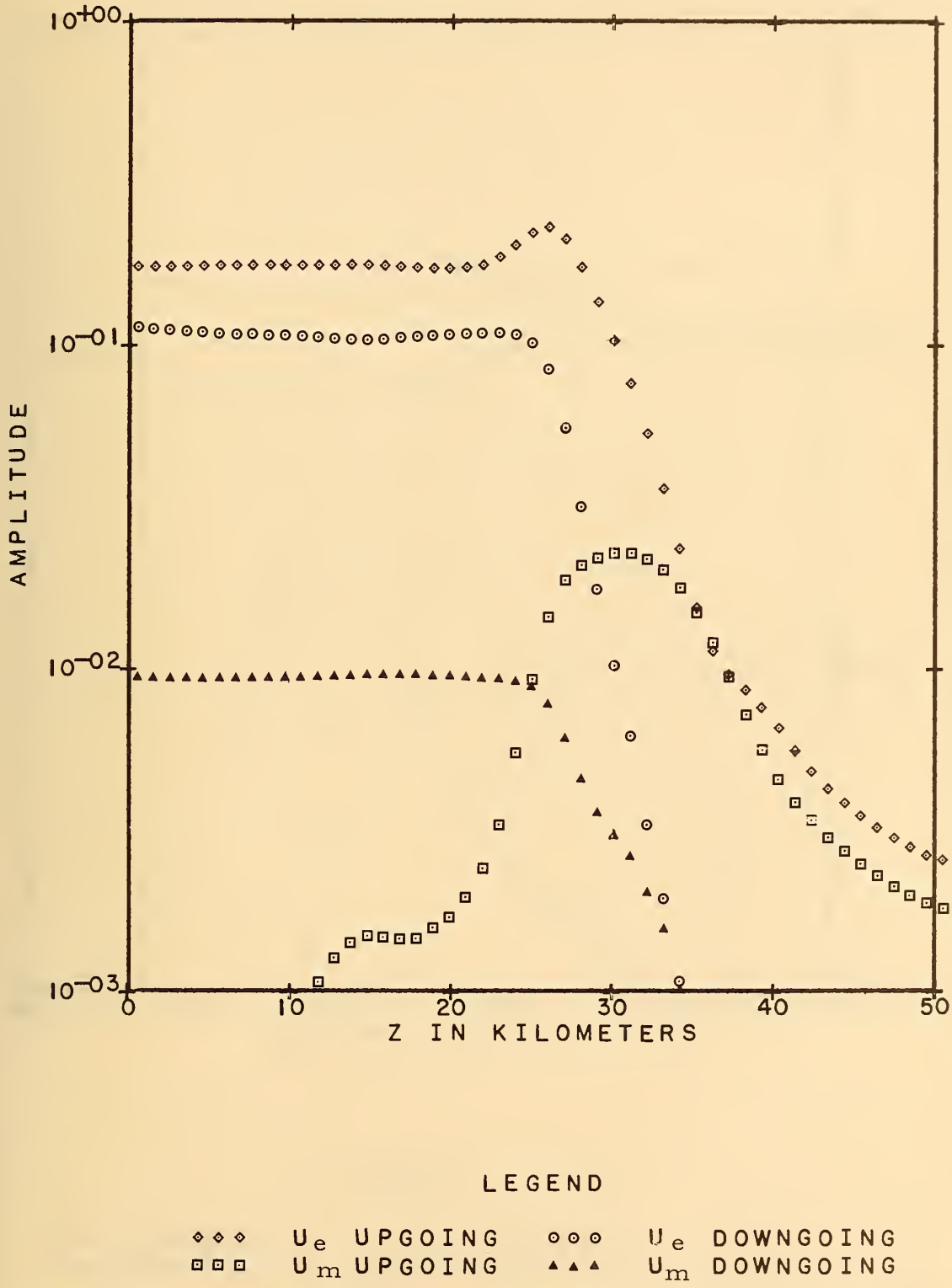

Figure 30. Penetration of vertically polarized wave into model ionosphere, $\phi_a = 0°$, $\phi_i = 80°$, f = 5 kc/s, h = 40 km, J profile.

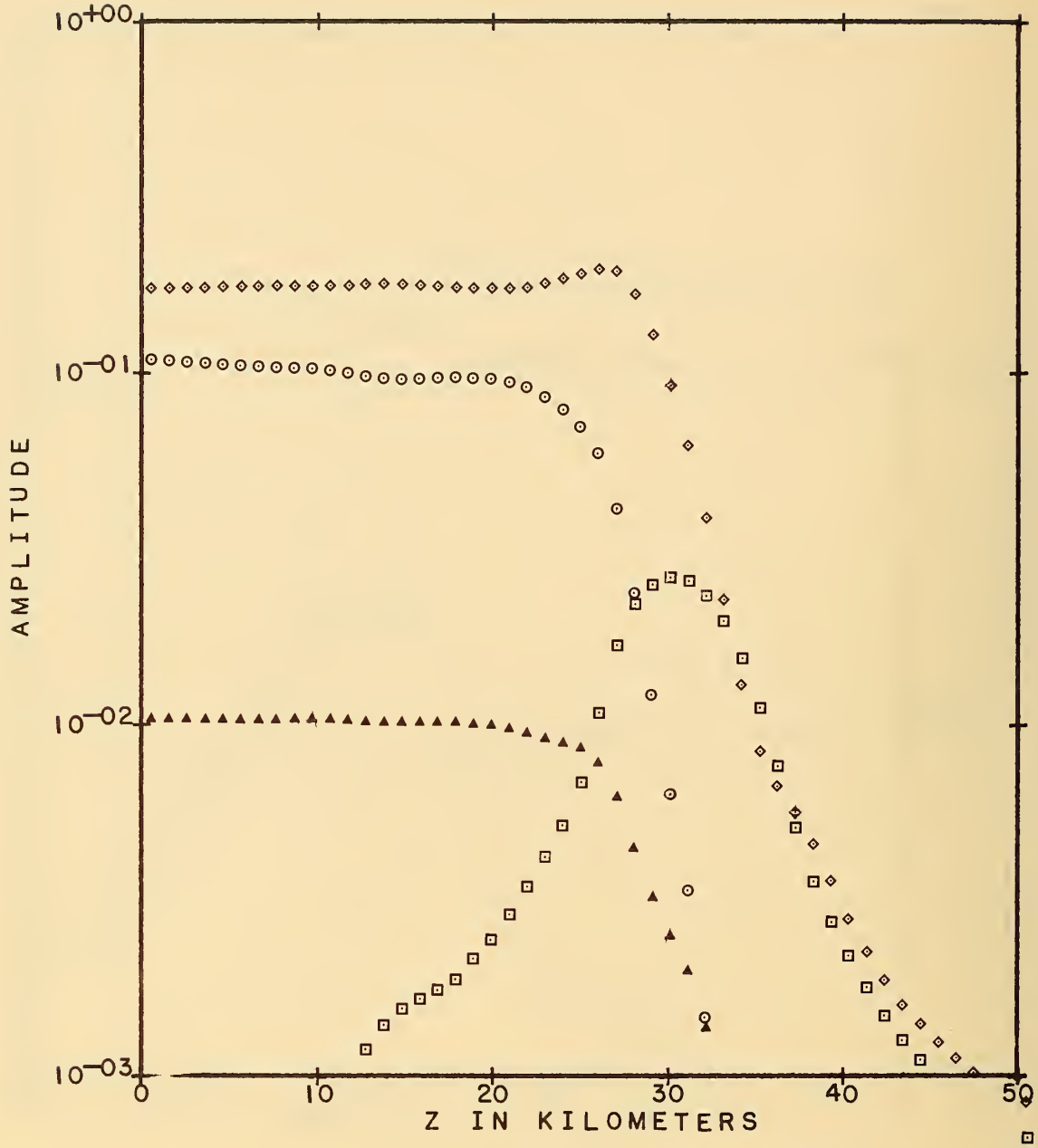

Figure 31. Penetration of vertically polarized wave into model ionosphere, $\phi_a = 0°$, $\phi_1 = 80°$, f = 10 kc/s, h = 40 km, J profile.

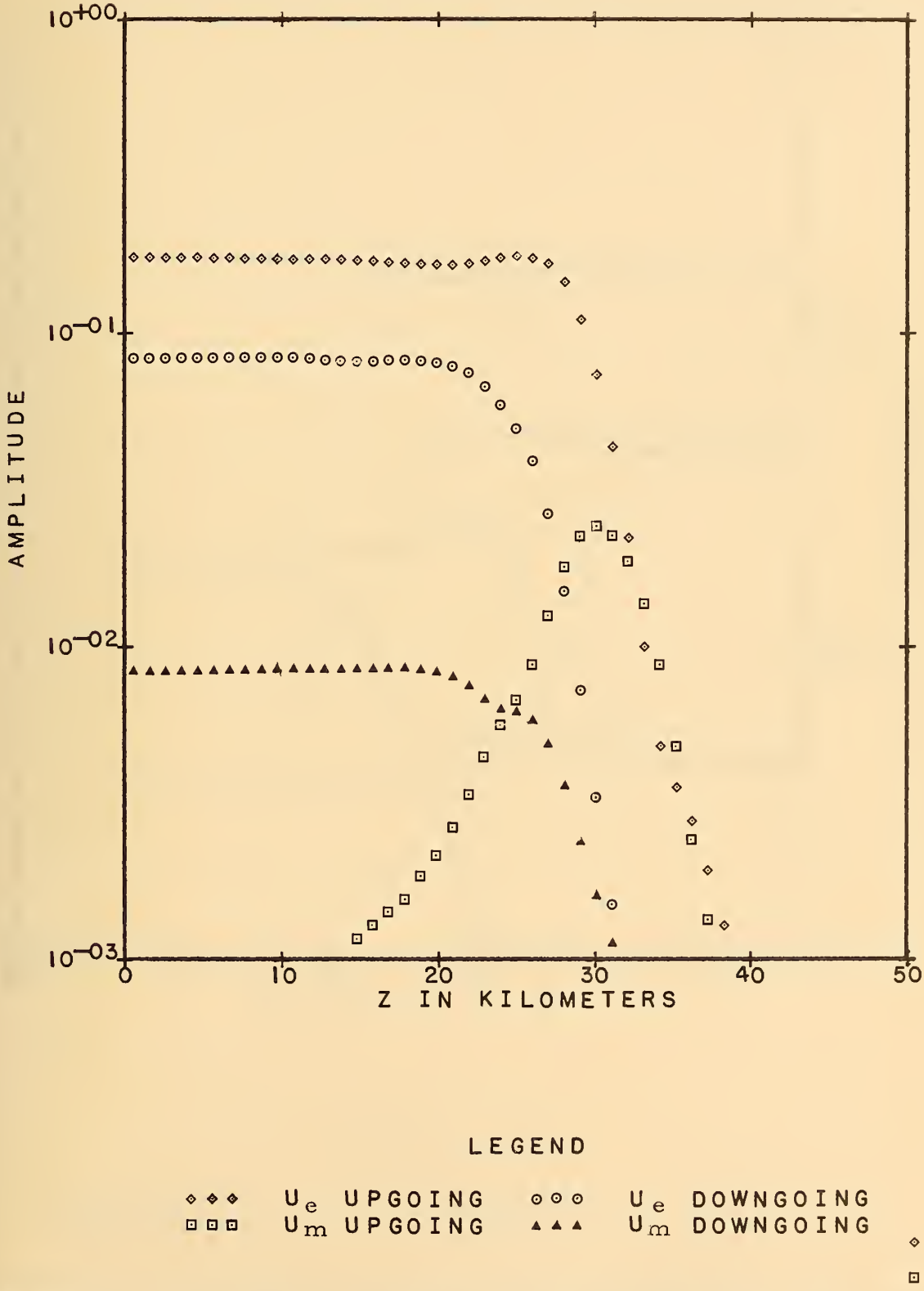

Figure 32. Penetration of vertically polarized wave into model ionosphere, $\phi_a = 0°$, $\phi_i = 80°$, f = 20 kc/s, h = 40 km, J profile.

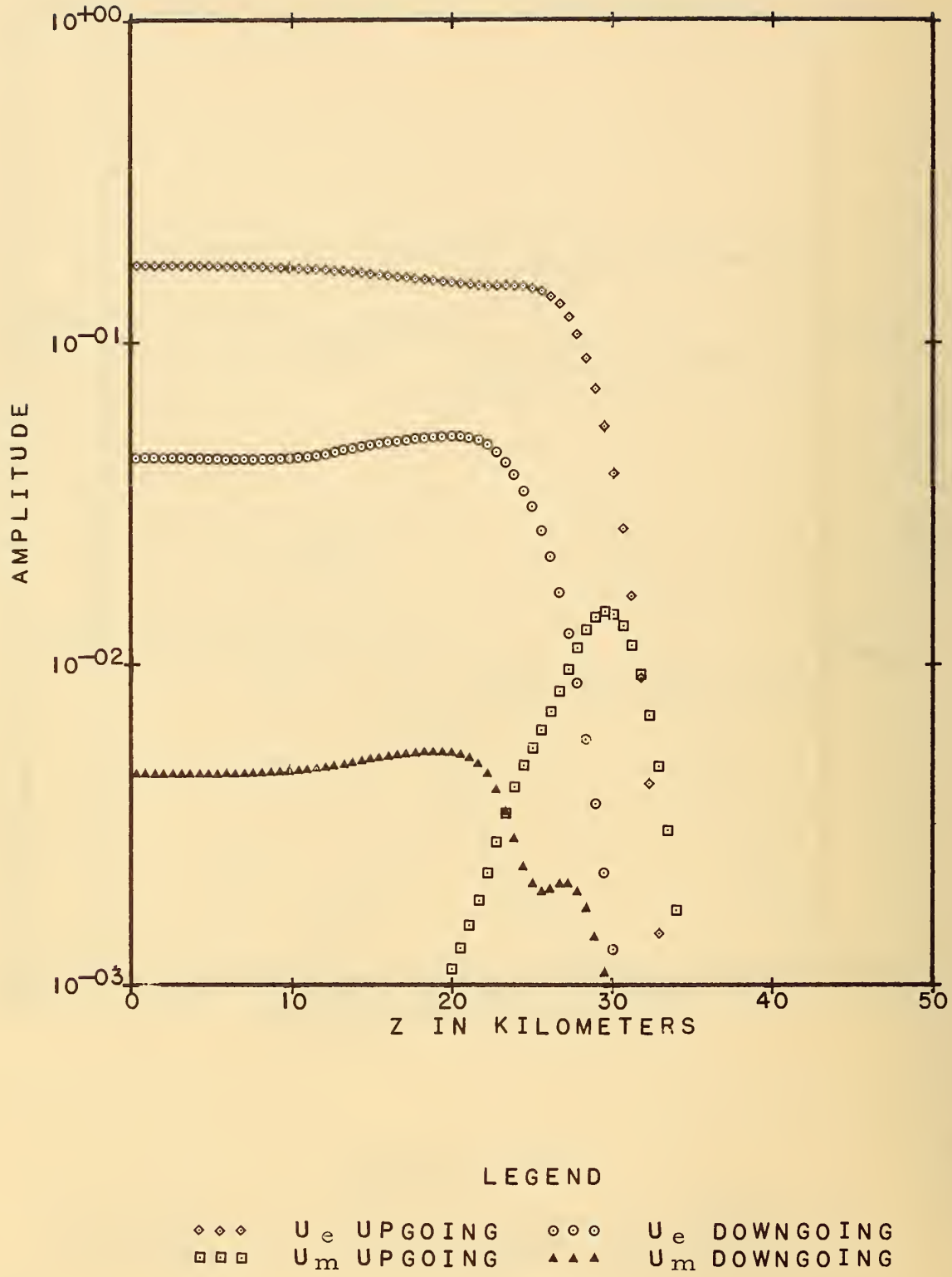

Figure 33. Penetration of vertically polarized wave into model ionosphere, $\phi_a = 0°$, $\phi_i = 80°$, f = 50 kc/s, h = 40 km, J profile.

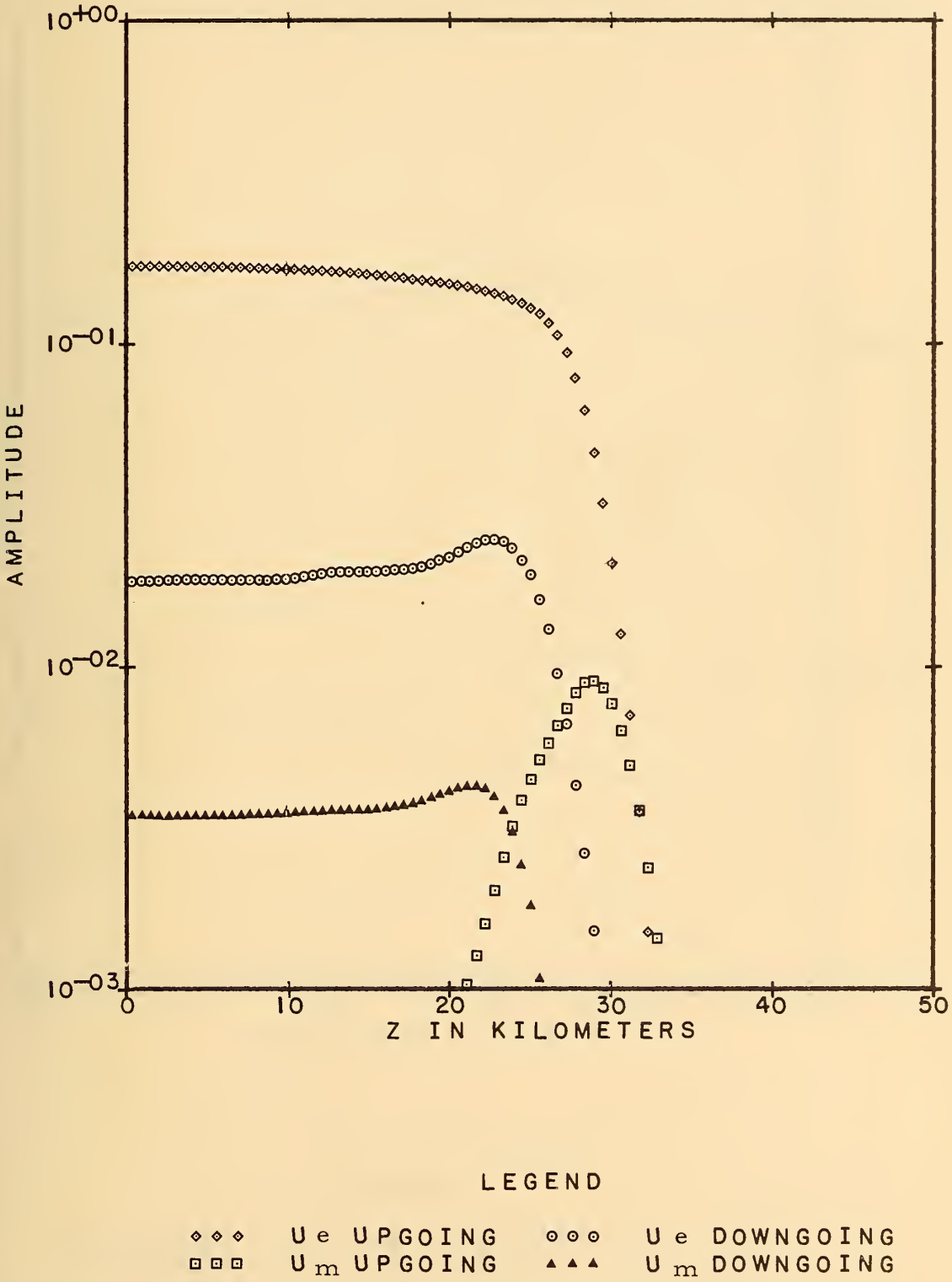

Figure 34. Penetration of vertically polarized wave into model ionosphere, $\phi_0 = 0°$, $\phi_1 = 80°$, f = 100 kc/s, h = 40 km, J profile.

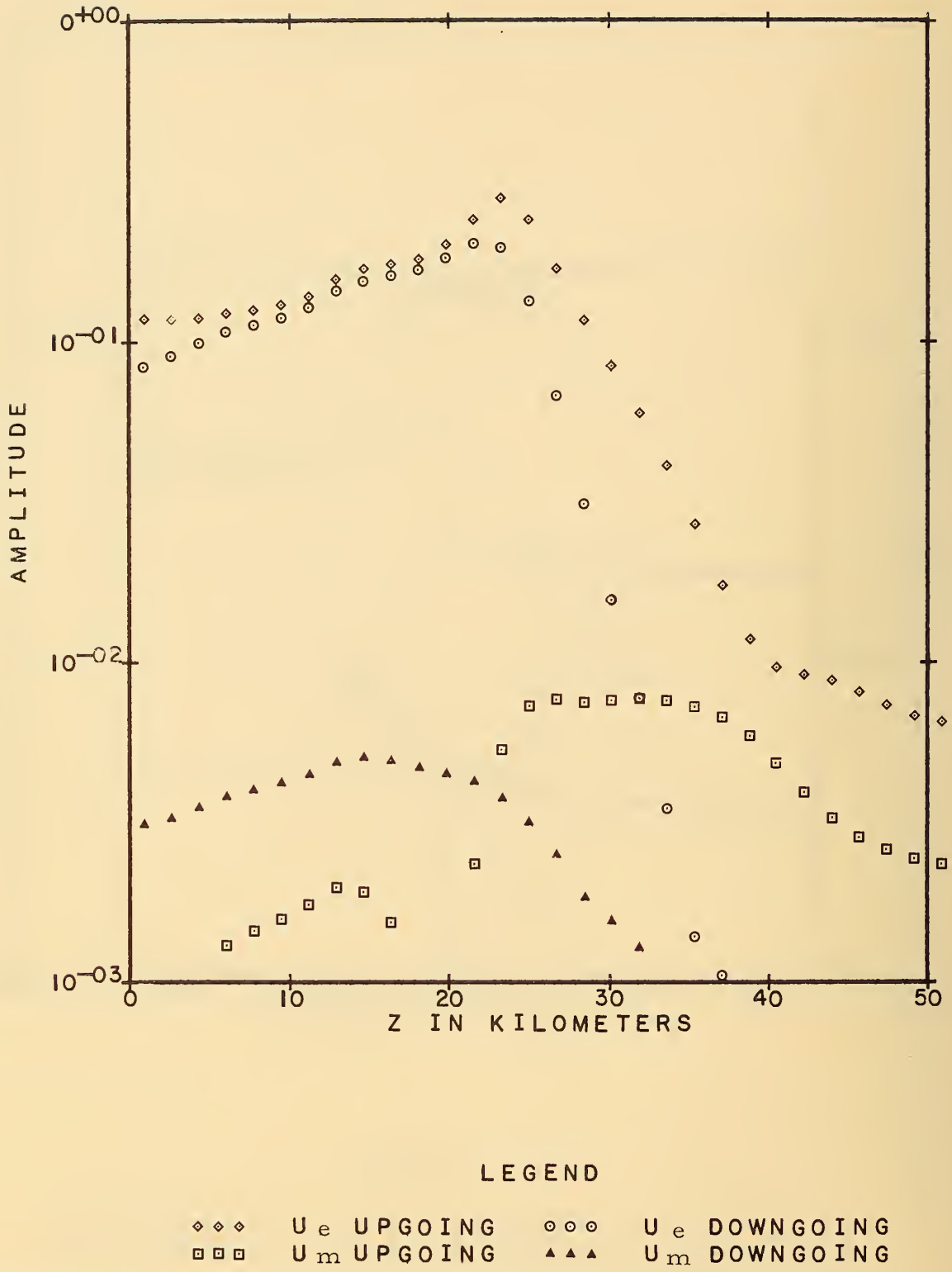

Figure 35. Penetration of vertically polarized wave into model ionosphere, $\phi_a = 0°$, $\phi_i = 83°$, f = 1 kc/s, h = 40 km, J profile.

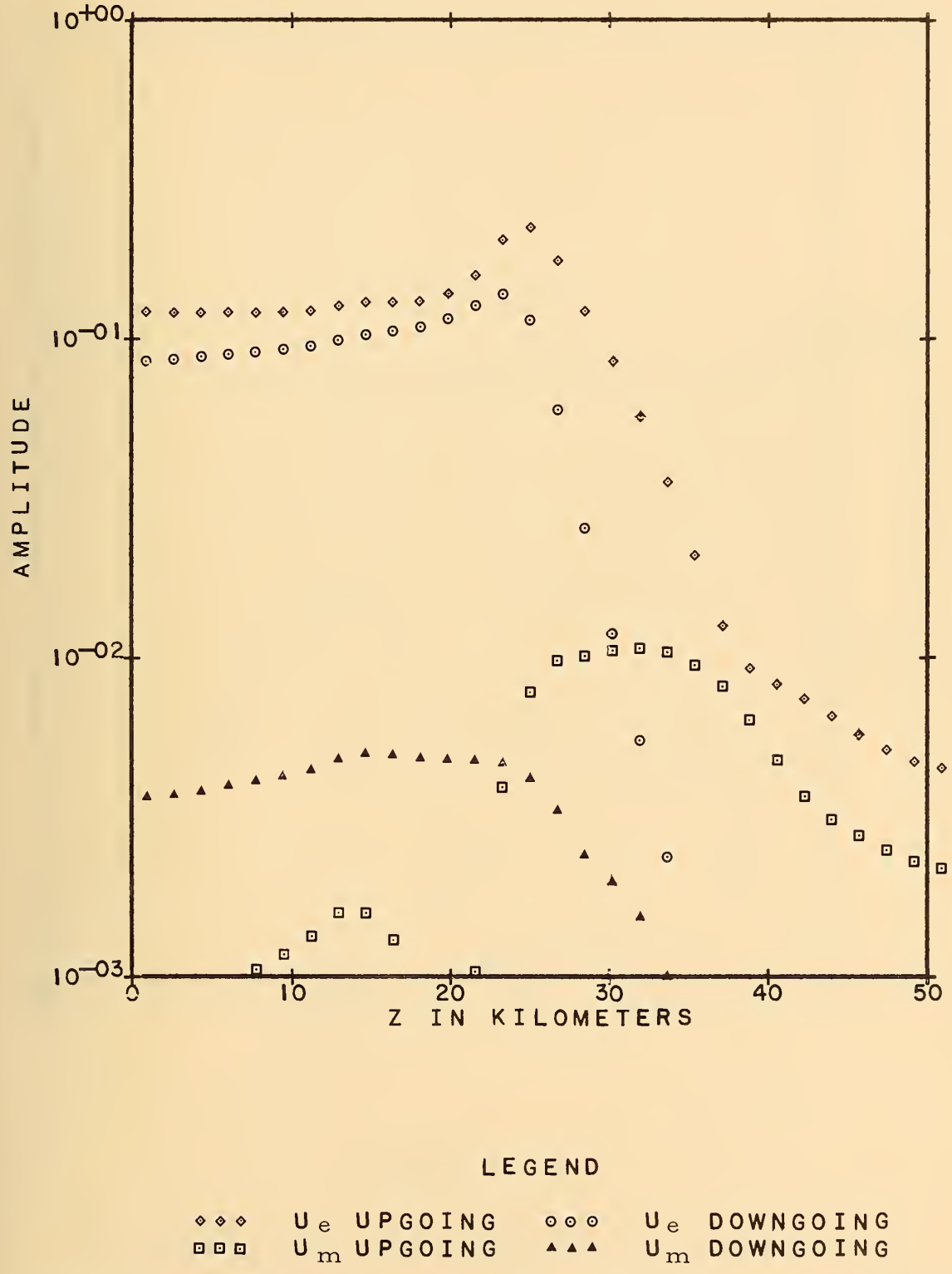

Figure 36. Penetration of vertically polarized wave into model ionosphere, $\phi_a = 0°$, $\phi_i = 83°$, f = 2 kc/s, h = 40 km, J profile.

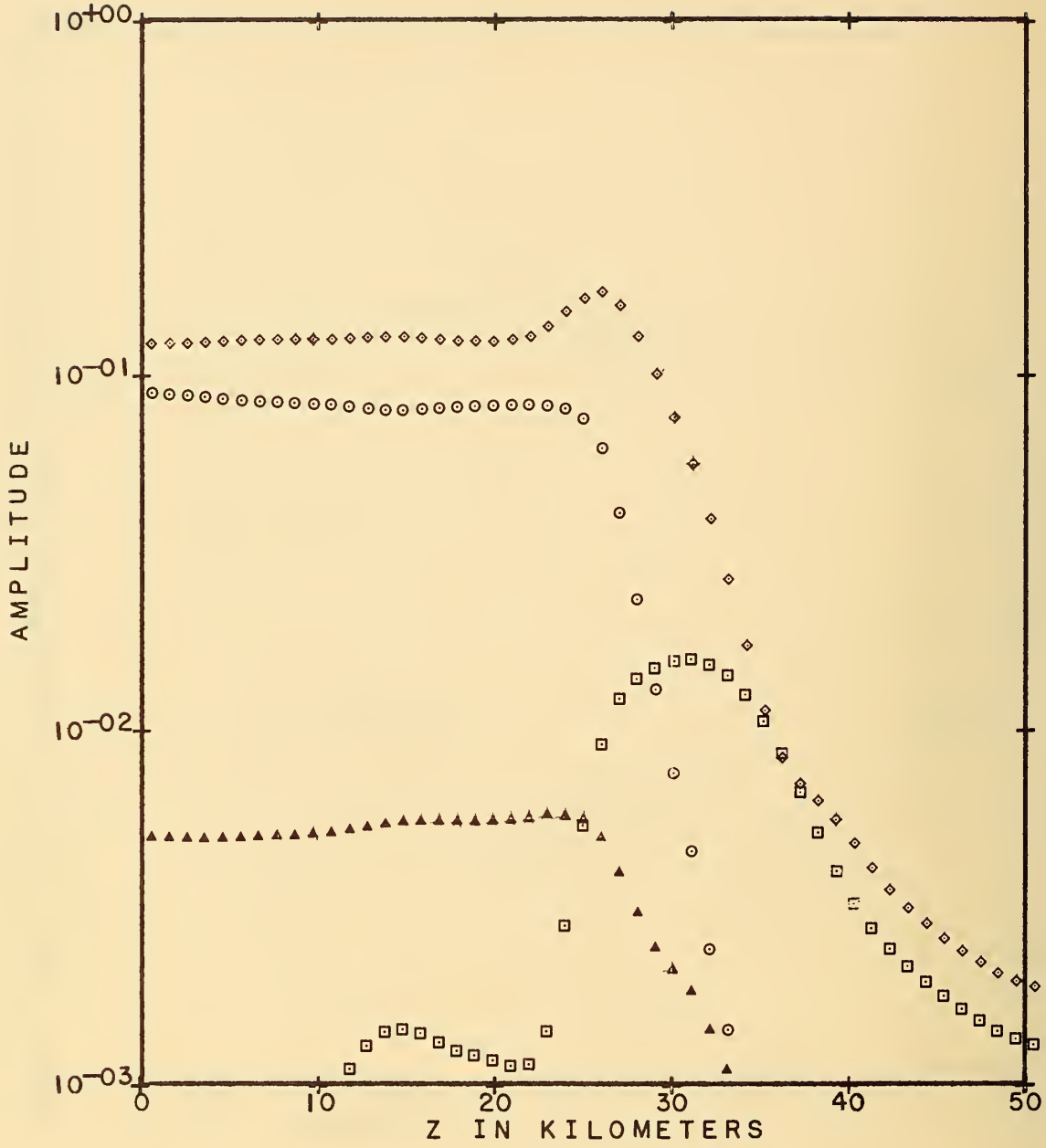

Figure 37. Penetration of vertically polarized wave into model ionosphere, $\phi_a = 0°$, $\phi_1 = 83°$, f = 5 kc/s, h = 40 km, J profile.

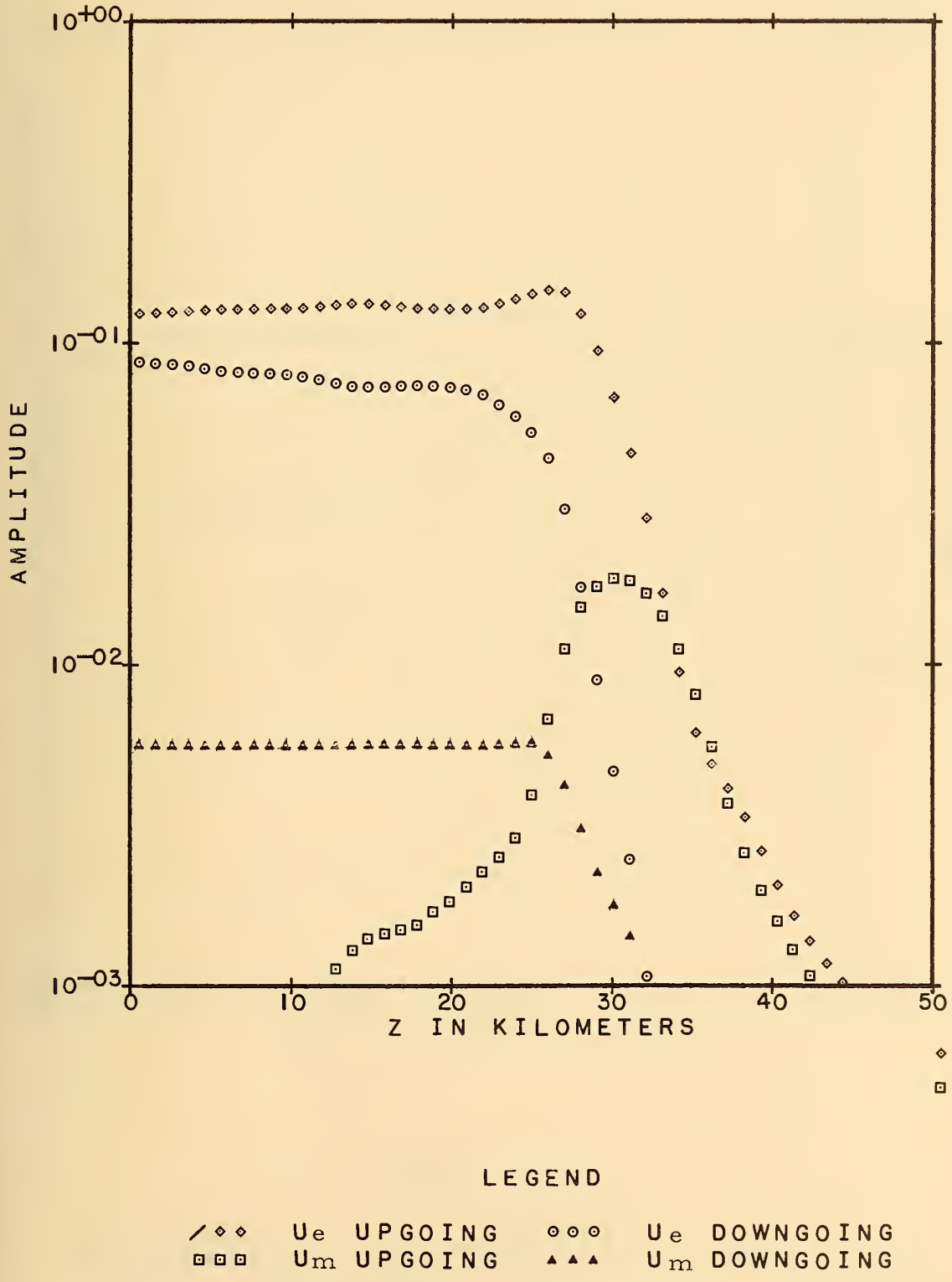

Figure 38. Penetration of vertically polarized wave into model ionosphere, $\phi_a = 0°$, $\phi_i = 83°$, f = 10 kc/s, h = 40 km, J profile.

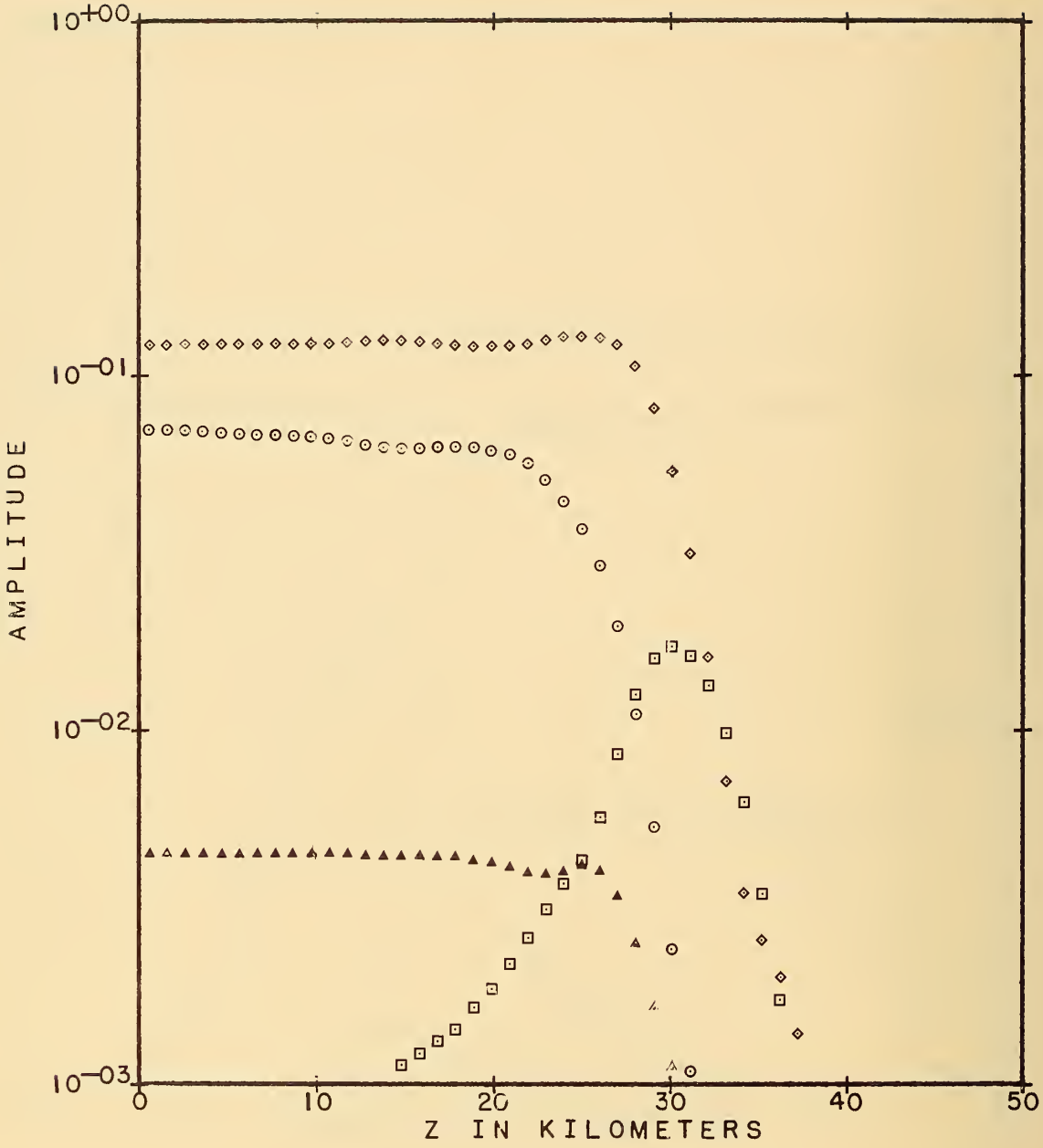

Figure 39. Penetration of vertically polarized wave into model ionosphere, $\phi_a = 0°$, $\phi_1 = 83°$, f = 20 kc/s, h = 40 km, J profile.

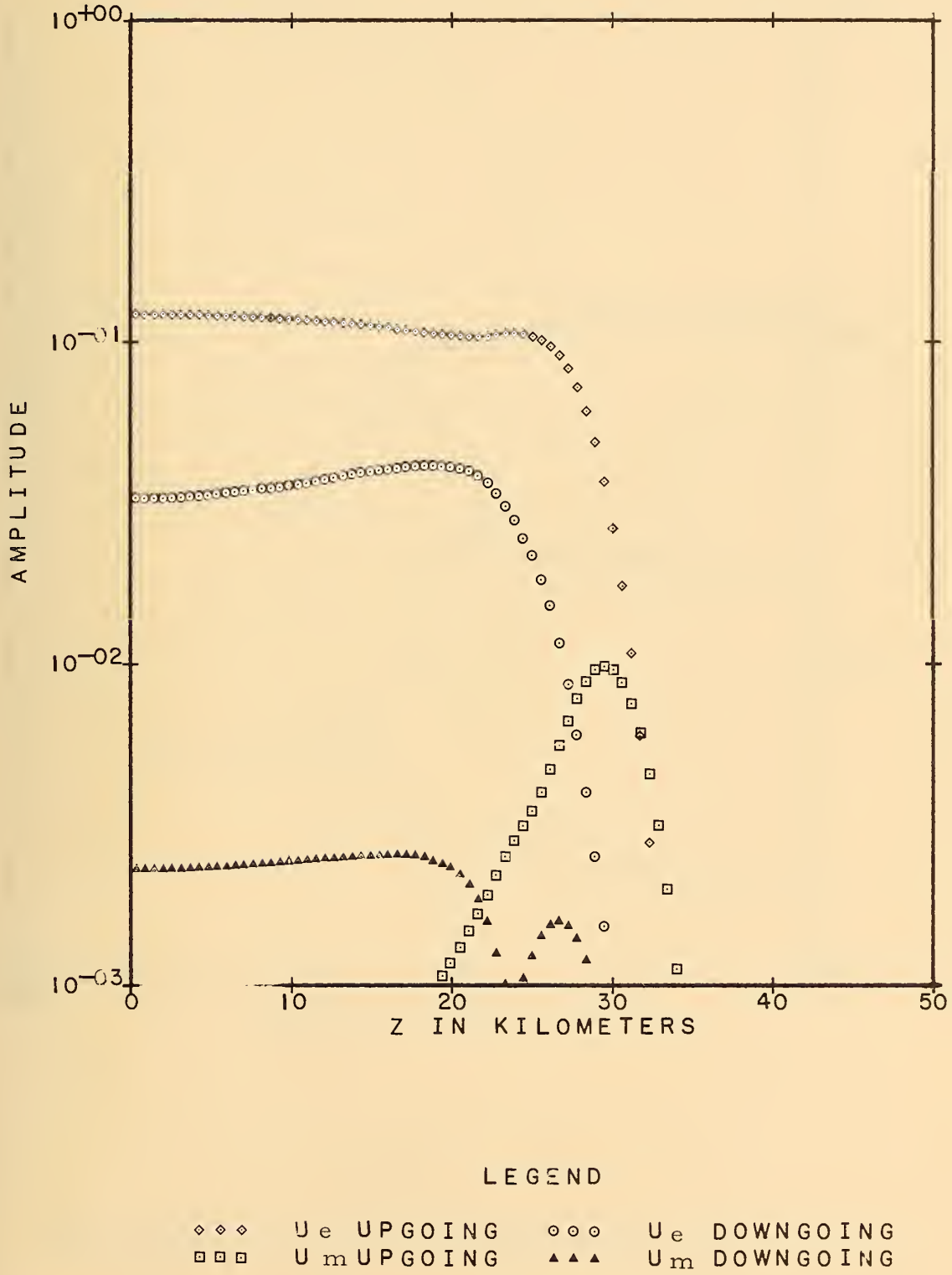

Figure 40. Penetration of vertically polarized wave into model ionosphere, $\phi_a = 0°$, $\phi_i = 83°$, f = 50 kc/s, h = 40 km, J profile.

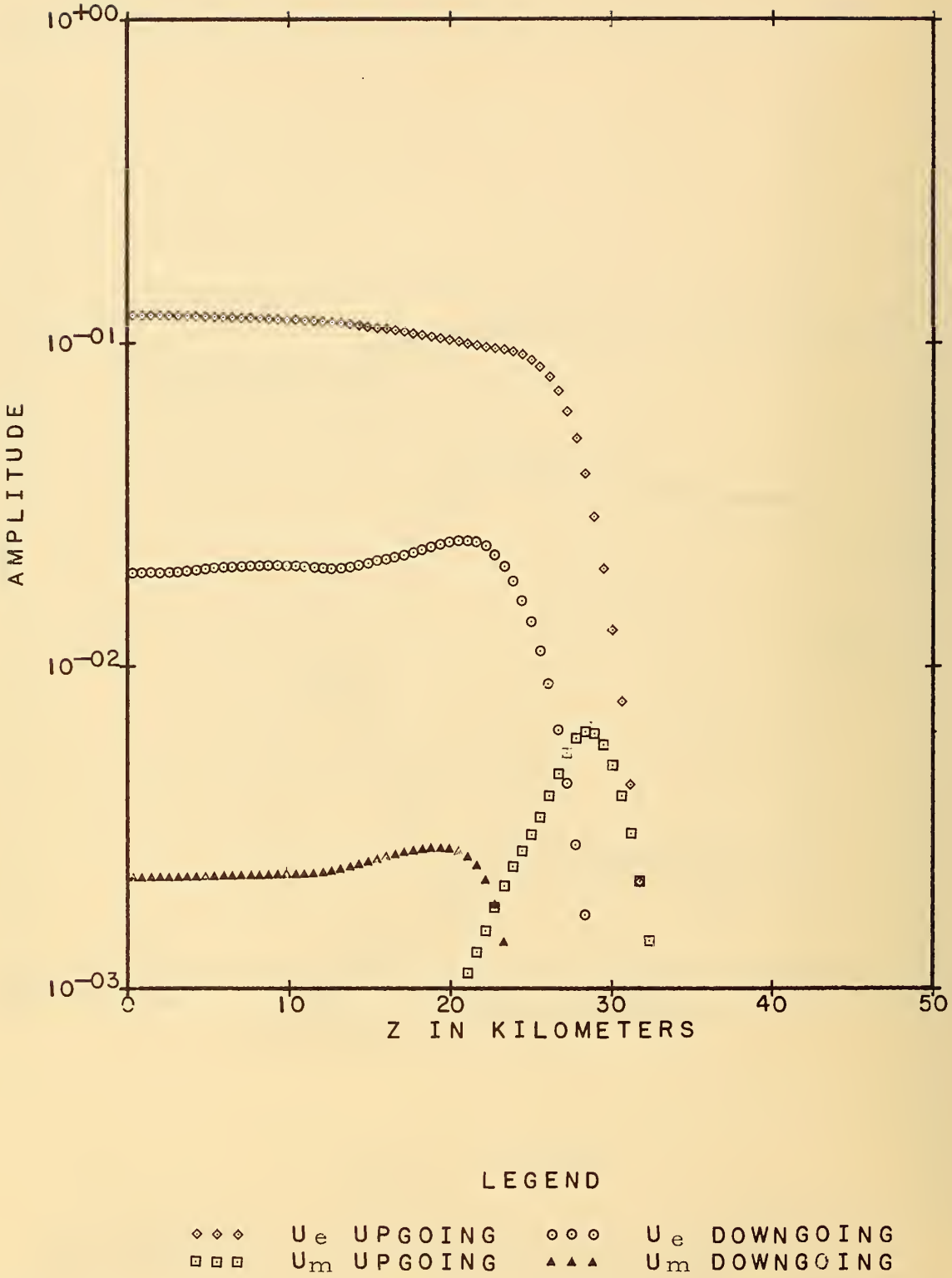

Figure 41. Penetration of vertically polarized wave into model ionosphere, $\phi_a = 0°$, $\phi_i = 83°$, f = 100 kc/s, h = 40 km, J profile.

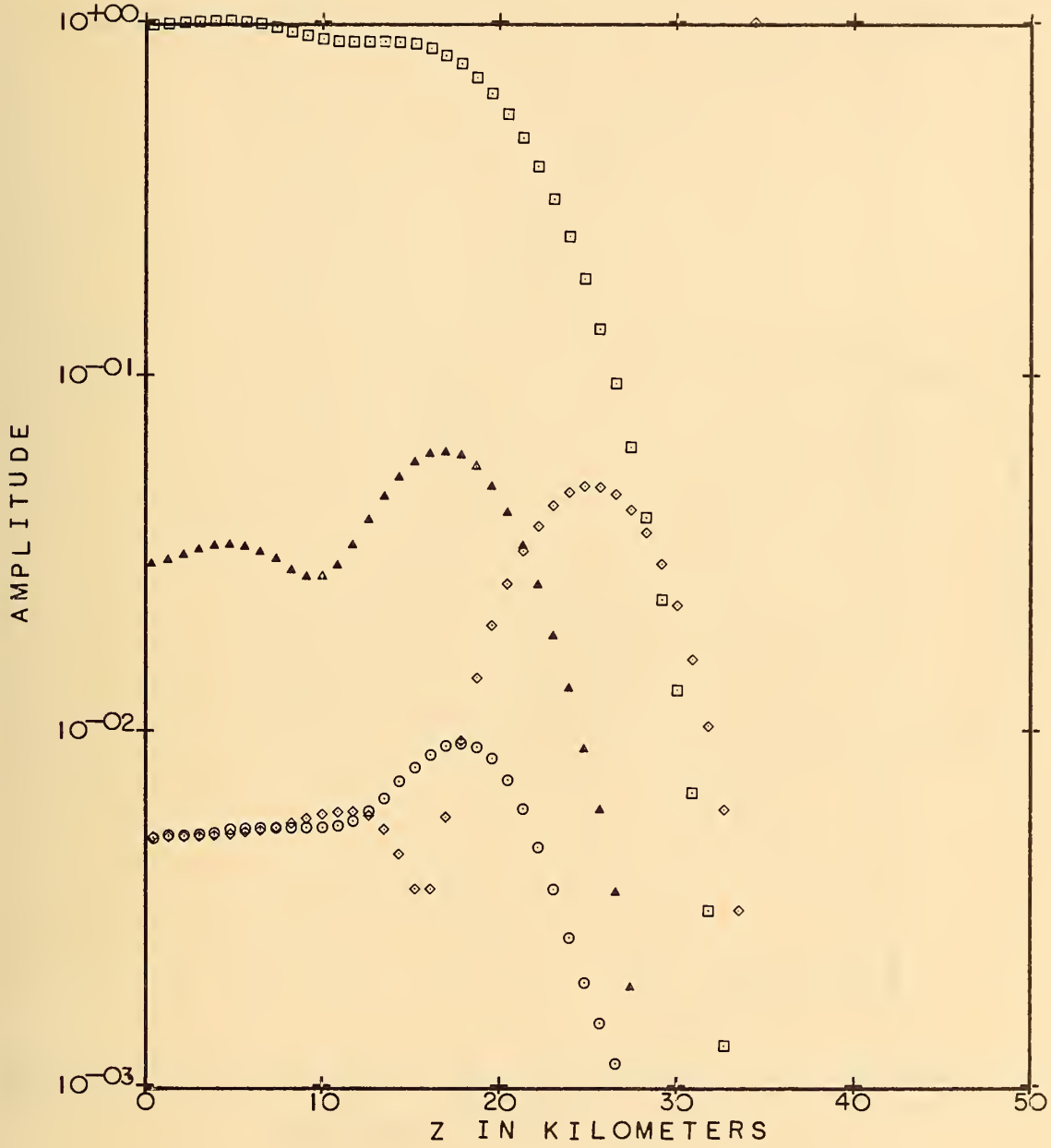

Figure 42. Penetration into nuclear model ionosphere, $Q_o = 10^4$, gas mixture, daytime, h = 36 km, f = 100 kc/s, $\varphi_i = 82°$, $\varphi_a = 270°$.

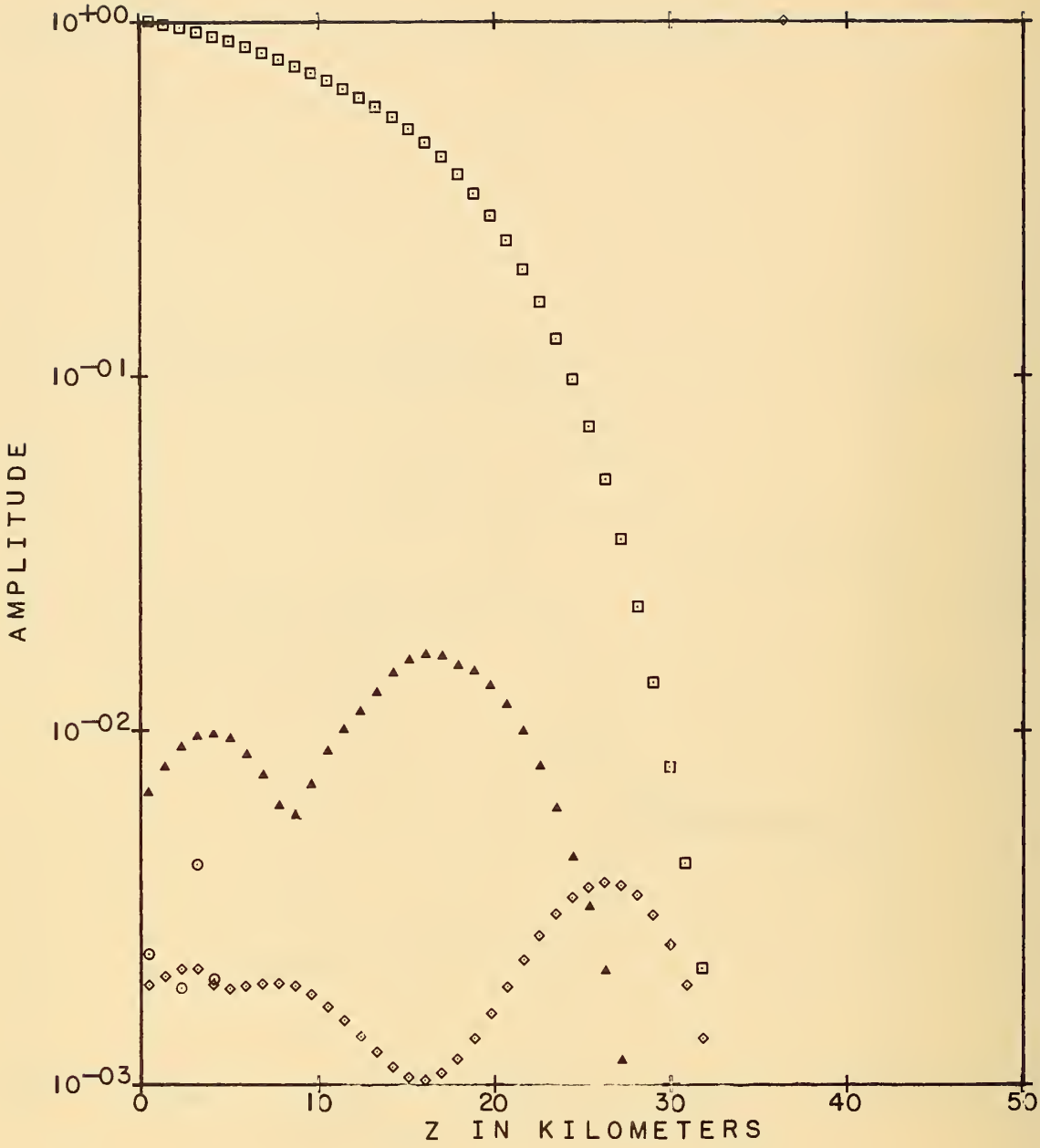

Figure 43. Penetration into nuclear model ionosphere, $Q_o = 10^6$, gas mixture, daytime, h = 26 km, f = 100 kc/s, $\varphi_1 = 82°$, $\varphi_a = 270°$.

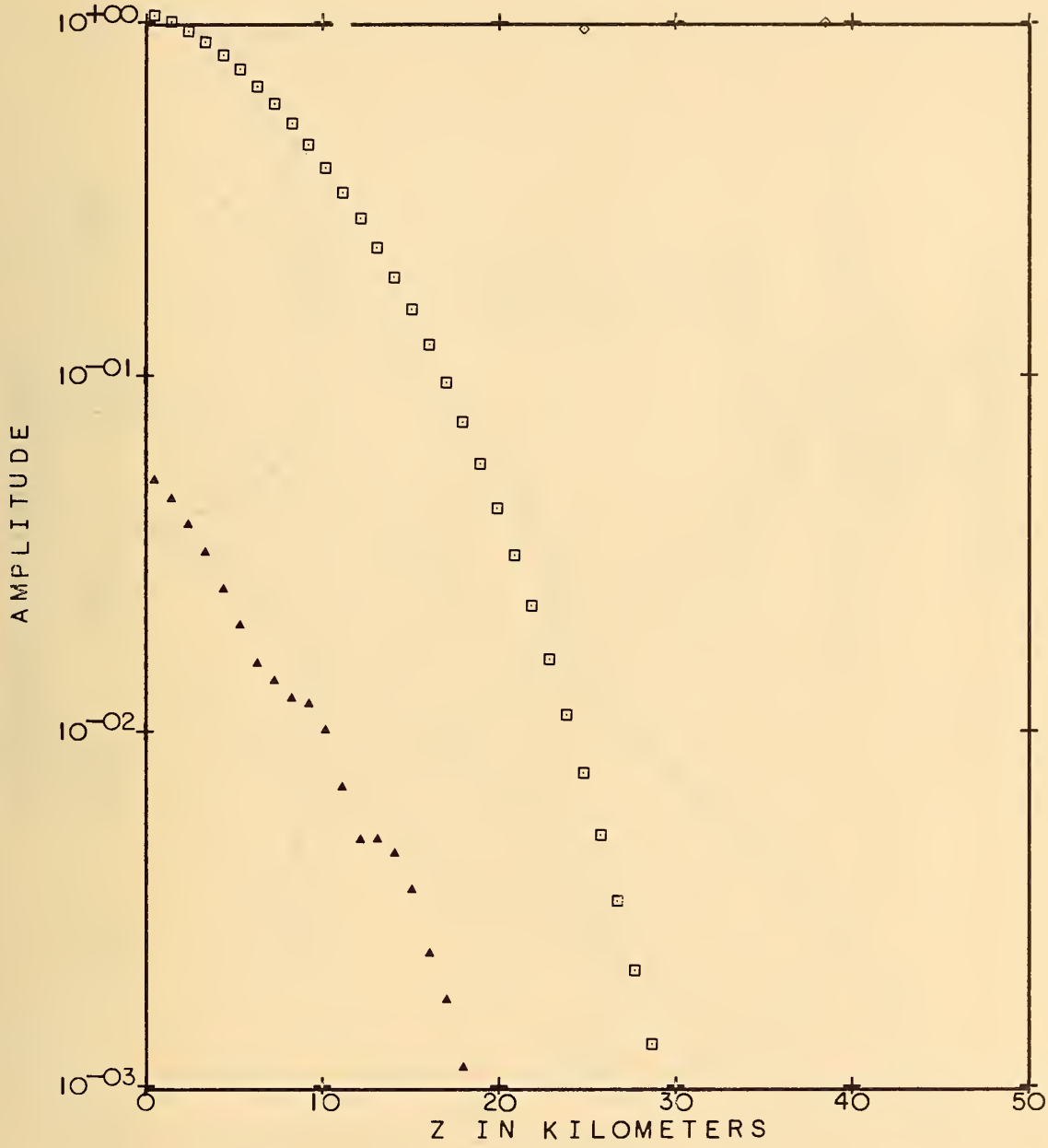

Figure 44. Penetration into nuclear model ionosphere, $Q_o = 10^8$, gas mixture, daytime, h = 12 km, f = 100 kc/s, $\varphi_i = 82°$, $\varphi_a = 270°$.

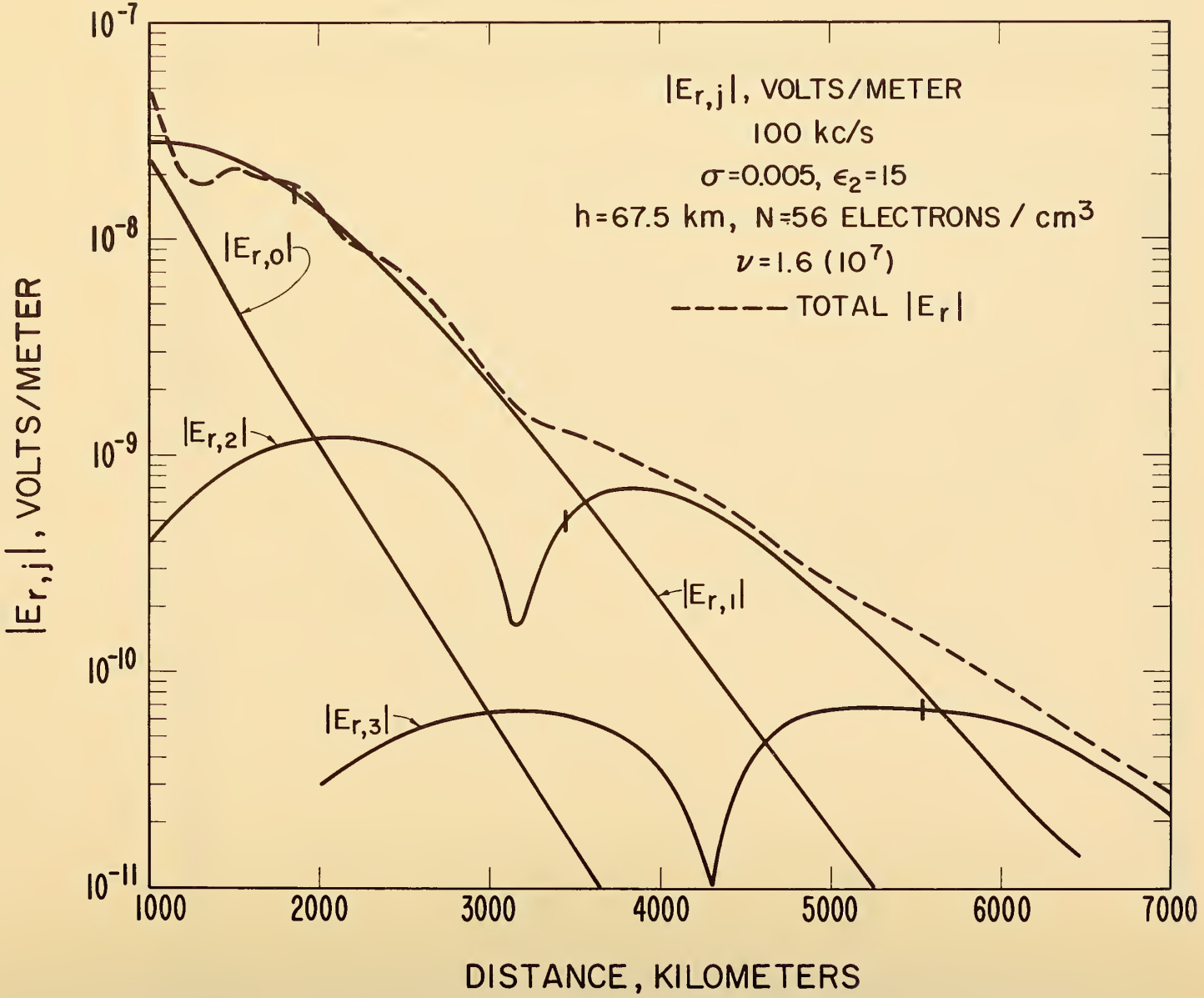

Figure 45. Propagation of 100 kc/s wave overland on ambient day.

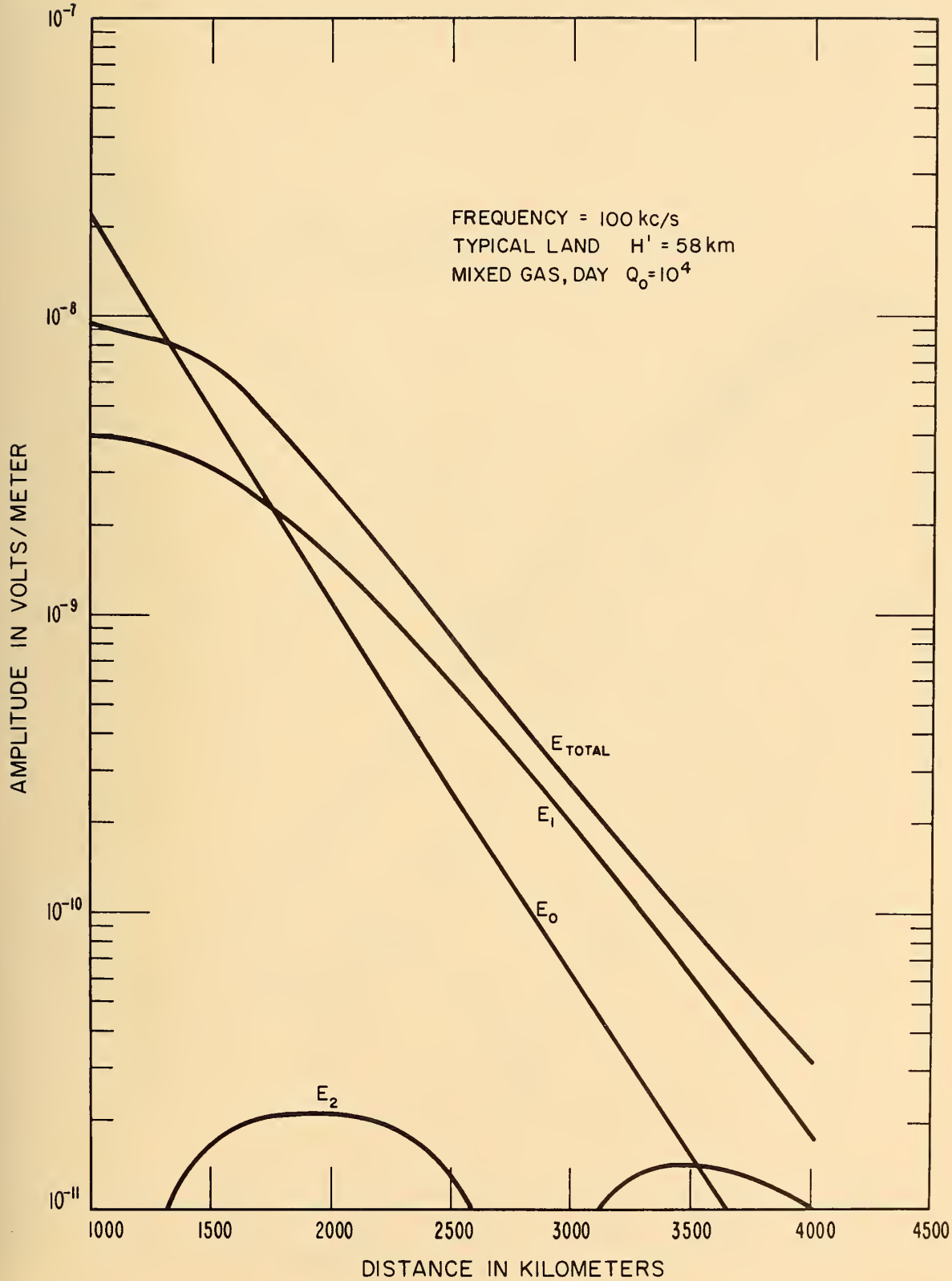

Figure 46. Propagation of 100 kc/s wave overland, $Q_o = 10^4$.

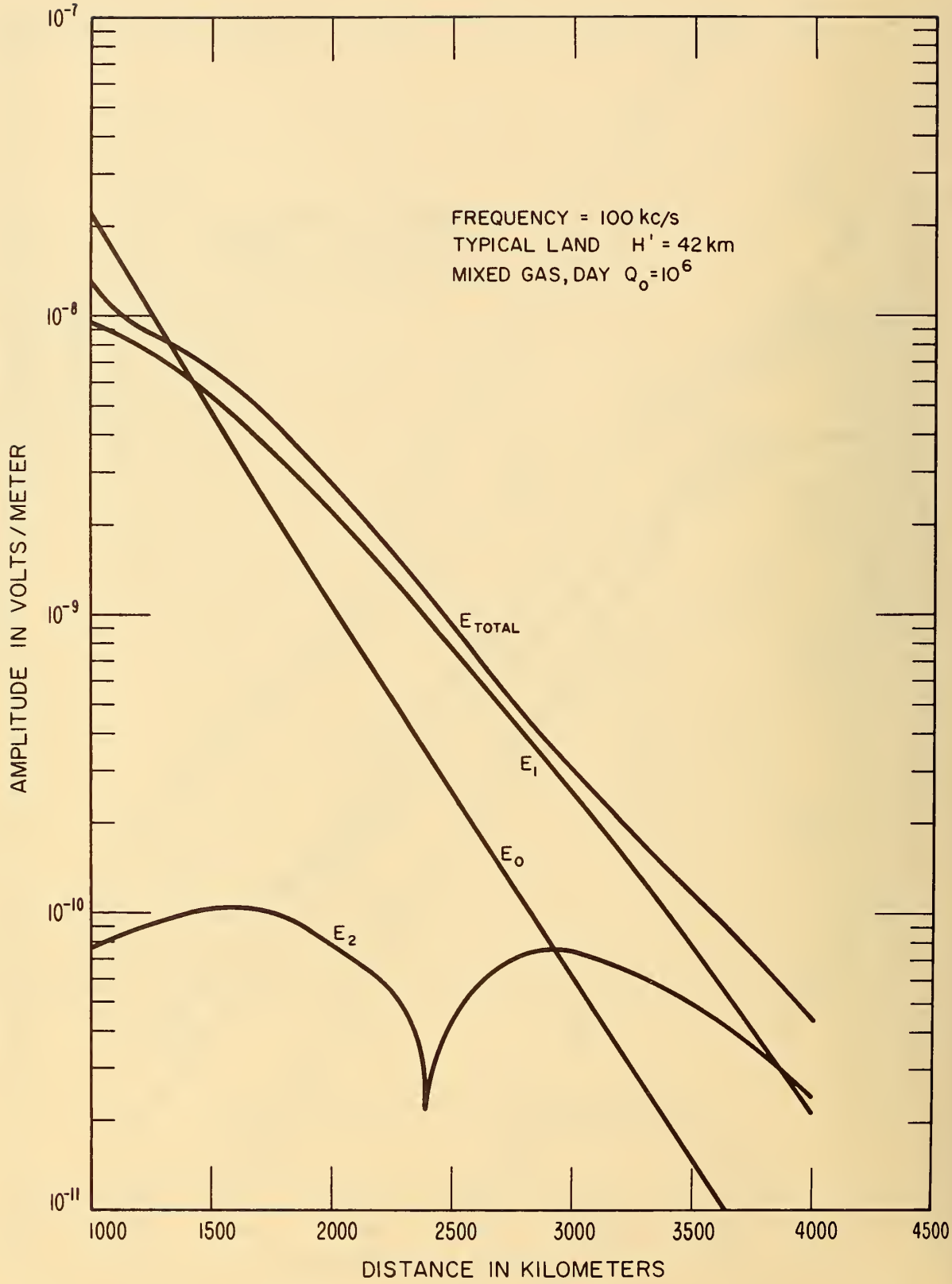

Figure 47. Propagation of 100 kc/s wave overland, $Q_o = 10^6$.

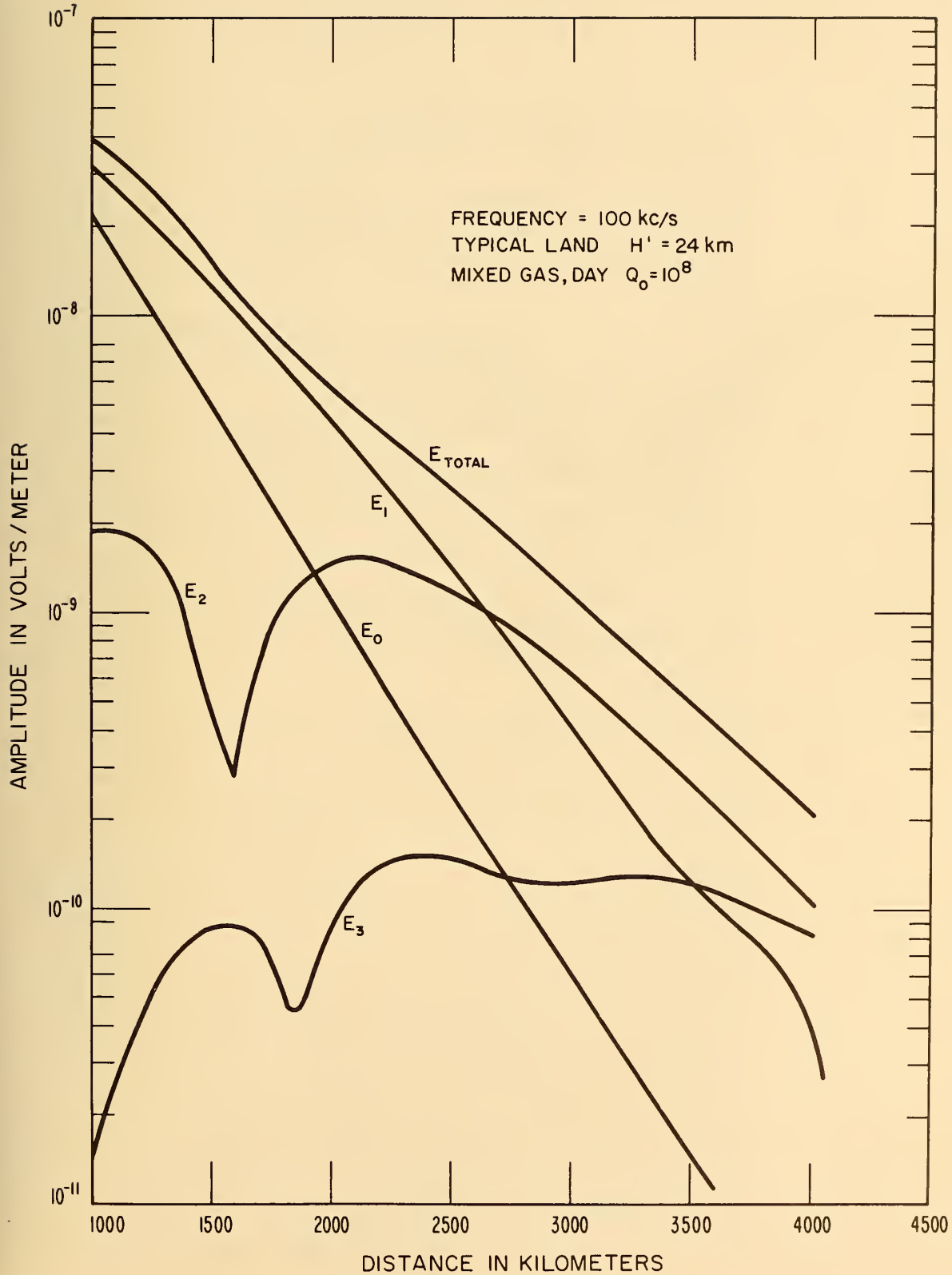

Figure 48. Propagation of 100 kc/s wave overland, $Q_o = 10^8$.

Glossary

A	=	electron attachment coefficient (1.1), (1.2).
Å		Angstron (1.18).
B		electron-ion recombination coefficient (1.1), (1.3).
C		photo detachment coefficient (1.1), (1.4).
C		$1/i\omega\epsilon_0$
C_i		i = 1, 2, 3 . . . collision process parameter (2.2).
D		detachment coefficient (1.1).
D_A		associative detachment coefficient (1.6).
D_C		collisional detachment coefficient (1.5).
E		ion-ion recombination coefficient (1.1), (1.7).
E		electric field in Maxwell's equations (2.3).
E_a		electron affinity, electron-volts (1.5).
e		electronic charge (2.1 et seq.).
ϵ_0		permittivity (2.3).
η		index of refraction (complex) (2.14 et seq.).
Y		Gregorian calendar year (1.10).
H		magnetic field is Maxwell's equations (2.3).
H		hydrogen (1.2).
h		height above surface or ground (1.9).
$\mathcal{H}$		fixed magnetic field (2.3).
I_∞^α		Lyman α incident flux at great height (1.12).
$I_\infty'(x)$		intensity of solar maximum (1.19)
I_∞^x		x-ray flux at great height (1.19)
I_h		Lyman α incident flux at any height (1.12).
I		magnetic dip (2.14 et seq.).
J		current in Maxwell's equations (2.11)

$\lambda' = N_-/N_e$ (2.16 to 2.27).

λ wavelength (1.17).

m mass (2.2).

μ_m mass absorption coefficient (1.17).

μ_0 permeability (2.3).

N number density (1.1).

N_2 nitrogen (1.2).

ν collision frequency (2.16 to 2.27).

N_s number density at surface (1.9).

N_h number density at height, h (1.9).

N_j number density of j constituent (1.13).

O_2, O oxygen (1.2).

O_3 ozone (1.4).

ω angular frequency (2.3).

ω_N^2 angular plasma frequency squared (2.14 et seq.).

ω_H gyro frequency (2.14 et seq.).

P_r probability that detachment occurs for a particular ion (1.5).

φ_a magnetic azimuth reckoned clockwise.

φ_1 angle of incidence of EM wave on plasma (2.14 et seq.).

Q production rate (1.1).

Q_0 $\frac{\rho_0}{\rho}$ production rate (1.28).

q_c production rate of cosmic rays at any height, h.

q_0 cosmic radiation production rate per atmosphere pressure (1.8).

q_n^x x-ray production rate at any height, h.

ρ density of atmosphere at any height, h (1.28 et seq.).

ρ_σ atmospheric pressure.

ρ_0 surface density of atmosphere (1.28 et seq.).

S complex number root of a quartic equation (2.14).

T temperature, degrees Kelvin (1.2).

t time.

θ = geomagnetic latitude (1.8).

U_e transmission coefficient for transverse magnetic waves (3.1).

U_m transmission coefficient for transverse electric waves (3.2).

V velocity (2.1).

[ ] indicates number density of a particular species (1.2).

GPO 850-128


DEPARTMENT OF COMMERCE
NATIONAL BUREAU OF STANDARDS